

MOLECULAR MECHANISM OF ORLISTAT HYDROLYSIS BY THE
THIOESTERASE OF HUMAN FATTY ACID SYNTHASE FOR TARGETED DRUG
DISCOVERY

Valerie Fako Miller

Submitted to the faculty of the University Graduate School
in partial fulfillment of the requirements
for the degree
Doctor of Philosophy
in the Department of Pharmacology and Toxicology,
Indiana University

August 2014

Accepted by the Graduate Faculty, of Indiana University, in partial
Fulfillment of the requirements for the degree of Doctor of Philosophy.

Jian-Ting Zhang, Ph.D., Chair

Doctoral Committee

Travis J. Jerde, Ph.D.

May 2, 2014

Jing-Yuan Liu, Ph.D.

Beth R. Pflug, Ph.D.

Karen E. Pollok, Ph.D.

Ahmad R. Safa, Ph.D.

This thesis is dedicated to my late grandmother Jessie Thomas and my late father-in-law Dennis Miller, whose lives were cut devastatingly short by pancreatic cancer. It is my hope that the research performed herein may one day make a difference, no matter how small, in improving the outcomes of patients who are diagnosed with cancer.

Acknowledgments

First and foremost, I would like to express my utmost gratitude for my mentor, Dr. Jian-Ting Zhang, and also to Dr. Jing-Yuan Liu, for the tremendous amount of guidance and mentorship that they have given me throughout my time of working in their laboratories. Both have always been available to discuss any issues that I had, and were always willing to take time to make sure that my research was making progress. Thank you also to my thesis committee chair, Dr. Travis Jerde, and to my thesis committee members, Drs. Beth Pflug, Karen Pollok and Ahmad Safa, for the time that they have taken to meet with me and for all of the instruction, suggestions and support that they have provided me. I would have not have succeeded in this graduate program without the help of my mentors and my research committee, and I owe them all many more thanks than I could possibly express here.

I would also like to thank the many members past and present of Dr. Zhang's lab and Dr. Liu's lab, all of whom have provided expertise as I completed my thesis work. I would especially like to thank Dr. Xi Wu and Dr. Zizheng Dong who were always willing to answer to my questions and provide assistance whenever possible. Thank you also to Dr. David Jones, who spent a lot of time meeting with me and helping me with the kinetics aspects of this research project. Thank you to all of the professors and researchers in the PharmTox department who have attended my seminars, and who have provided so much useful feedback and constructive critiques that have helped better my research. Thank you to the PharmTox administrative staff Amy Lawson and Lisa King for all the behind the scenes work they do every day to keep me on track and to make sure our department runs smoothly, and thank you to grants coordinator Ali Guzik and

former grants coordinator Miriam Barr for all of their help as I submitted a grant and progress reports for that grant.

I greatly thank National Cancer Institute at the NIH for awarding me a Ruth L. Kirschstein National Research Service Award to support my research, which would not have been possible without letters of recommendation provided by Drs. Bill Sullivan, John Turchi and Paul Hergenrother. I would also like to thank the Indiana University Simon Cancer Center for awarding me a travel grant to attend the American Association for Cancer Research Annual Meeting in 2012, and I would like to thank the Department of Pharmacology and Toxicology Paradise Travel Award Committee for granting me an award to attend the Molecular Therapeutics of Cancer Research Annual Meeting in 2013.

Lastly, I would like to express my deepest gratitude to my friends and family for all of their support and encouragement throughout my time in graduate school. To all of the students in the PharmTox department, thank you for making my time here at IU so much fun. To my friends Betsy Lungwitz, Jessica Pellman and Sarah Wilson, I am so grateful that I had you ladies by my side from the very beginning as we went through this experience together. Thank you for providing shoulders to lean on, and for always being understanding and supportive. Thank you especially for reminding me to take some time to enjoy life. To my parents Steve and Betsy Fako, thank you for always believing in me and reassuring me that I can accomplish anything I put my mind to. Finally, to my husband Chris, all I can say is thank you for being you, and for accompanying me on this journey and reminding me every day how lucky I am to have you in my life. What a ride it has been.

ABSTRACT

Valerie Fako Miller

MOLECULAR MECHANISM OF ORLISTAT HYDROLYSIS BY THE THIOESTERASE OF HUMAN FATTY ACID SYNTHASE FOR TARGETED DRUG DISCOVERY

Fatty acid synthase (FASN) is over-expressed in many cancers, and novel inhibitors that target FASN may find use in the treatment of cancers. It has been shown that orlistat, an FDA approved drug for weight loss, inhibits the thioesterase (TE) of FASN, but can be hydrolyzed by TE. To understand the mechanisms of TE action and for designing better FASN inhibitors, I examined the mechanism of orlistat hydrolysis by TE using molecular dynamics simulations. I found that the hexyl tail of orlistat undergoes a conformational transition, destabilizing a hydrogen bond that forms between orlistat and the active site histidine. A water molecule can then hydrogen bond with histidine and become activated to hydrolyze orlistat. These findings suggest that rational design of inhibitors that block hexyl tail transition may lead to a more potent TE inhibitor. To search for novel inhibitors of TE, I performed virtual DOCK screening of FDA approved drugs followed by a fluorogenic assay using recombinant TE protein and found that proton pump inhibitors (PPIs) can competitively inhibit TE. PPIs, which are used for the treatment of gastroesophageal reflux and peptic ulcers, work to decrease gastric acid production by binding irreversibly with gastric hydrogen potassium ATPase in the stomach. Recently, PPIs have been reported to reduce drug resistance in cancer cells

when used in combination with chemotherapeutics, although the mechanism of resistance reduction is unknown. Further investigation showed that PPIs are able to decrease FASN activity and cancer cell proliferation in a dose-dependent manner. These findings provide new evidence that FDA approved PPIs may synergistically suppress cancer cells by inhibiting TE of FASN and suggests that the use of PPIs in combinational therapies for the treatment of many types of cancer, including pancreatic cancer, warrants further investigation.

Jian-Ting Zhang, Ph.D., Chair

Table of Contents

List of Tables	xii
List of Figures	xiii
List of Abbreviations	xv
Chapter 1: Introduction	1
A. Fatty Acid Synthesis Pathway in Humans	1
B. Fatty Acid Synthase Over-Expression in Cancer.....	7
C. Drug Resistance in Cancer.....	13
D. Pancreatic Cancer.....	14
E. FASN and Pancreatic Cancer.....	17
F. Effects of FASN Inhibition on Cancer Cell Survival	20
G. Proton Pump Inhibitors and Use in Cancer Treatment	26
H. Hypothesis and Specific Aims	30
Chapter 2: Materials and Methods	33
I. Specific Aim I: Orlistat Parameterization and Molecular Dynamics	
A. Orlistat Parameterization	33
B. MM and QM Dihedral Angle Scans	37
C. Molecular Modeling and MD Simulations	39
D. MD Simulation Trajectory Analysis.....	41
E. Free Energy Calculations	43
II. Specific Aim II: In Silico and High-Throughput Ligand Screening	
A. In Situ Receptor and Ligand Preparation.....	45
B. DOCK Ligand Screening.....	46

C. Cloning and Subcloning the FASN TE Plasmid.....	47
D. Expression and Purification of Recombinant FASN TE	53
E. FASN TE Kinetic Studies and Candidate Ligand Screening.....	56
III. Specific Aim III: Lead Candidate Evaluation	
A. Human Cell Culture	59
B. MTT Assays to Measure Cellular Proliferation.....	60
C. Colony Formation Assays.....	61
D. Radioactive FASN Lipid Synthesis Assay	61
E. Measuring FASN Protein Expression via Western Blot.....	62
F. Probing the FASN TE Active Site.....	64
G. Determination of Inhibition Mechanism of FASN TE by Lansoprazole.....	65
H. PARP-1 Cleavage Apoptosis Assay	66
I. Cell Death Detection Apoptosis Assay.....	66
J. Extracellular and Intracellular pH Measurement.....	67
K. Rescue with Palmitate Supplementation.....	68
L. IC ₅₀ and Statistical Calculations	69
Chapter 3: Aim I: Mechanism of Orlistat Hydrolysis by the Thioesterase of Human	
Fatty Acid Synthase	70
A. Background and Rationale.....	70
B. Results.....	73
B1. Covalent-Orlistat Molecular Mechanic Parameter Verification by	
Quantum Mechanics.....	73
B2. Two Distinct Conformations of the Hexyl Tail in Covalent-Orlistat.....	76

B3. Compatibility of Covalent-Orlistat MM Parameters with AMBER	78
B4. Conformational Transition of the Hexyl Tail in the FASN TE Domain...	81
B5. Interactions of the Hexyl tail with the Short-Chain and Shift Pockets	86
B6. Crystal Packing Restrains the Hexyl Tail in Conformation I	89
B7. Accessibility of Water Molecules to the Active Site	92
B8. Catalytically Critical Interactions at the Active Site.....	92
B9. Activation of Catalytic Water Molecules.....	94
B10. Correlation of Interactions at the Active Site.....	94
B11. Simulation of Truncated Orlistat Lacking the Hexyl Tail.....	98
C. Conclusions and Discussion	100
Chapter 4: Aim II: Identification of FDA Approved Proton Pump Inhibitors as	
Inhibitors of Human Fatty Acid Synthase Thioesterase	105
A. Background and Rationale.....	105
B. Results.....	108
C. Conclusions and Discussion	120
Chapter 5: Aim III: Validation of Proton Pump Inhibitors as Inhibitors of Human	
Fatty Acid Synthase Thioesterase and Determination of their	
Therapeutic Potential as Anti-Cancer Agents in Pancreatic Cancer.....	125
A. Background and Rationale.....	125
B. Results.....	127
B1. PPIs Inhibit Cellular Proliferation and Colony Forming Ability	127
B2. PPIs Inhibit Fatty Acid Synthesis in Whole Cells.....	132
B3. Lansoprazole Competitively Inhibits the Active Site of FASN TE.....	136

B4. Lansoprazole Induces Cell Death In Vitro	138
B5. Palmitate Supplementation Rescues the Effect of Lansoprazole on Cellular Proliferation and Apoptosis	140
B6. Effect of Lansoprazole on Extracellular and Intracellular pH	142
B7. Lansoprazole Treatment has a Greater Effect in Cells with Higher FASN Activity.....	142
C. Conclusions and Discussion	145
Chapter 6: Summary and Future Directions	149
A. Summary and Future Directions for Specific Aim I.....	149
B. Summary and Future Directions for Specific Aims II and III	153
C. Final Remarks	155
Appendices	
Appendix A: Gaussian and Molecular Dynamics Input Files	157
Appendix B: Covalent-Orlistat AMBER Parameters	174
Appendix C: DOCK Input Files	179
Appendix D: Novel FASN Inhibitor.....	183
References.....	186
Curriculum Vitae	

List of Tables

Chapter 3:

Table 1: Summary of simulated trajectories and average RMSD, temperature, and energy.....	80
Table 2: Time span of conformation I and II, B factor, ω angles, hexyl tail RMSD and free energy for all three simulations	85
Table 3: Average distance of the hexyl tail to pocket I and pocket II in TE	85
Table 4: Catalytically important interactions at the active site.....	97

Chapter 4:

Table 1: 34 selected FDA approved compounds from DOCK screening.....	110
Table 2: Chemical structure, IC_{50} and K_i of PPIs.....	120

Chapter 5:

Table 1: IC_{50} values of PPIs from MTT assays	128
Table 2: IC_{50} values of PPIs from colony formation assays	130

Appendix B:

Table 1: Charge and AMBER atom type for each covalent-orlistat atom	176
---	-----

List of Figures

Chapter 1:

Figure 1: Overview of the fatty acid synthesis pathway in humans2
Figure 2: Chemical reactions of fatty acid synthesis6

Chapter 2:

Figure 1: Schematic illustration of the covalent-orlistat parameterization.....34
Figure 2: Schematic illustration of the 3-mer peptide containing covalent-orlistat.....38

Chapter 3:

Figure 1: Catalytic mechanism of orlistat hydrolysis by FASN TE75
Figure 2: Potential energy of the 3-mer peptide containing covalent-orlistat and ω angle scan.....78
Figure 3: RMSD, B-factor, ω dihedral angle, and distance of the hexyl tail of covalent-orlistat in the first simulation84
Figure 4: Hexyl tail interactions with short-chain and shift-pocket residues88
Figure 5: Crystal lattice simulation ω dihedral angle and RMSD91
Figure 6: Catalytically important interactions at the active site96
Figure 7: Simulation of truncated orlistat99

Chapter 4:

Figure 1: Determination of FASN TE kinetic parameters115
Figure 2: Pantoprazole inhibits FASN TE activity117
Figure 3: Dose-dependent inhibition of FASN TE by PPIs.....119

Chapter 5:

Figure 1: Dose-response curves of PPIs from MTT assays	128
Figure 2: Dose-response curves of PPIs from colony formation assays.....	130
Figure 3: FASN protein expression and activity in PANC-1 and BxPC3 cells...	132
Figure 4: Lansoprazole inhibits FASN lipid synthesis	134
Figure 5: PPIs inhibit FASN lipid synthesis	135
Figure 6: Direct inhibition of FASN TE by lansoprazole.....	137
Figure 7: Initiation of apoptosis by lansoprazole.....	139
Figure 8: Palmitate supplementation rescues the effects of lansoprazole.....	141
Figure 9: Effect of lansoprazole on intracellular pH and differential effects of lansoprazole in paired cells with varying FASN activity	144

Chapter 6:

Figure 1: Orlistat derivatives	152
--------------------------------------	-----

Appendix B:

Figure 1: Orlistat atom type and charge indicator	175
---	-----

Appendix C:

Figure 1: Novel compound 13C inhibits recombinant FASN TE activity and tumor cell proliferation	185
--	-----

List of Abbreviations

4-MU:	4-methylumbelliferone
4-MUH:	4-methylumbelliferyl heptanoate
5-FU:	Fluorouracil
ACC:	Acetyl CoA carboxylase
ACP:	Acyl carrier protein
AMPK:	AMP-activated protein kinase
BSA:	Bovine serum albumin
CDKi:	Cyclin-dependent kinase inhibitor
COX-2:	Cyclooxygenase-2
DMEM:	Dulbecco's modified eagle medium
DMSO:	Dimethyl sulfoxide
dNTP:	Deoxynucleotide
DPC4:	Deleted in pancreatic carcinoma 4
DPM:	Disintegrations per minute
EGCG:	Epigallocatechin-3-gallate
EGF:	Epidermal growth factor
EGFR:	Epidermal growth factor receptor
ESP:	Electrostatic potential
ER:	Endoplasmic reticulum
FASN:	Fatty acid synthase
FLOPS:	Floating operations per second
FU:	Fluorescence units
GF:	Growth factor
GFR:	Growth factor receptor
HRP:	Horseradish peroxidase
HTS:	High-throughput screening
IPMN:	Intraductal papillary mucinous neoplasm
IPTG:	Isopropyl β -D-1-thiogalactopyranoside
KS:	Ketoacyl synthase
MD:	Molecular dynamics
MM:	Molecular mechanics
MTT:	(3-(4,5-dimethylthiazol-2-yl)-2,5-diphenyltetrazolium bromide
NADH:	Nicotinamide adenine dinucleotide
NADPH:	Nicotinamide adenine dinucleotide phosphate
MCN:	Mucinous cystic neoplasm
NEB:	New England Biolabs
NFDM:	Non-fat dry milk
Ni-NTA:	Nickel-nitrilotriacetic acid
PAGE:	Polyacrylamide gel electrophoresis

PanIN:	Pancreatic intraepithelial neoplasia
PARP-1:	Poly(ADP-ribose) polymerase-1
PBS:	Phosphate buffered saline
PCR:	Polymerase chain reaction
PI3K:	Phosphatidylinositol-3 kinase
PMSF:	Phenylmethylsulfonyl fluoride
PPI:	Proton pump inhibitor
PVDF:	Polyvinylidene difluoride
QM:	Quantum mechanics
RESP:	Restrained electrostatic potential
RMS:	Root mean square
RMSD:	Root mean square deviation
RMSF:	Root mean square fluctuation
SDS:	Sodium dodecyl sulfate
SEM:	Standard error of the mean
SNP:	Single nucleotide polymorphism
SREBP:	Sterol regulatory element-binding protein
TBS:	Tris buffered saline
TBST:	Tris buffered saline with Tween-20
TE:	Thioesterase
TGF- β :	Transforming growth factor- β
VEGF:	Vascular endothelial growth factor

Chapter 1: Introduction

A. Fatty Acid Synthesis Pathway in Humans

Lipogenesis is the process by which fatty acids are synthesized from a surplus of acetyl-CoA and are subsequently stored as triglycerides or used in the creation of other cellular lipids [1,2]. Glucose, created from the breakdown of excess carbohydrates in the diet, is converted to pyruvate via the glycolysis pathway. Pyruvate is transported into the mitochondria and is converted to acetyl-CoA by pyruvate dehydrogenase. Acetyl-CoA typically enters the citric acid cycle, which yields energy in the form of adenosine triphosphate (ATP), as well as the reducing agent nicotinamide adenine dinucleotide (NADH). However, when excess acetyl-CoA is synthesized, it is instead converted to citrate by citrate synthase and shuttled back into the cellular cytoplasm via the citrate shuttle. Once in the cytoplasm, citrate is re-converted to acetyl-CoA by citrate lyase, where it can then be incorporated into fatty acids [3-5] (Fig. 1).

FIGURE 1

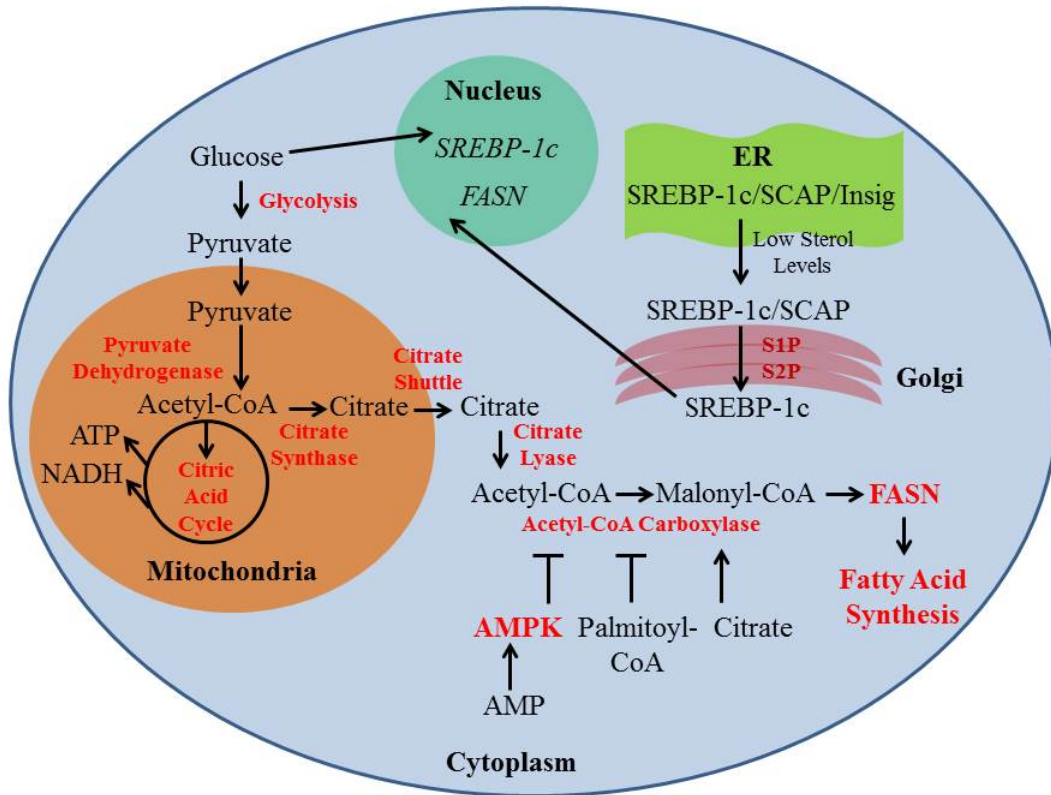


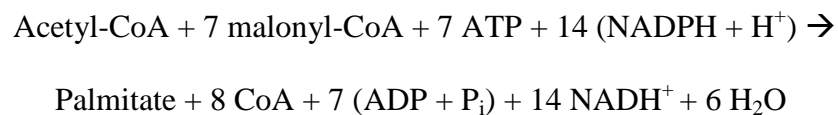
Figure 1. Overview of the fatty acid synthesis pathway in humans. *FASN* and fatty acid synthesis is controlled transcriptionally and enzymatically, both of which are initiated by high levels of glucose. The transcription of the *SREBP-1c* gene is controlled by insulin, which is increased in the presence of glucose. *SREBP-1c* is a transcription factor that regulates the transcription of the *FASN* gene. Excess glucose also leads to an excess of acetyl-CoA that does not enter the citric acid cycle, and is instead shuttled out of the mitochondria as citrate, which is then converted back to acetyl-CoA. Citrate allosterically activates acetyl-CoA carboxylase, which controls the rate-limiting step of fatty acid synthesis: the conversion of acetyl-CoA to malonyl-CoA. All enzymes and pathways are indicated in red.

In humans, long-chain fatty acids, mainly 16-carbon palmitate, are synthesized by the 270 kDa homodimeric enzyme fatty acid synthase (FASN). FASN is a seven-domain enzyme and is the sole protein in the human genome capable of synthesizing fatty acids *de novo* [6-8]. Crystal structure analysis of the FASN protein revealed that FASN adopts a 'X-shape' structure, with each side of the dimer containing a full set of active sites that coordinate FASN activity [9,10]. The gene encoding the FASN protein is found on chromosome 17q25 [11], and transcription of the FASN gene is controlled directly by the sterol regulatory element-binding protein-1c (SREBP-1c) transcription factor. The presence of the hormone insulin, stimulated by increased levels of glucose in the blood stream, enhances the transcription of SREBP-1c gene [12,13], whereas glucagon, stimulated by low levels of glucose, suppresses SREBP-1c transcription [14,15]. SREBP-1c is post-transcriptionally regulated by two proteins, SCAP and INSIG. Following synthesis, SREBP-1c forms a complex with SCAP in the endoplasmic reticulum (ER) [16,17]. When sterol levels are in excess, the SCAP/SREBP-1c complex binds to INSIG, which prevents the SCAP/SREBP-1c complex from leaving the ER [18,19]. However, when sterol levels are decreased, the SCAP/SREBP-1c complex is released from INSIG and is transported via vesicle to the golgi apparatus for proteolytic processing by site-1 protease (S1P) and site-2 protease (S2P) [20,21]. SREBP-1c is then free to travel to the nucleus to transcribe the FASN gene [22-24] (Fig. 1).

FASN activity is tightly regulated by acetyl-CoA carboxylase (ACC), which acts as the gate keeper and rate-limiting enzyme of fatty acid biosynthesis [25]. ACC uses ATP to convert two-carbon acetyl-CoA to three-carbon malonyl-CoA by transferring a CO₂ group from bicarbonate to acetyl-CoA using biotin as a carrier [6,26]. ACC, and thus

fatty acid synthesis, is tightly controlled both allosterically and by covalent modification. ACC is down-regulated allosterically by palmitoyl-CoA and up-regulated allosterically by citrate. ACC is also controlled via covalent modification with phosphorylation. AMP-activated protein kinase (AMPK), which acts as a cellular energy sensor, phosphorylates and inactivates ACC when AMP levels in the cell are high, and thus cellular energy levels are low. AMPK de-phosphorylates and activates ACC when AMP levels are low, indicating that cellular energy levels are high and excess acetyl-CoA can be converted to fatty acids [27,28] (Fig. 1).

Fatty acids are synthesized with acetyl-CoA, malonyl-CoA, ATP and NADPH via the following net reaction:



In the first step of fatty acid synthesis, the acetyl group from acetyl-CoA is transferred to the flexible acyl carrier protein domain (ACP), which then transfers the molecule to the β -ketoacyl synthase (KS) domain. The malonyl group from malonyl-CoA is transferred to the ACP, and then the acetyl group from acetyl-ACP is transferred to malonyl-ACP by the malonyl/acetyl transferase (MAT) domain, yielding a 3-keto acyl ACP. This 3-keto acyl group is converted to a saturated carbon chain in a series of three reactions. First, the keto group is reduced to an alcohol group by the β -ketoacyl reductase (KR) domain of FASN. Then, dehydration of the alcohol group by the β -hydroxylacyl dehydratase (DH) domain yields a double bond in the carbon chain. Finally, the enoyl reductase (ER) domain reduces the double bond to a single bond. Both reduction reactions require the cofactor NADPH. This newly formed chain is moved to the KS domain, a new molecule

of malonyl-CoA is transferred to the ACP and the cycle continues until the carbon chain reaches the desired length [6-8] (Fig. 2). The thioesterase (TE) domain of FASN, a serine hydrolase with an Asp-His-Ser catalytic triad, hydrolyzes the thioester bond between the fatty acid and ACP. The sulfur atom of ACP accepts a hydrogen atom from the His residue in the TE active site, which is then released as the fatty acid is covalently bound to the Ser residue in the TE active site, forming an acyl-enzyme intermediate. A water molecule is activated by forming a hydrogen bond with the catalytic nitrogen atom of the His residue and nucleophilically attacks the carbonyl carbon of the acyl-enzyme intermediate, causing the release of the fatty acid from the Ser residue [29].

In bacteria and plants, fatty acid synthesis is performed by a series of dissociated monofunctional proteins that correspond to each domain of the FASN polypeptide found in humans [30]. In fungi, fatty acids are synthesized by a heterododecamer with the domains situated across the two polypeptides [31]. Although there are clear variations in structural organization of the domains, the chemical reactions of fatty acid biosynthesis are conserved for all organisms [30]. With the exception of thioesterase, the domains of FASN are truly unique, in that similar domains have only been found in the polyketide synthases of bacteria [32]. Synthesized palmitate can be used to covalently modify the cysteine residues of various proteins in a process called palmitoylation. A protein with very similar function to FASN thioesterase, palmitoyl protein thioesterase, removes palmitate from palmitoylated proteins by cleaving the thioester bond between the palmitate molecule and the cysteine residue of the protein, similar to the way TE cleaves the bond between palmitate and ACP [33].

FIGURE 2

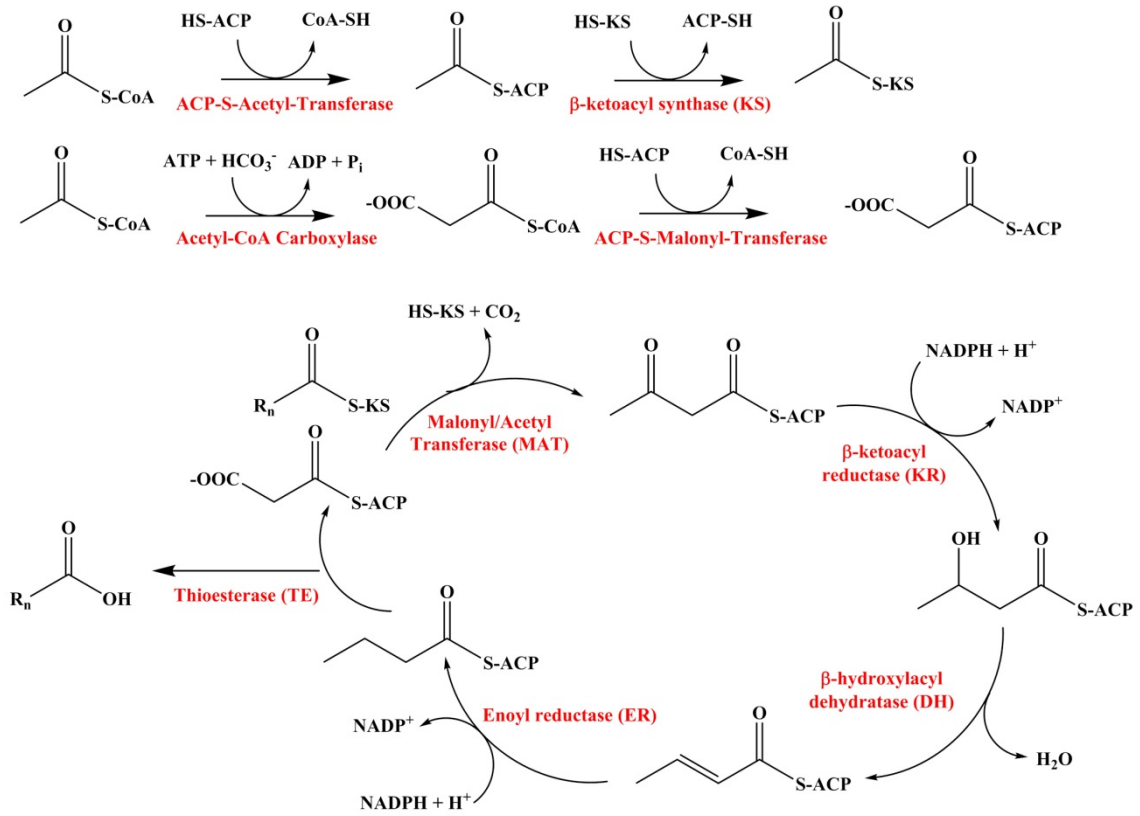


Figure 2: Chemical reactions of fatty acid synthesis. Fatty acid synthesis begins when acetyl-CoA is transferred to the ACP domain and then the KS domain of FASN, and malonyl-CoA, created from acetyl-CoA by ACC, is transferred to the ACP domain. A coordinated series of reactions by the domains of FASN create a growing fatty acid chain from the condensation of acetyl-CoA and malonyl-CoA, followed by several reduction reactions. The cycle continues until the fatty acid chain reaches a certain length, when the TE domain catalyzes the release of the fatty acid chain from the ACP.

Following the synthesis and release of the saturated fatty acid chains by FASN, these fatty acids have the potential to be used in a number of different ways. Most commonly, these fatty acids are linked to a glycerol backbone and converted to triglycerides for energy storage by liver cells and adipose cells [34]. As discussed above, palmitate can be covalently attached to proteins. The hydrophobicity of proteins can be increased by palmitoylation, which may in turn enhance their membrane association. Palmitoylation can also modulate protein-protein interactions, and affects subcellular trafficking [35]. Additionally, products of fatty acid synthesis could be elongated or desaturated in the mitochondria or ER, which are then incorporated into many other types of cellular lipids, such as phospholipids or cholesterol esters [36,37]. However, in humans who intake adequate fatty acids in their diets, FASN expression and activity is typically suppressed in most tissues throughout the body, with the exception of liver cells [38], adipose cells [39], lactating mammary tissue [40] and cycling endometrium [41]. Thus, the de novo synthesis of fatty acids by FASN is a minor anabolic pathway, as most tissues will preferentially use exogenous dietary fats instead of synthesizing fatty acids de novo [42].

B. Fatty Acid Synthase Over-Expression in Cancer

High levels of aerobic glycolysis, in which cells produce energy by lactic acid fermentation in the cytosol, instead of oxidation of pyruvate in the mitochondria, has been noted as one of the hallmarks of cancer cells [43,44]. The increased glucose production in transformed cells has subsequently been linked to an increase in the activity of lipogenic enzymes in these cells [45], and contrasting with normal tissue, cancer cells

have been found to derive esterified fatty acids almost exclusively from de novo fatty acid synthesis [46], despite adequate nutritional supply [47]. Although the relationship between increased glycolysis and de novo fatty acid synthesis has been well documented since the 1950s, a definitive link between FASN enzyme activity and cancer progression was not noted until 1994 when Kuhajda *et al.* determined that a marker for poor prognosis in breast cancer patients, oncogenic-antigen 519 (OA-519), was actually FASN [48]. Since this discovery, marked differences between fatty acid synthesis in normal and cancer cells have been noted. Unlike normal cells from healthy tissues types, in which endogenous fatty acids are typically used for energy storage in the form of triglycerides, the majority of fatty acids synthesized by cancer cells are esterified to phospholipids and incorporated into new membranes as these cells rapidly proliferate [48,49]. Also, cancer cells can lose control of the fatty acid synthesis pathway by nutritional or hormonal signals and can also adopt new control by growth factors (GFs) and growth factor receptors (GFRs) such as epidermal growth factor (EGF) and the EGF receptor (EGFR) [50]. GFs and GFRs increase FASN gene transcription through the activation of the phosphatidylinositol-3 kinase (PI3K)-Akt signaling pathway [51] and the mitogen-activated protein kinase (MAPK)/extracellular signal-regulated kinase (ERK1/2) pathway [52]. Blockade of the PI3K/Akt or MAPK/ERK1/2 pathways with specific inhibitors of PI3K or MEK1 resulted in a reduced expression of both FASN and SREBP1 [52], but did not cause a complete abrogation of the synthesis of fatty acids. A possible explanation is that blockade of PI3K/Akt or MAP/ERK1/2 did not affect the activation or expression acetyl-CoA carboxylase, which ultimately controls the fatty acid synthesis pathway [6]. It is also possible that mutations downstream of the PI3K/Akt or MAPK/ERK1/2 pathways

could also be contributing to FASN over-expression. In prostate and ovarian cancers, loss of the tumor suppressor phosphatase and tensin homologue (PTEN) caused the activation of the PI3K/Akt pathway, which correlated to FASN over-expression [53,54]. In breast cancer cells, the HER2/Neu pathway, likely working through the PI3K/Akt pathway, has also been implicated in the up-regulation of FASN [55-57]. Steroid hormones not associated with nutritional response, such as progestins, androgens and E₂, have also been shown to regulate FASN expression [58-61]. The activation of FASN gene transcription by growth factor and steroid hormone pathways is driven by the aberrant stimulation of SREBP-1c expression and activation [62-65]. Copy number gain of the FASN gene has also been implicated as a cause of FASN protein over-expression in cancerous lesions [66,67]. There are a number of known single nucleotide polymorphisms (SNPs) of the FASN gene, and several studies have associated some SNPs with an increase in body mass index and obesity [68,69]. However, only two studies have looked into a correlation between any FASN SNPs and an increase in cancer risk. The first study failed to find a correlation between FASN SNPs and an increase in breast cancer risk [70]. However, another study determined that several FASN SNPs were associated with an over-expression of FASN, as well as an increase in risk for development and progression of prostate cancer [71], but it is unknown how these FASN SNPs play a role in FASN over-expression. Following translation, the FASN enzyme is not known to be allosterically regulated or covalently modified in normal cells, but there has been one report of direct FASN phosphorylation by Her2 in breast cancer, which may modify or modulate FASN activity [72]. Additionally, ubiquitin-specific protease USP2a, which rescues proteins

from degradation by removing ubiquitin tags, stabilizes FASN in prostate cancer cells [73,74].

Stresses in the cellular microenvironment may also lead to the up-regulation of FASN. Under conditions of hypoxia, induction of hypoxia inducible factor 1 (HIF1) activates Akt, which significantly up-regulates SREBP-1c, leading to increased FASN expression [75]. Also, acidic extracellular pH was found to up-regulate transcription of the FASN gene in an epigenetic manner, leading to over-expression of FASN protein [76].

Since the discovery that FASN expression and de novo lipogenesis are deregulated in cancer cells, FASN over-expression has been noted in a wide variety of cancer cell types including endometrial carcinoma [77,78], melanoma [79], esophageal cancer [80-82], mesothelioma [83], gastrointestinal stromal tumors [84], Paget's disease of the vulva [85], oral squamous carcinomas [86], head and neck squamous cell carcinoma [87], non-Hodgkin lymphoma [88], oral melanoma [89], meningioma [90], liposarcoma [91], multiple myeloma [92], and glioma [93]. In addition to being present in the aforementioned cancer types, FASN over-expression has also been found to definitively correlate with aggressiveness, cancer stage and worsened prognosis in patients with cancer of the prostate [94,95], breast [96,97], ovary [98,99], tongue [100,101], soft tissue [102], endometrium [103,104], lung [105], pancreas [106], renal cell [107], larynx [108], head and neck [109], bladder [110], and esophagus [111], as well as melanoma [112] retinoblastoma [113,114], nephroblastoma [115], osteosarcoma [116], meningioma [117,118], and glioma [119]. The over-expression of FASN throughout the process of tumorigenesis has been monitored using the transgenic adenocarcinoma of

mouse prostate (TRAMP) model, which demonstrated that with increasing age and tumor progression, as well as in metastatic lesions, FASN activity also increased [120]. Examination of prostate carcinomas from patient samples also revealed that there is a strong association between tumor initiation and progression and FASN expression, with the highest level of expression found in bone metastases [66]. FASN is currently being investigated as a possible prognostic or diagnostic tumor marker, as its expression has been found in the serum of patients with breast cancer [121], pancreatic cancer [122] and colorectal cancer [123].

There is indication that the up-regulation of fatty acid synthesis may be an early event in tumorigenesis, as FASN over-expression has been found in benign, pre-cancerous and early cancerous lesions of several tissue types. Breast tissue [124,125]; colorectal tissue [126]; early stages of squamous cell lung carcinoma [127]; prostate tissue [128-130]; precancerous foci of the stomach [131]; pre-cancerous intraductal papillary mucinous neoplasms [122]; ulcerative colitis in the colon [132]; benign and atypical granular cell tumors [133]; hyperkeritotic oral epithelium [134]; esophageal mucosa of patients with esophagitis, Barrett's esophagus and esophageal adenocarcinoma [82,135,136]; and benign tumors of the salivary gland [137] all have been shown to have increased FASN expression. Due to an abundance of evidence that FASN up-regulation often occurs in the pre-cancerous lesions of many tissue types and is correlated to tumor aggressiveness and worsened prognosis in patients whose tumors over-express FASN, the theory that FASN may act as a "metabolic oncogene" has been proposed [76,138]. In one such study supporting this theory, FASN was ectopically over-expressed in immortalized human breast epithelial cells, which activated the HER1/HER2 tyrosine kinase receptors

and induced a cancer-like phenotype in these epithelial cells [139]. In 2009, Migita *et al.* demonstrated that FASN can act as a metabolic oncogene in prostate cancer by over-expressing FASN in immortalized human prostate epithelial cells, androgen receptor-overexpressing epithelial cells, and human prostate adenocarcinoma, which increased cellular proliferation in these cell types. When injected into immunodeficient mice, epithelial cells with over-expressed FASN that also over-expressed the androgen receptor formed invasive tumors. Additionally, prostate intraepithelial neoplasms formed when FASN was transgenically expressed in mice, and FASN over-expression protected epithelial cells from apoptosis when treated with chemotherapeutic drugs [140]. One mechanism by which FASN may be contributing to the development of cancerous phenotypes is through the WNT/ β -catenin signaling pathway. FASN over-expression in immortalized prostate epithelial cells led to increased levels of Wnt-1 palmitoylation, which in turn stabilized cytoplasmic β -catenin, leading to the activation of the WNT/ β -catenin signaling pathway, which has been implicated in prostate carcinogenesis [141].

Arachidonic acid, a polyunsaturated fatty acid, is the rate-limiting precursor of a number of biologically active pro-inflammatory metabolites including hydroxyeicosatetraenoic acids (HETEs) and leukotrienes produced by lipoxygenase, and prostanoids such as prostaglandins and thromboxanes produced by cyclooxygenase. Altered metabolism of arachidonic acid to produce these metabolites has been implicated in promoting cancer progression and metastasis by modifying the tumor microenvironment (reviewed in [142]). Arachidonic acid also activates androgen steroid hormone synthesis, which contributes to prostate cancer progression [143]. As arachidonic acid is produced directly via hydrolysis from the sn-2 position of membrane

phospholipids by the enzyme phospholipase A2 [144], and it has been demonstrated that lipids produced by FASN in cancer cells are mainly incorporated into membrane phospholipids such as phosphatidylcholine and phosphatidylserine [145], it is possible that there is a connection between FASN and arachidonic acid production in cancer cells. Indeed, one study has connected the fatty acid synthesis pathway to the production of arachidonic acid. Reduction of FASN by RNAi in prostate cancer cells suppressed the expression of the PLA2G4A and HSD17B12 genes, which encode the enzymes phospholipase A2 and 17- β -hydroxy-steroid dehydrogenase, respectively [146]. 17- β -hydroxysteroid dehydrogenase, which is involved in the synthesis of steroid hormones, has also been correlated to the production of very long chain fatty acids, including arachidonic acid [147]. This report demonstrates that altered lipid production by FASN may be an upstream event that contributes to aberrant arachidonic acid metabolism in cancer cells.

C. Drug Resistance in Cancer

Not only is FASN associated with increasing aggressiveness and worsened prognosis, FASN over-expression has also been implicated in resistance of tumor tissues to chemotherapeutic treatment. FASN was found to be over-expressed in a doxorubicin-selected multi-drug resistant breast cancer cell line [148], suggesting that FASN may be involved in the development of drug resistance following chemotherapeutic treatment. Ectopic over-expression of FASN also led to increased drug resistance in breast cancer cells [148]. FASN up-regulation has also been associated with resistance to gemcitabine

and radiation treatment in pancreatic cancer cells [149], as well as resistance to radiation treatment in nasopharyngeal carcinoma [150].

There are several proposed mechanisms by which FASN over-expression confers drug resistance in cancer cells. Regulation of drug-induced apoptosis may be one such mechanism, as a recent study demonstrated that FASN over-expression in breast cancer cells inhibited apoptosis and caspase-8 activation upon treatment with doxorubicin, by inhibiting the production of TNF α and ceramide [151]. FASN over-expression may also mediate the DNA damage response following treatment with DNA damaging chemotherapeutics by causing the up-regulation of a key DNA damage response enzyme, Poly (ADP-ribose) polymerase-1 (PARP-1), leading to increased DNA repair following drug treatment [152]. Also, a study examining the cellular membrane of doxorubicin-resistant breast cancer cells found that the resistant cells had an altered cellular membrane composition, which was more condensed and less fluid than the membrane of sensitive cells [153]. Although FASN expression was not specifically examined, it is possible that FASN over-expression-mediated drug resistance may be due to changes in lipid composition, which could affect drug uptake [152].

D. Pancreatic Cancer

According to the American Cancer Society, there are two main types of cancerous lesions of the pancreas: cancer of the exocrine pancreas and cancer of the endocrine pancreas. Endocrine pancreatic cells, known as islets or islets of Langerhans, are responsible for producing the nutritional hormones insulin and glucagon. Exocrine pancreatic cells produce the enzymes that are released into the intestines to aid digestion.

These glands and ductal cells make up 95 % of the pancreas. A vast majority of pancreatic cancers occur in the exocrine pancreas, and 95 % of cancers of the exocrine pancreas are ductal adenocarcinomas. The general term ‘pancreatic cancer’ refers specifically to these types of cancers. On the other hand, cancers of the endocrine pancreas are known as pancreatic neuroendocrine tumors, and constitute a completely different tumor type. The American Cancer Society estimates that approximately 46,420 people (23,530 men and 22,890 women) will be diagnosed with pancreatic cancer, and 39,590 people (20,170 men and 19,140 women) will die of pancreatic cancer in the United States in 2014. Of patients diagnosed with pancreatic cancer, the 5-year survival rate for the least aggressive tumor stage was only 14 %, and dropping to as low as 1 % for the most aggressive tumor stage [154]. Pancreatic carcinomas are the fourth leading cause of cancer related deaths [155] and majority of patients who are diagnosed with pancreatic cancer die within 4 to 6 months of diagnosis [156]. Despite continued research and advancing technology and medical developments over the last decade, pancreatic cancer incidence and mortality rates have not improved [157]. The especially poor prognosis of pancreatic cancer is a direct result of difficulty in diagnosing the disease at an early stage, due to the inaccessible location of the pancreas and the lack of specific symptoms. By the time a diagnosis is made, metastasis has typically already occurred and chemotherapy, radiotherapy and surgery have been found to increase survival rate and quality of life in only ~10 % of patients diagnosed with pancreatic cancer [158].

There are several types of precancerous lesions that have been described in pancreatic cancer, including pancreatic intraepithelial neoplasia (PanIN), intraductal papillary mucinous neoplasm (IPMN), and mucinous cystic neoplasm (MCN) [159], and

a number of genetic mutation events that likely lead to the initiation and maintenance of pancreatic cancer have been described [160]. One of the earliest genetic mutations arising in pancreatic cancer is a mutation in the *KRAS2* oncogene. The protein encoded by *KRAS2*, which becomes constitutively active by the mutation, mediates a number of pro-survival protein functions including cellular proliferation, cytoskeleton remodeling and migration [161,162]. This mutation, which is present in approximately 90-95 % of pancreatic cancer cases [161], has also been found to be present 36 %, 44 % and 87 % of progressive PanIN lesions (PanIN-1A, PanIN-1B and PanIN-2/3 precancerous lesions, respectively) suggesting that this mutation may initiate the formation of pancreatic cancer [159]. In addition to the activation of the KRAS oncogenic pathway, there are three main tumor suppressor genes that are inactivated in pancreatic cancer. The most common, which is inactivated in approximately 90 % of pancreatic cancers, is the *p16/CDKN2A* gene. This gene encodes proteins of the cyclin-dependent kinase inhibitor (CDKi) family, which prevent progression through the cell cycle [163]. The tumor suppressor gene *TP53* is inactivated in approximately 70 % of pancreatic cancers [164]. The p53 tumor suppressor protein regulates the cell cycle, maintains cellular arrest and induces apoptosis in cells with DNA damage, and loss of the protein leads to the survival and proliferation of cells, even with DNA damage present [165]. In approximately 55 % of pancreatic cancers, the *DPC4/SMAD4* (DPC4 standing for deleted in pancreatic carcinoma 4) tumor suppressor gene is inactivated [166]. The protein encoded by this gene, smad4, activates the transforming growth factor- β (TGF- β) signaling pathway, which regulates target genes that have growth-inhibitory effects [167]. Thus, the loss of smad4 confers a growth advantage in pancreatic tumor cells with this mutation.

In addition to the genetic mutations listed above, a global genomic analysis study of pancreas tumors revealed that, on average, pancreatic cancers contain 63 genetic alterations, most of which are point mutations. This study also defined 12 major cellular signaling pathways that are genetically altered in 67-100 % of pancreatic tumors. Altered genes represented pathways involved in cancer such as those that regulate apoptosis; DNA damage control; G₁/S phase cell cycle transition; hedgehog signaling; cell adhesion; integrin signaling; KRAS signaling; c-Jun N-terminal kinase signaling; invasion regulation; small GTPase signaling; TGF- β signaling; and Wnt/Notch signaling. Although common pathways were altered in each pancreatic tumor examined, the specific components of each pathway containing the alterations varied greatly. The study concluded that, due to the tremendous amount of heterogeneity in these tumors, targeting individual components in these pathways is not likely to be a useful strategy for therapeutic development for the treatment of pancreatic cancer. Instead, the focus should lie in targeting mediators and processes that are downstream of these pathways. The authors of the study suggested that discovering agents that cause metabolic disturbances may be one such strategy [168]. As FASN lies downstream of the PI3K/Akt and MAPK/ERK1/2 pathways in cancerous tissues, it is reasonable to predict that targeting FASN may be a useful strategy for the treatment of pancreatic cancer.

E. FASN and Pancreatic Cancer

Very few treatment options exist for patients with advanced pancreatic cancer and very little progress has been made in elucidating new treatment modalities for this disease. The only curative treatment for pancreatic cancer is surgical resection, however,

fewer than 20 % of patients are candidates for surgery [169]. In 1997, the nucleoside analog gemcitabine was established as the first-line chemotherapeutic treatment option for pancreatic cancer. This landmark study demonstrated very modest increase in median survival with gemcitabine treatment compared to the chemotherapeutic drug fluorouracil (5-FU), increasing to 5.65 months from 4.41 months [170]. Gemcitabine (difluorodeoxycitidine) is a prodrug that is phosphorylated to difluorodeoxycitidine triphosphate upon cellular uptake [171]. This triphosphate gemcitabine metabolite then competes with the nucleoside deoxycitidine triphosphate for incorporation into DNA, causing termination of DNA elongation and apoptosis [172]. Gemcitabine also reduces the available stores of deoxynucleoside triphosphates, likely by inhibiting ribonucleotide reductase [173]. In 2011, a study evaluating the efficacy of FOLFIRINOX (oxaliplatin, irinotecan, fluorouracil and leucovorin) for use in pancreatic cancer treatment demonstrated an even further increase in median survival (11.1 months vs. 6.8 months with gemcitabine alone). However, FOLFIRINOX treatment was more toxic to patients, and more adverse effects were noted in patients in this treatment group [174]. The combination of gemcitabine with a number of other chemotherapeutic drugs has been investigated, with very little success. No significant increase in survival was seen when gemcitabine was used in combination with other standard chemotherapeutics such as the platinum DNA cross-linkers cisplatin and oxaliplatin; the topoisomerase inhibitor irinotecan; or the folate antimetabolite pemetrexed (reviewed in [175]). The combination of gemcitabine with several targeted cancer therapies such as the EGF inhibitor cetuximab; the farnesyltransferase inhibitor tapifarnib; the leukotriene B4 receptor agonist Lys93111; the matrix metalloprotease inhibitor marimastat; the VEGF inhibitor

bevacizumab; or the antiangiogenic agent cliengitide has also been met with no success (reviewed in [175]). To date, two drug combinations with gemcitabine have demonstrated a statistically significant increase in survival compared to gemcitabine alone, however the increases in survival were very modest. The combination of gemcitabine with the EGF inhibitor erlotinib versus gemcitabine alone increased survival from 5.9 months to 6.2 months [176]. Another study demonstrated that the combination of gemcitabine with the 5-FU prodrug capecitabine could increase survival from 6.2 to 7.1 months compared to gemcitabine alone [177]. Despite ongoing research, very few advances have been made with currently available therapy options. Therefore, the discovery of new therapies to prevent the development of this cancer, or to prolong the life of these patients following diagnosis, is critically needed.

Indeed, as with many other types of cancer, FASN expression has been implicated in pancreatic cancer. In one study, FASN was over-expressed in over 85 % of primary pancreatic adenocarcinoma samples and over 90 % of pre-cancerous IPMN lesions resected from patients, yet FASN expression was not detected in the normal ductal epithelium of these patients. Serum FASN expression levels were also found to be significantly higher in patients with pancreatic ductal adenocarcinoma, IPMN lesions and chronic pancreatitis than in healthy controls, indicating that FASN serum levels in patients may also be a useful marker for the early detection of pancreatic cancer or other neoplasms. The results of this study demonstrated that not only is FASN over-expression likely an early event in pancreatic tumorigenesis, as indicated by the high percentage of pre-cancerous lesions that over-express FASN, but also that targeting FASN may be a highly specific way to treat pancreatic cancers, as FASN is not expressed in normal

pancreatic tissue but is nearly ubiquitously over-expressed in tumor tissue. [122]. Over-expression of FASN in the tumors of patients with pancreatic cancer has also been correlated with higher tumor stage, recurrence and lower overall survival, which was determined by monitoring the expression of FASN in the tumors of 30 patients with pancreatic adenocarcinoma over a 5-year period [178]. One way in which FASN over-expression may result in a poorer outcome by conferring resistance to chemotherapeutic treatment. Inhibiting FASN decreased the resistance of pancreatic cancer cells to both gemcitabine and radiation treatment, whereas ectopically over-expressing FASN increased the resistance of pancreatic cancer cells to both gemcitabine and radiation treatment, indicating that FASN activity and over-expression may be one of the reasons for the poor performance of gemcitabine as a single agent chemotherapeutic [149]. Although further investigation is needed to elucidate the mechanism by which FASN expression causes treatment resistance, it is clear that targeting FASN may be a useful treatment strategy when used in conjunction with chemotherapeutic or radiation treatment, for an improvement in clinical outcome that remains to be seen in pancreatic cancer treatment.

F. Effects of FASN Inhibition on Cancer Cell Survival

FASN expression and activity are critical for tumor progression and survival, thus the fatty acid synthesis pathway appears to be an attractive target for cancer therapy. Although the inhibition of pathways such as the PI3K/Akt and MAPK/ERK1/2 pathways that lie upstream of FASN have been shown to reduce expression of SREBP-1 and FASN, and thus reduce fatty acid synthesis, this strategy for inhibiting the fatty acid

synthesis pathway is less than ideal, due to the presence of active acetyl-CoA carboxylase. Instead, blocking FASN directly with pharmacological inhibitors would likely lead to an enhanced effect in tumor cells. The effect of FASN inhibition in tumor cells has been demonstrated using RNAi knockdown in prostate cancer cells, which caused attenuation of tumor cell proliferation and induction of apoptosis, with no noticeable effect on non-malignant cells [179]. Microarray analysis following FASN knockdown with siRNA revealed that FASN inhibition is accompanied by an increase in the pro-apoptotic factors BNIP3, TRAIL, DAPK2 and ceramide [180]. Genome-wide analysis with gene expression profiling demonstrated that FASN knockdown with siRNA down-regulated pathways regulating lipid metabolism, glycolysis, the TCA cycle and oxidative phosphorylation while up-regulating genes implicated in cell cycle arrest and apoptosis [181]. Another study demonstrated that FASN knockdown in colorectal cancer cells reduced metastasis by attenuating the expression of CD44, a protein associated with increased metastasis, and other proteins known to affect adhesion, migration and invasion [182]. Additionally, it was demonstrated that treatment with first generation FASN inhibitors does not result in any hepatocellular injury or fat necrosis in test animals [183], indicating that targeting FASN with small molecule inhibitors may be a highly specific way to selectively affect malignant cells without harming normal tissues. As such, the quest to find pharmacological inhibitors of the various domains of FASN has been underway, and the inhibitors described below have proven to be very useful tools for elucidating the mechanisms by which FASN inhibition is cytotoxic to malignant cells.

One of the first small-molecule inhibitors of FASN described was cerulenin, a compound isolated from *Cephalosporium caerulens*, which contains an epoxide moiety

that can react covalently with the active cysteine of the β -ketoacyl synthase (KS) domain of FASN, thereby preventing the transfer of a molecule of acetyl-CoA from the ACP, which is necessary to begin the fatty acid synthesis cycle [184]. Cerulenin decreases the proliferation of malignant cells, the effect of which was abrogated by supplementing treated cells with supraphysiologic levels of palmitate [48,185], indicating not only that FASN inhibition is a valid strategy for targeting cancer cells, but also that end product starvation and subsequent disturbance of membrane function, may have deleterious effects in tumor cells. Cerulenin induced programmed cell death in breast cancer cells [186] and prostate cancer cells [187]; slowed tumor progression of ovarian xenografts *in vivo* [188]; and suppressed metastasis to the liver in a colon cancer mouse model [189]. Cerulenin was also shown to induce apoptosis through the inhibition of DNA replication and S-phase progression [190]. C75, a synthetic analog that is more chemically stable than cerulenin, inhibits FASN in cancer cells without adverse effects on bone marrow, the gastrointestinal tract, skin, or lymphoid tissues [191]. C75 treatment led to the ubiquitination and degradation of various proteins in the oncogenic PI3K pathway, including Akt and mTOR in ovarian cancer cells [192]. Cerulenin and C75 were used to demonstrate that fatty acid inhibition may be more effective in cells with mutant p53, inducing a cytotoxic effect in these cells, while inducing a cytostatic growth arrest in cells with wild-type p53 [193,194]. These compounds were also used to demonstrate the utility of blocking FASN activity as a method of chemoprevention in mammary cancers by suppressing the HER2/neu pathway and blocking malignant transformation [56,195]. Interestingly, blocking the fatty acid synthesis pathway by inhibiting the conversion of acetyl-CoA to malonyl-CoA did not have an adverse effect on cancer cells, and even

rescued the effects of treatment with cerulenin or C75, indicating that the buildup of malonyl-CoA, not end product starvation, was the cause of cellular distress in tumor cells [196]. These results demonstrate that blockade of FASN may exert its effects through multiple pathways. However, despite successful use as a tool for elucidating the mechanisms by which FASN inhibition is selectively harmful to cancerous cells, cerulenin and C75 are unlikely to be used clinically as they cause severe side-effects in test animals. This included weight loss induced by stimulating fatty acid oxidation, and anorexia due to inhibition of neuropeptide Y production in the hypothalamus [183,197]. To overcome the potency and side effect limitations of cerulenin and C75, a synthetic cerulenin analog, C93, was developed [198], and was shown to successfully inhibit the growth of lung cancer xenografts, without stimulating fatty acid oxidation and subsequent weight loss and anorexia in test animals [199]. This study indicated that the FASN pathway can be blocked without necessarily inducing fatty acid oxidation. C93 treatment was associated with reduced Akt activity in lung tumor tissues [200], and activated AMPK in ovarian cancer cells [201].

Epigallocatechin-3-gallate (EGCG), an extract from green tea, was found to inhibit the ketoacyl reductase (KR) domain of FASN, possibly by blocking the NADPH binding site on the domain, thus preventing the reduction of the keto group to an alcohol on the growing fatty acid chain, thus halting the FASN cycle [202]. EGCG has selectively induced apoptosis in prostate cancer cells [203], however, EGCG is not a specific inhibitor of FASN, as it is known to inhibit other pathways that offer a chemotherapeutic effect [204]. FASN is also inhibited by a variety of other polyphenolic compounds including amentoflavone [205] and flavonoid compounds including luteolin,

quercetin, kaempferol, apigenin and taxifolin [206-208]. EGCG inhibits FASN without stimulating fatty acid oxidation or weight loss in test animals [209,210]. A class of novel synthesized polyphenols that inhibited the growth of breast cancer xenografts, without concurrent induction of fatty acid oxidation or weight loss as a side effect, has also been described [211].

In 2004, orlistat, an FDA approved drug for weight loss that works by inhibiting pancreatic lipases and thereby prevents the uptake of dietary fats in the gastrointestinal tract, was discovered to also act as an inhibitor of the TE domain of FASN during an activity-based screen that had intended to identify serine hydrolases in prostate cancer and search for inhibitors to those serine hydrolases simultaneously. As expected, orlistat inhibited the proliferation and induced apoptosis in prostate cancer cells both *in vitro* and *in vivo* [212]. Crystal structure analysis of orlistat within the active site of FASN TE revealed that Orlistat, a β -lactone compound, covalently modifies the active site serine of TE, and halts the fatty acid synthesis cycle by prohibiting the release of fatty acid from the ACP. However, crystal structure analysis also showed a hydrolyzed form of orlistat in the TE active site, indicating that FASN can easily catalyze and inactivate orlistat [213]. Orlistat has been found to induce apoptosis via caspase-9 and -3 induction and reduce cell proliferation and metastasis in a mouse melanoma model [214,215]; and increase tumor cell death and survival rates in mice with gastric tumors [216]. Fatty acid synthesis blockade by orlistat inhibits angiogenesis and proliferation of endothelial cells [217]; affects the cell cycle by down-regulating Skp2, arresting cells in G1/S phase [218]; induces ER stress and apoptosis in cancer cells [219]; and promotes caspase-8 mediated apoptosis and down-regulation of the mTOR pathway via the stress response gene DDIT4

[220]. Orlistat is unlikely to find use as a systemic cancer treatment due to the side-effect of weight loss, as well as low solubility, poor oral bioavailability, systemic availability and stability [221,222]. A number of orlistat analogs have been synthesized [223-226], but none have proven to be a successful alternative thus far.

A number of other FASN inhibitors have been reported. Triclosan, a common antibiotic that works by inhibiting the enoyl reductase enzymes of type II fatty acid synthases in bacteria, also inhibits the enoyl reductase (ER) domain of human FASN and is cytotoxic to human breast cancer cells. It has been suggested that triclosan increases the affinity of the ER domain for NADP⁺, forming a stable complex, thus preventing the interaction of NADPH with the domain, which is necessary for final reduction step of fatty acid synthesis [227]. Natural products have also been shown to effectively inhibit FASN activity including conjugated linoleic acid [228] and various plant extracts [229-235]. Other novel classes of FASN inhibitors have also been described [236-239], but thus far, no further research involving these novel inhibitors has been reported.

In addition to being a useful target for the treatment of cancer in its own right, FASN inhibition has also shown to be useful in combination therapy. FASN inhibition sensitized resistant breast cancer cells to trastuzumab, an antibody that targets Her-2/neu, possibly by affecting the composition of lipid rafts produced by FASN activity, perhaps affecting crosstalk between EGRF and HER2/neu, which has been implicated in trastuzumab resistance [240]. A synergistic chemosensitization of HER2/neu over-expressing breast cancer cells to docetaxel [241], vinorelbine [242], paclitaxel [243], 5-fluorouracil [244] was demonstrated upon FASN inhibition, possibly by suppressing the HER2/neu oncogene [57]. FASN blockade has also been shown to sensitize resistant

breast cancer cells to treatment with DNA-damaging agents mitoxantrone and doxorubicin [148] and resistant pancreatic cancer cells to gemcitabine and irradiation [149]. Clearly, an abundance of research has demonstrated that FASN is a potential target for cancer therapy, and inhibitors of FASN could be very useful when added to a combination chemotherapeutic regimen.

G. Proton Pump Inhibitors and Use in Cancer Treatment

Recently, there has been great interest in investigating the potential utility of an FDA approved class of drugs known as proton pump inhibitors (PPIs) for use in combination chemotherapy, which began in 2004 when a study demonstrated that PPIs could reduce the resistance of cancer cells to cytotoxic drugs [245]. PPIs are the standard treatment for a variety of acid-related diseases that plague the digestive system, including peptic ulcer, gastro-esophageal reflux, Barrett's esophagus and Zollinger-Ellison syndrome, as well as the treatment of upper gastrointestinal bleeding and *Helicobacter pylori* infection [246-248]. PPIs are substituted benzimidazole compounds [249] that exert their effects by accumulating in the gastric parietal cells. PPIs are weakly basic prodrugs that are membrane permeable, and upon entering the acidic environment of the parietal cells, they become protonated and then undergo a series of acid-base reactions, ultimately revealing a cationic sulfur ion that irreversibly binds with cysteine residues of gastric hydrogen-potassium ATPase proton pumps. By inhibiting proton pumps, PPIs directly inhibit the exchange of a proton for a potassium ion, thus inhibiting the secretion of acid into the gastric lumen [250-252]. Current FDA approved proton pump inhibitors include omeprazole [253], pantoprazole [254], lansoprazole [255], rabeprazole [256] and

esomeprazole, the (S)-enantiomer of omeprazole [257]. As a class, PPIs are extremely safe and well tolerated drugs, and adverse side effects with long term PPI treatment are rare [258].

The first study that examined the use of PPIs in combination chemotherapy demonstrated that upon pretreatment with omeprazole, esomeprazole or pantoprazole, various solid tumor types including melanoma cells, colon adenocarcinomas, breast cancer cells and ovarian carcinomas were sensitized to treatment with the chemotherapeutic agents cisplatin, 5-FU and vinblastine *in vitro* with up to a 2 log reduction in IC₅₀. Tumor cells pretreated with PPIs were found to have an increased extracellular and lysosomal pH, indicating PPIs may prevent the acidification of the tumor microenvironment by inhibiting the function of vacuolar vATPase [245]. Tumor cells have been found to exhibit increased vATPase activity, which help to generate the pH gradient in tumor microenvironments and maintain pH homeostasis within tumor cells, which is often altered due to increased cellular metabolism (reviewed in [259,260]). As a result, chemotherapeutics that are weakly basic may have a reduced effect caused by decreased uptake, as the extracellular pH of solid tumors is more acidic than in normal tissues [261,262]. It has been noted that with concurrent PPI treatment, cytotoxic drugs are more greatly retained in the cellular cytoplasm, possibly explaining their observed increased effect. Oral pretreatment with omeprazole also slowed tumor growth in test animals treated with cisplatin, when compared to cisplatin treatment alone [245].

PPIs alone can also effectively induce apoptosis. Omeprazole treatment induced caspase-dependent cell death in Jurkat immortalized T lymphocyte cells [263]. Treatment of B-cell tumors with omeprazole or esomeprazole induced apoptosis through a caspase-

independent mechanism. Each PPI caused an increase in the production of reactive oxygen species, leading to alteration of lysosomal pH and lysosomal membrane permeabilization, followed by membrane depolarization, cytochrome c release and subsequent induction of apoptosis upon activation of caspases [264]. Pantoprazole treatment selectively induced apoptosis in gastric cancer cells both *in vitro* and *in vivo*, without affecting normal gastric mucosal cells [265], and caused tumor growth retardation in murine T cell lymphoma [266]. Treatment of melanoma cells with esomeprazole caused accumulation of reactive oxygen species and induced apoptosis via a caspase-dependent pathway [267].

PPIs have also been proposed to decrease the resistance of certain cancers in ways other than affecting the pH of the tumor microenvironment. For example, omeprazole, lansoprazole and pantoprazole are substrates of the ATP-dependent efflux transporter P-glycoprotein, and directly inhibit its activity [268]. As P-glycoprotein can expel chemotherapeutic agents from cells, and has thus been implicated in the development of the multi-drug resistance phenotype in tumor tissue [269], inhibition of P-glycoprotein by PPI treatment may lead to the observed increase in efficacy of chemotherapeutic agents [259]. In one study, omeprazole was found to inhibit proliferation and modulate autophagy in pancreatic cancer cells through affecting the regulatory function of vATPase, without inhibiting the function of the pump itself, causing modulation of lysosomal transport and autophagy, leading to cell death [270]. Several studies have examined the effect of pantoprazole treatment on gastric cancer cell growth. Pantoprazole treatment was shown to decrease the expression of HIF-1- α , a protein implicated in tumor progression and aggressiveness, in human gastric carcinoma cells [271]. A decrease in

vATPase expression and components of the wnt/ β -catenin signaling pathway, leading to a disruption in gastric cancer cell growth and increase in apoptosis, has also been demonstrated upon pantoprazole treatment [272]. Pretreatment with pantoprazole also enhanced the effect of Adriamycin treatment on gastric cancer cells both *in vitro* and *in vivo*, and reduced the resistance of an Adriamycin resistant cell line to chemotherapeutic treatment. In addition to the down-regulation of vATPase protein levels, it was noted that upon pantoprazole treatment, the expression levels of several proteins that have been implicated in tumor proliferation, including mTOR, HIF-1- α , p-glycoprotein and multi drug resistant protein 1, were also down-regulated [273]. Pantoprazole pretreatment also selectively suppressed the secretion of IL-6, a pro-inflammatory cytokine, in gastric cancer cells, without affecting epithelial cells. A reduction in IL-6 subsequently decreased the activation of STAT3 and its downstream targets, which have also been implicated in tumor cell proliferation and survival [274].

As such, several clinical trials have been performed to evaluate the use of PPIs in combination with chemotherapeutic drugs for cancer treatment. A phase I/II clinical trial demonstrated that treatment with high dose lansoprazole concurrently with traditional chemotherapy reversed chemoresistance of tumors in dogs and cats with cancer. The high dose PPI treatment was well tolerated, and improved the quality of life in the animals [275]. Additionally, an ongoing phase II clinical trial is investigating the use of pantoprazole in combination with doxorubicin in advanced cancer patients with solid tumors [276]. All of these results demonstrate the ability of PPIs to inhibit tumor cell growth in many types of cancer, and clearly more studies are needed to determine the utility of PPIs as potential agents for use in chemotherapeutic regimens, as well as the

mechanism by which PPIs might be inhibiting cancer cell growth. In the study that examined the effect of omeprazole treatment on pancreatic cancer cells, it was noted that PPI treatment altered the composition of cellular lipid metabolites, indicating that the fatty acid synthesis pathway may be an important mechanism by which PPIs are acting in cancer cells, but the possibility of fatty acid synthesis disruption was not discussed [270].

F. Hypothesis and Specific Aims

As discussed in detail above, orlistat, an FDA approved drug for weight loss that works by inhibiting the esterase activity of pancreatic lipases in the gut, also acts as a reversible inhibitor of the thioesterase activity of FASN. In 2007, the crystal structure of the human FASN thioesterase domain with orlistat in the active site was elucidated by Pemble *et al* [213]. The catalytic triad of FASN thioesterase, Ser²³⁰⁸-His²⁴⁸¹-Asp²³³⁸, with Ser²³⁰⁸ forming a covalent bond with the C1 carbon of the β -lactone cyclic ester moiety of orlistat, was identified. Pemble *et al.* observed that orlistat was present within the active site of thioesterase in two forms: the covalently bound intermediate, and a hydrolyzed, inactivated form in which the bond between Ser²³⁰⁸ and orlistat had been cleaved, thus freeing orlistat and demonstrating that orlistat is not a stable inhibitor of the thioesterase domain. It was also noted that a hexyl tail moiety of orlistat had shifted position when comparing the position of covalent-orlistat to hydrolyzed orlistat within the crystal structure, indicating that this hexyl tail may be involved in orlistat hydrolysis. The goal of the thesis work described herein was to examine the mechanism of hydrolysis of orlistat by the thioesterase domain of FASN, and then use the findings to aid in the discovery of FASN inhibitors that can target thioesterase activity with greater stability.

The *central hypothesis* is that *the flexibility of the hexyl moiety of orlistat promotes its hydrolysis and limits its ability to target the thioesterase domain of FASN. Novel inhibitors of FASN TE, perhaps proton pump inhibitors, will have greater endurance in blocking the fatty acid synthesis pathway for therapeutic treatment.* To this end, the following specific aims were accomplished:

Specific Aim I: To determine the molecular process that occurs after orlistat has formed a covalent bond to the FASN TE domain using molecular dynamics simulations

Using the co-crystal structure of orlistat with the thioesterase domain of FASN, the orlistat residue bound to the Ser²³⁰⁸ residue in the thioesterase domain of FASN, an irregular residue, was manually parameterized for simulation. The AMBER9 suite of programs was used to examine this covalent-orlistat within the thioesterase domain in a solvated environment via molecular dynamics simulations, allowing for the examination of how the hexyl tail of orlistat may play a role in its hydrolysis.

Specific Aim II: To identify potential inhibitors of FASN thioesterase

Several libraries of compounds were virtually screened specifically for shape and chemical complementarity to the active site of the TE domain of FASN using the DOCK6.0 suite of programs. The inhibition potential of top-scoring compounds was examined using a fluorogenic activity assay with a recombinant thioesterase domain of FASN.

Specific Aim III: To evaluate the therapeutic potential of selected compounds

The therapeutic potential of compounds that inhibited FASN thioesterase activity in a dose-dependent manner was evaluated using several pancreatic cancer cell lines by

examining the ability of compound candidates to inhibit cellular proliferation, colony formation, and lipid synthesis. Apoptosis induction with the lead compound candidate and rescue with palmitate supplementation was also evaluated.

Chapter 2: Materials and Methods

Specific Aim I: Orlistat Parameterization and Molecular Dynamics

A. Orlistat Parameterization

The crystal structure of covalent-orlistat within FASN TE, elucidated by Pemble *et al.* [213], was downloaded from the RCSB Protein Data Bank (www.rcsb.org). The crystal structure (PDB ID: 2PX6) contained the initial coordinates of covalent-orlistat within TE in PDB file format, which contains structural information derived from x-ray diffraction studies. Covalent-orlistat was then manually parameterized following the procedure for determining the atomic charges for the AMBER parm94/parm99 parameter sets described by Cornell *et al.* [277], with guidance from the AMBER online tutorial (<http://ambermd.org/tutorials/advanced/tutorial1/>) for preparing irregular residues. Using the Chimera visualization and structure building program (University of California, San Francisco) [278], the irregular covalent-orlistat Ser²³⁰⁸ residue and the two adjacent tyrosine residues flanking covalent-orlistat (Tyr²³⁰⁷ and Tyr²³⁰⁹) were removed from the rest of the enzyme by virtually deleting the remainder of the protein. The remaining small peptide was capped by removing the side chains from the tyrosine residues and retaining only the protein backbone, and then virtually adding hydrogen atoms to create an N-terminal blocking cap that consists of a $-(CO-CH_3)$ group and a C-terminal blocking cap that consists of a $-(NH-CH_3)$ group (Fig. 1). The newly capped residue was saved as a PDB file using UCSF Chimera.

FIGURE 1:

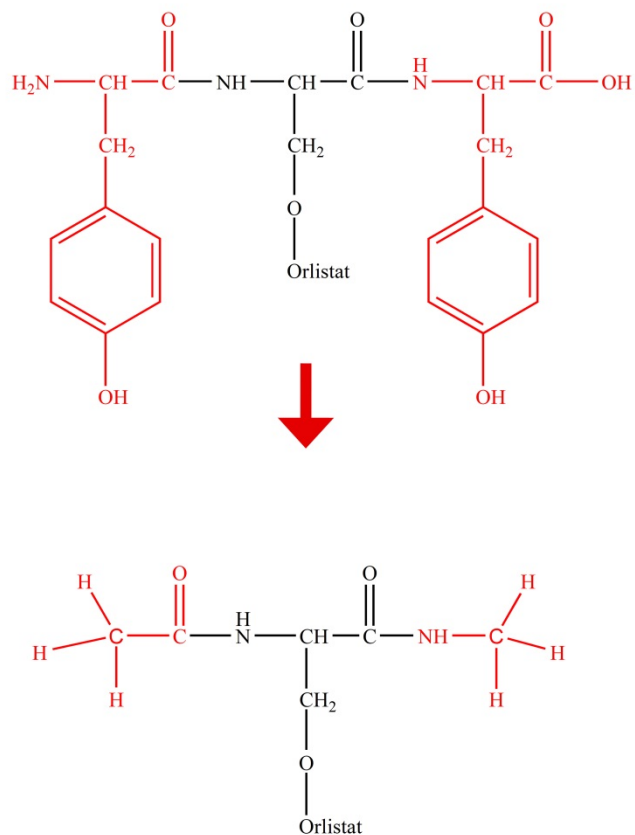


Figure 1: Schematic illustration of the covalent-orlistat parameterization. The side chains of the tyrosine residues (red, top) flanking the covalent orlistat-Ser²³⁰⁸ residues are removed. The tyrosine residues are then replaced by an N-terminal cap $-(\text{CO}-\text{CH}_3)$ and a C-terminal cap $-(\text{NH}-\text{CH}_3)$, leaving only the peptide backbone atoms (red, bottom).

The quantum mechanics (QM) package Gaussian03 (Gaussian Inc.) was used to optimize the geometry of the capped covalent-orlistat complex using the B3LYP/6-31G* level of quantum mechanical theory. All calculations were performed using the Big Red supercomputer (Indiana University). The Gaussian input file (.gau) was generated directly from the PDB file prepared in the previous step using the WebQC molecular formats converter (<http://www.webqc.org/molecularformatsconverter.php>). The optimization was performed in Cartesian coordinates and the opt=modredundant keyword was specified in the input file in order to freeze dihedral angles between all heavy atoms. Dihedral angles were frozen by indicating the number of each heavy atom in the dihedral, in accordance with the atom number assigned to each atom of covalent-orlistat in the PDB file. Dihedral angles were frozen to ensure that the geometry of the ligand, and thus the charge development, of orlistat reflects the charge distribution of the conformation seen in the crystal structure. An example of a Gaussian optimization input file (.gau) can be found in Appendix A. In order for a structure to be properly optimized, it must achieve convergence, in which the threshold value of four criteria must fall below a certain value. These criteria are: maximum force on atoms in the system; root mean square (RMS) force on atoms in the system; maximum displacement and RMS displacement. Maximum displacement describes the maximum structural change of one atom coordinate and RMS displacement describes the average coordinate change of all atoms in the system in the previous two optimization cycles. Default convergence values were chosen for the optimization, which are 0.000450 atomic units (AU) for maximum force; 0.000300 AU for RMS force; 0.001800 AU for maximum displacement and 0.001200 AU for RMS displacement. The generated checkpoint file (.chk) from the completed optimization was

converted to a formcheck file (.fchk) using the formchk utility of Gaussian, which can be recognized and visualized by Chimera. The optimized capped covalent-orlistat was then re-saved in PDB format.

The electrostatic potential (ESP) of the optimized ligand was calculated with Gaussian03 using the HF/6-31G* level of quantum mechanical theory. The input file used for the ESP calculation can be found in Appendix A. The .chk file from the optimization was copied and then used in the input file for the ESP calculation. The ESP data generated by Gaussian was then converted into restrained electrostatic potential (RESP) input format with the resp functionality within AMBER, using the script esp.sh, which can be found in Appendix A. The number of ESP Fit Centers needed to run the esp.sh script was gathered from the Gaussian output file from the ESP calculation. As Gaussian does not print any ESP Fit Center numbers past 9,999, the number of ESP Fit Centers was calculated by taking the difference in the line numbers in the output file.

Next, the atomic charges of the ligand were calculated in two steps. First, the charges of the caps, which sum to zero, were defined as by Cornell *et al.* [277] and the charges for the remainder of the atoms were calculated by RESP. In the second step, to ensure that rotationally-degenerate atoms had equivalent charges, the charges for all atoms were fixed except for hydrogen atoms in methyl (-CH₃) and methylene (-CH₂) groups and the charges were recalculated. Further explanation of RESP charge fitting, along with input files used, can be found in Appendix A.

The caps flanking the irregular covalent-orlistat residue were then virtually removed using UCSF Chimera and a library file for the residue containing topology, charge and atom type information for each atom in the residue was created using the

xleap program within AMBER. Xleap also recognized any missing information for the residue, and analogy to parm99 parameters was used to define all missing values for covalent-orlistat, which were placed in a .frcmod file. Using UCSF Chimera, the orlistat-Ser²³⁰⁸ residue was reattached to the enzyme by aligning the newly optimized molecule with the original orlistat molecule in the FASN TE crystal structure [213].

B. MM and QM Dihedral Angle Scans

A 3-mer peptide was created using Chimera as follows: First, optimized covalent-orlistat and the two adjacent tyrosine residues flanking covalent-orlistat were separated from the rest of the TE protein and the tyrosine residues were converted to N- and C-terminal glycine residues (Fig. 2). Next, the torsion angles of the 3-mer peptide backbone were adjusted into an extended conformation to avoid electrostatic interaction between the amino group of the N-terminal glycine residue and the carboxyl group of the C-terminal glycine residue. Finally, thirty-six rotamers of the ω dihedral angle, each differing by 10 degrees, were created and saved as individual files.

FIGURE 2:

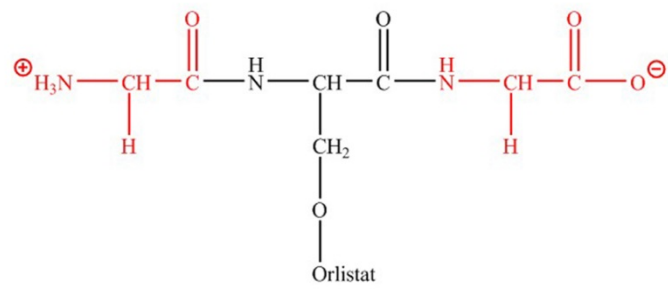


Figure 2: Schematic illustration the 3-mer peptide containing covalent-orlistat. Orlistat is flanked by N-terminal and C-terminal glycine residues (red).

To perform the dihedral angle energy scan using QM methods, the PDB file of the 3-mer peptide was converted to Gaussian Z-matrix input format using the Babel file converter on the Quarry supercomputer (Indiana University). An example input file can be found in Appendix A. The single point ab initio energy of each rotamer was calculated using Gaussian03 with the HF/6-31G* level of quantum mechanical theory and full convergence was requested using the scf=tight keyword. The single-point energy calculated for each rotamer was then compiled into a single file and visualized using the xmgrace plotting tool. To perform the dihedral energy scan using MM methods, the potential energy surface of the 3-mer peptide was calculated using the sander module of AMBER9. Using a non-periodic vacuum model, each rotamer was individually minimized using 500 steps of steepest descent minimization. During the minimization, all atoms were weakly restrained by $25 \text{ kcal/mol/\text{Å}^2}$ in Cartesian space using harmonic potential to ensure that the conformation of each rotamer was not dramatically changed during the minimization. An example input file can be found in Appendix A. Following the minimization, the exact ω dihedral angle for each minimized rotamer was determined using Chimera, and the angles and energies for each rotamer calculated during the minimization was compiled into a single file and visualized using the xmgrace plotting tool. As the energy units from the QM and MM scans do not match, each curve was scaled and then overlaid to compare the results from the two energy scans.

C. Molecular Modeling and MD Simulations

Unresolved residues from the crystal structure (loop I residues 2326-2328, loop II residues 2344-2360 and loop III residues 2450-2460) were built using the online software

ModLoop (<http://modbase.compbio.ucsf.edu/modloop/>) (UCSF) [279]. The LeAP module of AMBER9 created the necessary topology and coordinate files for the MD simulation by assigning FF03 parameters and hydrogen atoms to the protein and adding TIP3 water molecules to solvate the structure in a box with a distance of 8 Å between the wall and the closest atom in the system. Appropriate sodium counter ions to neutralize the system were also added by LeAP. The tleap script used to prepare the system can be found in Appendix A. Particle Mesh Ewald was used to calculate the long-range electrostatic interactions and the non-bonded cutoff was set to 8.0 Å.

Using the Big Red supercomputer, the solvated FASN TE covalent-olistat system was then equilibrated by a five-step protocol prior to beginning the MD simulation. First, with all protein and ligand atoms in the system being restrained by 500 kcal/mol/Å² in Cartesian space using harmonic potential, the solvated system was minimized by 500 steps of steepest descent minimization followed by 500 steps of conjugate gradient minimization to minimize the energy of the water molecules and counter ions. Next, the atomic restraints were removed and the energy of the whole system was minimized by 10000 steps of steepest descent minimization followed by 15000 steps of conjugate gradient minimization. Third, over a duration of 50 ps with a restraint of 10 kcal/mol/Å², the system was heated from 0 to 300 K. This gradual heat step was controlled by Langevin dynamics with a collision frequency of 2 ps⁻¹. Then, with a weak restraint of 10 kcal/mol/Å² to the protein, the system was equilibrated by constant pressure dynamics simulation with isotropic position scaling for 0.05 ns at 300 K. The reference pressure was set as 1 bar, with a pressure relaxation time of 1.0 ps. Finally, the system was further equilibrated for 60 ps at 300 K using constant volume periodic boundaries, which was

controlled by Langevin dynamics with a collision frequency of 2 ps^{-1} and a pressure relaxation time of 2 ps. Each step of the simulation applied the SHAKE procedure, which weakly constrained bonds involving hydrogen atoms. To perform the MD simulation, a total of 35 ns (3500 frames) were simulated using the same conditions as the final equilibration step. Input files for all steps of the MD simulation can be found in Appendix A. To ensure that the results and observations obtained were reproducible, two replicate simulations were performed using the same initial structure and the same conditions as outlined above.

Several additional MD simulations were also performed using the same procedure as described above. A truncated version of covalent-orlistat, in which the hexyl tail was virtually truncated to a methyl group using Chimera, was optimized, parameterized and simulated. Additionally, the 3-mer peptide containing orlistat was solvated and a total of 100 ns of production MD were simulated. Additionally, a crystal lattice containing two chains of FASN TE, chain A and chain B, was simulated for 35 ns using the same procedure described above, but this time with a 5 ns equilibration period.

D. MD Simulation Trajectory Analysis

The resulting trajectories from the MD simulations were processed using the ptraj module of AMBER9. A .mdcrd file describing the entire simulation trajectory was created by ptraj by uploading the .mdcrd files created in each production step and centering the trajectory in the box of water molecules using the center and image familiar commands. To ensure that the resulting trajectories were properly equilibrated, the temperature and total energy, along with potential and kinetic energy, were monitored

throughout the simulation by extracting these values from the MD simulation output files. Structural stability was examined using ptraj to calculate the root mean square deviation (RMSD) of the protein and root mean square fluctuation (RMSF) of the protein and covalent-orlistat ligand. All ptraj input files can be found in Appendix A.

A potential conformational transition was studied by analyzing several pieces of information. The RMSD of covalent-orlistat, the ω dihedral angle of the hexyl tail, and the distance of the center of mass between the hexyl tail and its two binding pockets were calculated by ptraj. The time in which the conformational transition in each simulation took place was determined by examining the RMSD of covalent-orlistat. The conformational transition was determined to begin when the RMSD of covalent-orlistat began to change dramatically, indicating that a deviation from the initial starting structure was taking place. The conformational transition was determined to end when the RMSD stabilized. The time of the simulation during which the conformational transition was taking place was not included in calculations. Using ptraj, the distance of the hexyl tail was monitored, to ensure that a transition between the two binding pockets took place, as well as the ω dihedral angle, to ensure that a change in angle took place.

To calculate the number of water molecules entering the active site of FASN TE during the simulations, the MD visualization program VMD (University of Illinois at Urbana-Champaign) was used to search for the oxygen atoms of water molecules in each frame of the trajectory that met specific criteria. In order for a water molecule to be considered to be within the TE active site, its oxygen atom must be found within 3.5 Å of the catalytic nitrogen of His²⁴⁸¹ and within 4.0 Å of the carbonyl carbon of covalent-orlistat that would be nucleophilically attacked by a catalytic water molecule. To

determine the percentage of time in which a water molecule occupied the active site during each part of the conformational transition, the number of frames in which a water molecule met the criteria was divided by the total number of frames in which the hexyl tail adopted each respective conformation.

Hydrogen bonds between polar atoms (N, O, S, F) in the system were examined using VMD with the criteria of a donor-acceptor distance of 3.5 Å and an angle cutoff of 20 degrees. The donor-acceptor distance for strong hydrogen bonding required for catalysis between water molecules and His²⁴⁸¹ was set to 3.0 Å.

To determine the percentage of time in which activated water molecules, which could potentially catalyze the bond between Ser²³⁰⁸ and orlistat, were found in the active site in each conformation, the number of frames were determined in which water molecules were found to strongly hydrogen bond (< 3.0 Å) of the catalytic nitrogen of His²⁴⁸¹, appeared within 4.0 Å of the carbonyl carbon of covalent-orlistat, and had an optimal orientation angle of $105^\circ \pm 5^\circ$ with the carbonyl carbon and carbonyl oxygen of orlistat. This number of frames was divided by the total number of frames in which the hexyl tail adopted each respective conformation.

E. Free Energy Calculations

To examine the free energy of the covalent-orlistat ligand in each hexyl tail conformation, the MM_PBSA module of AMBER was used to extract a total of 50 snapshots over the course of each conformation in each simulation, and then the total free energy was calculated. See Appendix A for input files used for the free energy calculations. The following equation describes how the MM_PBSA module calculates

the total free energy: $PB^{tot} = PB^{sol} + gas$, where $PB^{sol} = PB^{sur} + PB^{cal}$ and $gas = ELE + VDW + INT$. PB^{sur} is described as the hydrophobic contributions to solvation free energy for PB calculations, and PB^{cal} is described as the reaction field energy calculated by PB. ELE is the non-bonded electrostatic energy + 1,4-electrostatic energy, VDW is the non-bonded van der Waals energy + 1,4-van der Waals energy, and INT is the bond, angle and dihedral energies. Additionally, a total of 50 snapshots were extracted over the course of each conformation from each 100-ns trajectory with the 3-mer peptide containing orlistat. The free energy of the 3-mer peptide in each hexyl tail conformation was then calculated again with MM_PBSA to examine the free energy in each conformation without influence from the protein.

Specific Aim II: In-Silico and High-Throughput Ligand Screening

A. In Situ Receptor Model Preparation

To virtually screen the TE domain of FASN for potential ligand inhibitors, the crystal structure of FASN TE containing a polyunsaturated fatty acyl adduct, which has a higher resolution than the crystal structure of FASN TE with orlistat, was retrieved from the RCSB Protein Data Bank (ID: 3TJM) [280]. This crystal structure lacks residues 2342-2355 due to poor electron density, which was modeled using ModLoop [279]. The UCSF DOCK6.0 suite of programs, including sphere and grid generation, was used to complete the *in-silico* ligand screening with rigid ligand docking [281,282]. To prepare TE receptor for *in-silico* screening, the DOCK6.0 tutorial (http://dock.compbio.ucsf.edu/DOCK_6/tutorials/index.htm) was used in conjunction with the UCSF Chimera visualization program. First, the PDB file of FASN TE with the fatty acyl adduct was loaded into Chimera, and the fatty acyl ligand was deleted from the protein. Next, the Dock Prep tool within Chimera completed the receptor preparation by deleting solvent, adding hydrogen atoms and charges to the protein, and saving the receptor as a .mol2 file. All hydrogen atoms were stripped from the protein and saved as a PDB file for molecular surface generation. The molecular surface of the receptor was created by opening the receptor PDB containing no hydrogen atoms prepared as described above. Then the Chimera tool Surface was used to create the molecular surface for the FASN TE receptor, and Write DMS was used to create and save this newly created molecular surface.

Spheres to describe the shape of each potential binding pocket of the enzyme were created using the sphgen_cpp program available from the DOCK website

(http://dock.compbio.ucsf.edu/Contributed_Code/sphgen_cpp.htm). Spheres were created using the values as described in the DOCK tutorial, which is shown in Appendix C. The generated sphere clusters were examined in Chimera and all spheres that did not describe the active site of the protein were deleted manually with Chimera.

Next, the scoring grids to evaluate the orientation of each ligand candidate in the active site of FASN TE were created by first generating a box around the active site of the protein using the DOCK command showbox. The grid program within DOCK was used to calculate the scoring grids. Values described in the tutorial were used for box generation and for the grid input file, which are shown in Appendix C.

B. DOCK Ligand Screening

To perform the *in-silico* ligand screening, a library of FDA approved drugs, containing approximately 2,000 unique compounds, was downloaded from the ZINC database [283-285]. The *in-silico* ligand screening was then completed in two steps. In the first step, grid scores were generated for compounds in the library using the DOCK6.0 program with rigid ligand scoring on Big Red Supercomputer. The top 200 scoring compounds were output into a file renamed lig.mol2. Input files for the grid score screening can be found in Appendix C. Next, the second round of DOCK scoring, in which AMBER scores were generated for the top 200 scoring compounds from the grid screen, was completed by first using the prepare_amber.pl program extension available within DOCK6.0. This program prepared the receptor file by adding hydrogen atoms to the system, determining AMBER force field atoms types, calculating atomic charges, and generating the topology and coordinate files necessary for AMBER MD simulations. The

program also determined the charges and generated topology and coordinate files for each ligand. Finally, the second round of DOCK was performed for each ligand at a temperature of 300 K with 100 steps of steepest descent minimization followed by 3000 MD steps (3 ns), allowing each ligand to be flexible, but keeping the receptor stationary. The AMBER score (E_{Binding}) of each ligand was calculated as the $E_{\text{complex}} - (E_{\text{receptor}} + E_{\text{ligand}})$. Input files for AMBER scoring can be found in Appendix C.

Each of the 200 ligands that were subjected to AMBER scoring was clustered into groups based on chemical structure using the Library MCS (Chem Axon). All compounds were examined visually within the active site of FASN TE using the View Dock module of Chimera. Any ligands with a positive AMBER score were discarded, as were any ligands that appeared outside the FASN TE active site. Of the 200 ligands scored, 34 of the top scoring ligands were chosen for further examination, by ensuring that different clusters of compounds were represented and choosing compounds that may interact favorably in the active site of FASN TE.

C. Cloning and Subcloning the FASN TE Plasmid

To test the ability of compound candidates selected from the *in-silico* screen to inhibit FASN TE activity, a recombinant form of TE protein was cloned, expressed and purified as described previously [212,213]. First, new PCR primers were designed in order to amplify the FASN TE portion of the FASN gene and were synthesized by Invitrogen. The forward primer sequence used was (5' to 3'): GGGGATCCACGCCCAA GGAGGATGGTCTGGCCCAGCAG and the reverse primer sequence used was (5' to 3'): GGCTCGAGTTAGCCCTCCCGCACGCTCACGCGTGGCT. The primers were

dissolved in nuclease free H₂O to a concentration of 0.5 µg/µL. A 50 ng/µL primer stock for PCR was created by diluting the primers 10X. A total of 350 µL of PCR reaction mixture (enough for 3 100 µL PCR reactions) was prepared in the following order: 7 µL of template cDNA, 14 µL each of the diluted forward and reverse primer stocks, 35 µL of 10X pfu buffer, 7 µL of 10 mM deoxynucleotide (dNTP) mix, 10.5 µL of DMSO and 262.5 µL of ddH₂O. The samples were boiled for 10 minutes and divided into 3 reactions of 100 µL each. 1 µL of pfu polymerase was added to each reaction tube. The template cDNA, 10X pfu buffer, dNTP mix and pfu polymerase were obtained from Stratagene (Agilent). PCR was performed using a Bio-Rad thermocycler with the following protocol: 72 °C for 2 minutes; 35 cycles of 94 °C for 1 minute, 53 °C for 45 seconds, 72 °C for 1.5 minutes; 72 °C for 7 minutes; hold at 4 °C. To ensure that the desired PCR product (approximately 1 kb) was amplified, 9 µL of the PCR product, along with 1 µL of 10X agarose gel loading buffer, was loaded onto a 1.5 % agarose gel, prepared with TBE buffer (90 mM Tris-Cl, 90 mM boric acid, 2 mM EDTA) and 3 µL ethidium bromide. 4 µL of 1kb plus DNA marker (Invitrogen) was also loaded onto the gel. The gel was run at a constant 100 V and visualized using the FluorChem HD2 imaging system (Protein Simple).

The DNA product was precipitated using an ethanol precipitation. 1/10 the volume of 3M sodium acetate was added to the DNA product, followed by 3 volumes of 100 % ethanol. The mixture was incubated at -70 °C for 1 hour, centrifuged at room temperature at 12,000g for 15 minutes and the supernatant was removed. 200 µL of 70 % ethanol was added to the pellet, which was then centrifuged at 12,000g at room temperature for 5 minutes. The supernatant was removed and the addition of 70 %

ethanol followed by centrifugation and supernatant removal was repeated twice more. The DNA pellet was incubated for 1 hour in the culture hood and then resuspended in 57.2 μL of nuclease free H_2O . As DNA amplification with pfu polymerase creates blunt end PCR products, and ligation into the pGEM-T Easy vector requires “sticky” A-tailed DNA ends, the GoTaq polymerase kit (Promega) was used to add A-tails onto the FASN TE DNA. 16 μL of GoTaq Flexi buffer, 4.8 μL of 25 mM MgCl_2 solution, 1.6 μL of 10 mM PCR nucleotide mix and 0.4 μL of the GoTaq DNA Polymerase were added the 57.2 μL of DNA from PCR to create an 80 μL reaction mixture. The mixture was incubated at 70 $^\circ\text{C}$ for 30 minutes, and then separated on a 1.5 % agarose gel to purify the product. 2 μL of the product mixture was loaded into a separate lane to visualize the product with longwave UV, so as not to expose the majority of the product to UV radiation. After visualizing and determining the location of the product, the product band containing the rest of the DNA was cut away from the agarose gel and purified using the Qiagen Gel Extraction kit according to the instructions provided in the kit. The purified DNA was eluted using nuclease free H_2O and the concentration of DNA was measured using the Bio-Rad SmartSpec 3000 spectrometer by placing 2 μL of the DNA sample and 98 μL of ddH_2O into the black cuvette provided with the instrument.

To ligate the FASN TE PCR product into the pGEM-T Easy vector (Promega), a 10 μL reaction was created according to the kit instructions by mixing 5 μL of 2X Rapid Ligation Buffer with 1 μL of the vector, 0.5 μL of the PCR product (50 ng), 1 μL of T4 DNA ligase and 2.5 μL of nuclease free H_2O . The reaction was mixed by pipetting and incubated overnight at 4 $^\circ\text{C}$. The ligation product was transformed into DH5 α *E. coli* cells by adding all 10 μL of the ligation reaction mixture to a vial of the bacterial cells,

which were previously thawed on ice, and mixing by stirring with a pipet tip. The vial was incubated on ice for 30 seconds, followed by 45 seconds in a 42 °C water bath without any mixing or shaking. After 2 minutes of incubation on ice, 500 µL of pre-warmed (37 °C) LB bacterial growth media was added to the vial and then placed incubated at 37 °C for 1 hour. The vial was then placed on ice and the culture was spread onto LB agar plates with ampicillin, which had been equilibrated to room temperature. First, 50 µL of the bacterial solution was spread onto the first agar plate with a sterile spreader created in a flame from a 2 mL plastic volumetric pipette. Then, 100 µL of the bacterial solution was spread onto the second plate. The remaining 350 µL solution was spun down, 300 µL of the supernatant was removed, and the cells were re-suspended in the remaining 50 µL of LB, which was then spread onto the third agar plate. The plates were incubated upside down at 37 °C overnight, followed by refrigerating at 4 °C. Using sterile technique with a burner, 5 mL of LB media, along with 5 µL of ampicillin (50 µg/mL final concentration) were transferred into each of 12 sterile culture tubes. Next, 12 colonies were chosen, and 1 colony was added to each tube, and the bacteria were allowed to grow overnight by incubating at 37 °C with shaking. The DNA plasmids from each culture were collected by the QIAprep Spin Miniprep Kit (Qiagen), following the instructions provided by the kit, and the DNA concentration of each sample was measured as described previously.

To release the FASN TE gene from the pGEM-T Easy vector to ensure that proper ligation took place, a restriction digest with EcoRI was performed, as the pGEM-T Easy vector has EcoRI restriction sites on both sides of the FASN TE gene insert. A master mix, with enough of the mixture for 13 reactions, was created by mixing 159.9 µL

of nuclease free H₂O with 26 µL of EcoRI buffer (New England Biolabs, NEB) and 2.6 µL of bovine serum albumin (BSA) (100 µg/µL final concentration, NEB). For each plasmid sample, 14.5 µL of the reaction mixture was placed into a PCR tube, along with 5 µL of purified plasma DNA and 0.5 µL of EcoRI (NEB). Each tube was centrifuged briefly and then incubated at 37 °C for 1 hour. To ensure that successful digestion, and thus proper ligation, occurred, each sample was resolved on a 1.5 % agarose gel as described previously and two of the plasmid samples were submitted for DNA sequencing (DNA Sequencing Core Facility, Department of Biochemistry & Molecular Biology, Indiana University School of Medicine).

After the FASN TE sequence was determined to be correct by considering both the forward and reverse sequencing, and reconciling any mistakes by examining nucleotide peaks with Chromas DNA sequencing software, one of the samples was chosen for insertion into the pET-28a vector (Novagen). The vector was linearized and the FASN TE insert was prepared by restriction digestion with Xho I and BamHI restriction enzymes (NEB). To digest the FASN TE insert, a 50 µL reaction mixture was prepared by mixing 11.9 µL of nuclease free H₂O, 5 µL of NEB Buffer #4, 0.5 µL BSA, 30 µL of the FASN TE plasmid DNA, 1.3 µL of Xho I and 1.3 µL of BamHI. A restriction digest of the pET-28a plasmid was prepared by mixing 1.2 µL of nuclease free H₂O with 3 µL of NEB Buffer #4, 0.3 µL of BSA, 23.5 µL of the plasmid, 1 µL of Xho I and 1 µL BamH I. Each digestion was spun down briefly and incubated at 37 °C for 4 hours. The digestion products were stored at -20 °C. Digestion was confirmed later by resolving with a 1.5 % agarose gel. The bands corresponding to the FASN TE insert and

the pET-28a vectors were excised from the gel and purified using the Qiagen Gel Extraction kit according to the provided instructions.

The linearized vector and the FASN TE product were ligated together using a 3:1 molar ratio of insert to vector. A 10 μ L ligation reaction was prepared in the following order: 5 μ L of 2X Ligation Premix (Novagen), 1.58 μ L of the FASN TE insert (60 ng), 2.48 μ L of the pET-28a vector (100 ng), 1 μ L T4 DNA Ligase (Novagen). The mixture was gently mixed with a pipette tip, incubated at room temperature for 3 hours and then the entire reaction mixture was transformed into DH5 α competent cells and 12 plasmid samples were isolated as described above. To ensure that the FASN TE insert was properly ligated into the pET-28a vector, a restriction digest with Xho 1 and BamH 1 was again performed with 6.8 μ L of nuclease free H₂O, 0.2 μ L BSA, 2 μ L NEB Buffer #4, 0.5 μ L Xho I, 0.5 μ L BamH I, 10 μ L of the desired plasmid sample, which was then incubated at 37 °C for 4 hours. Each of the 12 isolated plasmids was digested in this manner. Proper insertion of the FASN TE gene was confirmed by running a 1.5 % agarose gel as described previously and two samples were sent for DNA sequencing. After confirming the correct sequence, 50 μ g of the pET-28a plasmid containing FASN TE from one of the samples was transformed into BL21 DE3 LRA *E. coli* cells, using kanamycin as the selection antibiotic, as described above. The bacterial sample was stored in LB with 10 % glycerol at -80 °C. Note: all excess DNA samples and plasmid products throughout the process described above were stored at -20 °C.

D. Expression and Purification of Recombinant FASN TE

The TE domain was overexpressed in BL21 DE3 LRA *E. coli* by first inoculating a total of 40 mL of LB growth media, created prior to beginning the experiment by dissolving 25 g of LB broth powder (Fisher) per 1000 mL of ddH₂O and autoclaving, with 40 μ L of *E. coli* containing the FASN TE plasmid, along with the antibiotic kanamycin, which was added to each culture at a final concentration of 50 μ g/mL. Sterile technique using a burner was employed. The culture was grown overnight at 37 °C with shaking. 20 mL of the culture was then transferred to each of 1 L of LB, along with kanamycin (final concentration 50 μ g/mL) and the culture was grown at 37 °C with shaking for approximately 4 hours until the OD₆₀₀ reached ~0.8-1. FASN TE expression was then induced by adding isopropyl β -D-1-thiogalactopyranoside (IPTG) to a final concentration of 0.5 mM, and the culture was grown at 25 °C with shaking for another 4 hours. The *E. coli* cells were collected by centrifugation (5000 rpm, 15 minutes), the LB was removed and the cell pellet was frozen at -70 °C.

To isolate and purify the expressed FASN TE protein, the bacterial cells were thawed for 15 minutes on ice and then re-suspended with 2 mL of lysis buffer per gram weight of cell pellet. Lysis buffer contained 50 mM NaH₂PO₄, 300 mM NaCl, 10 % glycerol, 0.1 % NP-40, 0.5 mM PMSF and 10 mM imidazole, pH = 8.0. Lysozyme (Sigma) was added to the lysis buffer/cell pellet mixture to a final concentration of 1 mg/mL, and the mixture was incubated on ice for 30 minutes. The cells were then subjected to 5 rounds of sonication, with 15 seconds of ablation with the sonication probe at 80 % amplification each round. The cell lysate was then centrifuged at 12,000g for 30 minutes at 4 °C to pellet any cellular debris, and the supernatant was saved. Note:

following sonication and pelleting of cellular debris, a small sample from each subsequent step of the purification listed below was saved and then examined using sodium dodecyl sulfate polyacrylamide gel electrophoresis (SDS-PAGE). As expression of the FASN TE protein with the pET-28a vector adds an N-terminal histidine tag to the protein, the protein product can be purified using nickel-nitrilotriacetic acid. First, 1 mL of nickel-nitrilotriacetic acid (Ni-NTA) agarose slurry (Qiagen) for every 4 mL of cleared lysate was equilibrated with lysis buffer by centrifuging the slurry at 1000g for 1 minute and removing the slurry solution. Then, 1 mL of lysis buffer was then added to the remaining Ni-NTA agarose, mixed, and centrifuged as before. The supernatant lysis buffer was removed from the Ni-NTA agarose and the cellular supernatant was added and mixed by gentle rotation at 4 °C for 1 hour to allow the His-tagged FASN TE protein to attach to the Ni-NTA agarose. The solution was centrifuged for 1 minute at 1000g, the supernatant was removed and 2 mL of wash buffer per 4 mL of lysate was added to the agarose beads. Wash buffer contained 50 mM NaH₂PO₄, 300 mM NaCl, 10 % glycerol, 0.1 % NP-40, 0.5 mM PMSF and 20 mM imidazole, pH = 8.0. The solution was rotated for 3 minutes at 4 °C, centrifuged and supernatant removed as above. The wash procedure was repeated four more times. 0.5 mL of elution buffer per 4 mL of lysate was then added to the slurry, and the solution was mixed by rotation for 5 minutes at 4 °C. Elution buffer contained 50 mM NaH₂PO₄, 300 mM NaCl, 10 % glycerol, 0.1 % NP-40, 0.5 mM PMSF and 250 mM imidazole, pH = 8.0. The solution was centrifuged as above, but the supernatant was saved in 1.5 mL centrifuge tubes. The elution procedure was repeated four more times, with the supernatant from each round saved in separate 1.5 mL

centrifuge tubes. The supernatant tubes were then centrifuged again and separated from any remaining Ni-NTA agarose.

The concentration of protein in each sample saved from the purification and each elution fraction was measured by Bradford Assay. To perform the assay, Bio-Rad Protein Assay Dye Reagent Concentrate (Bio-Rad) was diluted 1:5 with ddH₂O. A set of standards to create a standard curve was created by adding 1 mL of the diluted dye reagent to each of five small test tubes. To prepare the standards, one tube acted as a blank, and 1, 2, 4 or 8 μ L of a standard protein solution was added to each of the four tubes to create standards corresponding to protein concentrations of 1.40 mg/mL, 2.80 mg/mL, 5.60 mg/mL and 11.20 mg/mL protein. To measure the concentration of each elution sample, 1 μ L of the solution was added to 1 mL of the diluted dye reagent, and the concentration of each sample was measured in triplicate. The standard curve was created and the protein concentrations were measured using a Bio-Rad SmartSpec 3000 spectrometer. SDS-PAGE was then performed by adding 5 μ g total of protein from each sample along with SDS loading dye. Samples were boiled for 10 minutes, or incubated for 1 hour at room temperature, in order to denature the proteins, and then loaded onto a 12 % tris-glycine SDS-polyacrylamide gel with a 5 % stacking gel. PageRuler Pre-Stained Protein Ladder (Thermo) was also loaded onto the gel as a molecular weight marker. SDS-PAGE was performed in 1X SDS running buffer at 25 mA per gel and once the loading buffer reached the end of the gel, the gel was placed into coomassie blue staining solution, which consisted of 500 mg Brilliant Blue (0.1 %), 250 mL methanol (50 %), 50 mL glacial acetic acid (10 %) and 200 mL ddH₂O. The gel was stained in coomassie for 1 hour at room temperature with shaking, and then destained in destaining

solution (77:18:5 ddH₂O, methanol, acetic acid) overnight at room temperature with shaking. Completed gels were scanned using a computer scanner. The presence of purified FASN TE protein was confirmed by performing a Western Blot as described in methods section III E, and probing using a primary FASN antibody (Santa Cruz Biotechnology) raised against C-terminal residues 2205-2504, corresponding to FASN TE (1:1000 dilution), followed by probing with a horseradish peroxidase (HRP) conjugated anti-mouse IgG secondary antibody (1:3000 dilution).

After confirming the purify and presence of FASN in the elution fractions, the fractions were pooled and then dialyzed using a Slide-A-Lyzer dialysis cassette (Thermo) with a 3,500 Da molecular weight cutoff. If necessary, the protein was concentrated using Amicon ultra centrifugal filters (Millipore) with a 3,000 Da molecular weight cutoff, and then dialyzed overnight with spinning at 4 °C against 600 mL of buffer A (100 mM Tris-HCl, 50 mM NaCl, 0.05% Brij35 at pH 7.5). The dialysis solution was changed and dialyzed for 4 hours, followed by changing the dialysis solution and dialyzing for another 4 hours. The dialyzed protein solution was removed from the cassette and the protein concentration was once again measured using a Bradford assay as described above, and the protein was stored at -80 °C in buffer A with 10 % glycerol added as a cryoprotectant. Note: FASN TE cannot undergo multiple freeze-thaw cycles, and can therefore only be used once after thawing, thus it must be aliquoted.

E. FASN TE Kinetic Studies and Candidate Ligand Screening

The 34 candidate ligands from the DOCK *in-silico* screen were examined for their ability to inhibit FASN TE activity using a 4-methylumbelliferyl heptanoate (4-MUH)

fluorogenic assay first described by Jacks and Kircher [286] and described previously [224,236]. Before screening the candidate ligands, the kinetic parameters for the purified FASN TE protein were determined by first preparing a standard curve of the fluorescence produced at 355/460 nm for the 4-methylumbelliferone (4-MU) fluorescent product, to quantify the amount of fluorescence units (FU) yielded per μg of 4-MU. The kinetic assay was performed in opaque black, flat-bottom 96-well plates (Corning) containing 45 μL of 500 nM purified TE solubilized in buffer A (100 mM Tris-HCl, 50 mM NaCl, 0.05% Brij35 at pH 7.5). The kinetics of the protein were determined in the presence of DMSO, as would occur with the addition of a compound candidate, by first adding 5 μL of DMSO to each well, incubating at 37 °C for 30 minutes. 5 μL of varying concentrations of 4-MUH (1.2, 0.6, 0.3, 0.15, 0.075, 0.0375 mM starting concentrations, before addition to the wells) were added to each well in triplicate and incubated at 37 °C for 1 hour and the fluorescence was measured. To determine the K_m , which is equivalent to the concentration required to achieve 50 % of the maximal velocity (v_{max}), the data were fit using WinNonlin v2.0 software (Pharsight) with a 1 enzyme model with no weighing of the data.

The compound candidate screen was performed in opaque black, flat-bottom 96-well plates (Corning) containing 45 μL of 500 nM purified TE solubilized in buffer A and each compound candidate dissolved in DMSO was examined in triplicate, one reaction per well, by adding 5 μL of the compound to each well, with a final compound concentration of 100 μM . The plate was incubated at 37 °C for 30 min. 5 μL of 4-MUH (Sigma) dissolved in DMSO was then added to the reaction at a final concentration of

300 μ M and incubated at 37 °C for 1 hr. In addition to the reaction wells, the following control wells were also prepared:

- 1) Buffer A alone (no protein) + DMSO: used for blank
- 2) FASN TE Protein + inhibitor vehicle ONLY (no test inhibitor) + 4-MUH: used to measure the full activity of the protein
- 3) Buffer A alone (no FASN TE) + inhibitor vehicle ONLY (no test inhibitor) + 4-MUH: used to measure the auto-hydrolysis of 4-MUH, which was subtracted from the full activity of the protein
- 4) FASN TE Protein + inhibitor +4-MUH: used to measure the inhibition of FASN TE activity by each compound
- 5) Buffer A alone (no protein) + inhibitor + 4-MUH: used to determine if the inhibitor was adding to the fluorescent background, which was subtracted from the fluorescence value calculated from the protein + inhibitor + 4-MUH

The fluorescence due to liberated 4-MU was measured using a fluorescence plate reader with excitation/emission wavelengths of 355/460 nm. The K_i value for each inhibitor candidate was calculated using the online IC_{50} to K_i converter (<http://botdb.abcc.ncifcrf.gov/toxin/kiCalES.jsp>) [287] based on the Cheng and Prusoff equation [288].

Specific Aim III: Lead Candidate Evaluation

A. Human Cell Culture

PANC-1 cells (ATCC) were maintained in complete Dulbecco's modified eagle medium (DMEM) (Corning cellgro) supplemented with 10 % fetal bovine serum (Life Technologies) and 1 % penicillin-streptomycin (Corning cellgro). PANC-1/V4 and PANC-1/F7 cell lines [149] were maintained similarly to PANC-1 cells, but with the addition of G418 (Sigma) to the media at a final concentration of 200 $\mu\text{g/mL}$. BxPC-3 cells (ATCC) were maintained in RPMI 1640 (Corning cellgro) supplemented with 10 % fetal bovine serum and 1 % penicillin-streptomycin. All cell lines were maintained at 37 $^{\circ}\text{C}$ in 5 % CO_2 in 75 cm^2 vented tissue culture flasks.

Cells were ready for plating for experiments or for sub-culturing once they reached approximately 80 % confluency. Using sterile technique in a laminar flow hood, cells were passaged by removing media from the flask via vacuum aspiration, washing the cells with 2 mL of trypsin and removing via vacuum aspiration, and then incubating the cells in 2 mL of trypsin for approximately 20 minutes in the tissue culture incubator. Once cells had detached from the flask, 8 mL of new media was added to the flask, the walls of the flask washed by pipetting up and down with media, and then all media was removed from the flask and placed in a 50 mL centrifuge tube. Cells were pipetted up and down in the tube in order to break up any clumps of cells and to create a single cell solution, and then 1 mL of the cell suspension was then placed back into the tissue culture flask (1:10 splitting ratio), along with approximately 14 mL of new media. Cells were passaged twice weekly. To plate cells for subsequent experiments, cells were first counted by mixing 50 μL of the cell suspension with 50 μL of trypan blue solution

(Sigma), and then adding 10 μL of the mixture to each side of a hemocytometer. Cells in the four outer corners of each side of the hemocytometer were counted under magnification, ignoring any dead cells (stained blue with the trypan blue solution). Cell density was determined by the following formula:

$$\frac{(\text{Box } 1+2+3+4+ 5+6+7+8)}{4} = \text{Cell Density} \times 10^4 \text{ cells/mL}$$

B. MTT Assays to Measure Cellular Proliferation

PANC-1 or BxPC-3 cells were seeded in 96-well tissue culture plates (2,000 cells/well, 100 μL /well) and cultured for 24 h at 37 $^{\circ}\text{C}$ and 5 % CO_2 . Cells were treated in triplicate with proton pump inhibitors (PPIs) in DMSO or DMSO control (0.5 %) at various concentrations by removing the media from each well, and replacing with 200 μL of media containing the desired PPI at the desired concentration, prepared by serial dilution. Cells were then incubated for 72 h at 37 $^{\circ}\text{C}$; followed by performing an assay in which MTT dye is added to the culture media and is reduced from a soluble yellow tetrazole dye to an insoluble purple formazan by cellular reductases in living cells [289]. MTT stock solution was created by dissolving 5 mg/mL of thiazoyl blue tetrazolium bromide powder (Sigma) into 1X PBS solution (137 mM NaCl, 2.7 mM KCl, 10 mM $\text{Na}_2\text{HPO}_4 \cdot 2\text{H}_2\text{O}$, 2.0 mM KH_2PO_4 , pH = 7.4) and sterile filtering. MTT solution (20 μL) was added to each well and incubated for 4 hours in the tissue culture incubator. The plate was then spun down (1500 rpm, 10 minutes), and all media and MTT solution was removed from the plate via vacuum aspiration. Finally, 100 μL of DMSO was added to each well to solubilize the purple MTT dye and the absorbance at 570 nm was read on a plate reader.

C. Colony Formation Assays

Human pancreatic cancer cells were seeded in 6-well tissue culture plates (100 cells/well, 2 mL growth media for PANC-1, PANC-1/V4 and PANC-1/F7; 200 cells/well for BxPC-3 cells) and cultured for 24 h at 37 °C as described previously. Cells were treated in triplicate by adding 10 µL of PPIs in DMSO (various concentrations) or DMSO control directly to the treatment wells. The cells were cultured for 10 days, and colonies were visualized by removing the media, washing each well with 1 mL of PBS, staining with 750 µL of coomassie blue for 20 minutes at room temperature, re-washing with 1 mL of PBS and then allowing the plates to air dry. Colonies were counted manually.

D. Radioactive FASN Lipid Synthesis Assay

The basal FASN synthesis rate in each cell line, or the inhibition of fatty acid synthesis in the presence of PPIs, was measured by examining the incorporation of [¹⁴C]-acetate into fatty acids in whole cells. Cells were seeded in 12-well tissue culture plates (100,000 cells/well, 500 µL media) and cultured for 24 h at 37 °C. If lipid synthesis inhibition by PPIs were examined, cells were treated in triplicate with inhibitors (31.25-1000 µM) for 4 hours at 37 °C. To account for any differences in cell proliferation rate or for cell death caused by the PPIs, trypsin was added to wells of cells prepared specifically for cell counting prior to measuring radioactivity, and cells were counted to normalize radioactive counts to the number of cells. 1 µCi/mL of [¹⁴C]-acetate (Perkin Elmer) was added to each well and incubated for 2 hours at 37 °C. The cells were harvested and lipids extracted using the Folch extraction procedure [290]. The cell media was aspirated from each well and 900 µL of 2:1 chloroform/methanol (CHCl₃:MeOH) was added to

each well to lyse the cells. The lysate was transferred to 2 mL centrifuge tubes, along with 700 μ L of 4 mM $MgCl_2$. Each tube was vortexed and centrifuged for 30 seconds at 12,000g to separate the organic and aqueous layers. The top aqueous layer was removed by aspiration. 700 μ L of 2:1 $CHCl_3$:MeOH and 600 μ L of $MgCl_2$ was added to each tube, which were vortexed, centrifuged and the aqueous layer removed. The process was repeated once more with the addition of 600 μ L of 2:1 $CHCl_3$:MeOH and 500 μ L of $MgCl_2$. The samples were dried overnight in a fume hood, resuspended in 200 μ L of $CHCl_3$, added to 10 mL of scintillation fluid, and radioactivity, given as disintegrations per minute (DPM), was measured using a scintillation counter. All counts were normalized to 10^5 cells.

E. Measuring FASN Protein Expression via Western Blot

To measure the amount of FASN protein expression, $0.6-0.8 \times 10^6$ of cells were seeded in 10 cm tissue culture dishes with 3 mL of appropriate growth media and allowed to grow to approximately 80 % confluency. The media was aspirated and cells were washed with 1 mL ice cold PBS and collected in PBS by scraping. The cells were spun down for 10 seconds at 12,000g, PBS was removed, and cells were washed again with 1 mL PBS. PBS was removed and the cell pellets were resuspended in TNN lysis buffer (50 mM Tris-HCl, 150 mM NaCl, 0.5 % NP-40, 5 mM EDTA, 50 mM NaF, 1 mM Na_3VO_3 , with 1 mM PMSF and 1 mM DTT, added immediately before use, pH = 7.4), the amount of buffer ranging from 20-100 μ L, depending on the size of the cell pellet. Cells were vortexed, and incubated on ice for 15 minutes, followed by a second round of vortexing and incubation. Cells were then lysed with 5 rounds of sonication, with 7

seconds of ablation at 40 % of amplification each round. Cellular debris was pelleted by centrifuging at 12,000g for 15 minutes at 4 °C and protein concentration was measured by Bradford Assay as described in detail in section II D. Samples consisting of 20 µg of total protein were prepared with the addition 5X SDS loading dye, and the proteins were denatured by boiling for 10 minutes. The samples were resolved using SDS-PAGE with an 8 % Tris-glycine SDS-polyacrylamide gel with 5 % stacking gel, along with PageRuler Plus protein ladder (Fermentas) as a molecular weight marker. To prepare for Western Blot transfer, the resolved gel and two pieces of filter paper were soaked in Western Blot transfer buffer (48 mM Tris Base, 39 mM glycine, 5 mM SDS, 20 % MeOH), and a PVDF membrane was soaked in 100 % methanol. The transfer was performed wet overnight at 4 °C using the Mini Trans-Blot Cell system (Bio-Rad). The membrane was then blocked with 5 % non-fat dry milk (NFDM) (1X PBS with 0.1 % Tween-20) for 2 hours at room temperature. The blocking solution was discarded and replaced with primary FASN antibody (Santa Cruz) diluted 1:1000 and β-actin antibody diluted 1:3000 in 5 % NFDM. The membrane was incubated for 2 hours at room temperature and then washed three times for 10 minutes each with PBS with 0.1 % Tween-20. The membrane was incubated for 30 minutes at room temperature with HRP-conjugated anti-mouse IgG (1:3000 dilution) and again washed three times for 10 minutes each with PBS with 0.1 % Tween-20. The membrane was incubated with ECL Western Blotting Detection Reagents (Amersham) for 1 minute at room temperature and visualized with chemiluminescent detection using the FluorChem HD2 imaging system (Protein Simple).

F. Probing the FASN TE Active Site

The ability of lansoprazole (Sigma) to specifically inhibit the TE active site of full-length FASN was examined using a serine hydrolase probe as described previously [212]. PANC-1 cells were seeded (approximately $0.6\text{-}0.8 \times 10^6$ cells total) in 10 cm tissue culture dishes and allowed to grow to 80 % confluency. The media was aspirated and cells were washed with 1 mL ice cold PBS and collected by scraping. The cells were spun down for 10 seconds at 12,000g, PBS was removed, and cells were washed again with 1 mL PBS. PBS was removed and the cells were resuspended in 50 mM Tris-Cl (pH = 8.0). Cells were then lysed with five rounds of sonication, using 15 seconds of ablation at 40 % amplification. The soluble and insoluble protein fractions were separated by centrifugation at 12,000g for 15 minutes at 4 °C, and the protein concentration was measured by Bradford assay as described previously. Samples of cell lysate (40 μL , 1 $\mu\text{g}/\mu\text{L}$) were treated with varying concentrations of lansoprazole (1 μL in DMSO, 12.5-200 μM final concentration) or DMSO control for 30 minutes at room temperature, followed by treatment with the ActivX Desthiobiotin-fluorophosphonate (FP) serine hydrolase probe (Thermo) (1 μL in DMSO, 5 μM final concentration) for 30 minutes at room temperature. Reactions were stopped by addition of 10 μL 5X SDS-PAGE loading buffer and boiling for 10 minutes, and resolved using SDS-PAGE with an 8 % tris-glycine SDS-polyacrylamide gel with PageRuler Plus protein ladder (Fermentas) as a molecular weight marker. The protein was transferred to a PVDF membrane overnight at 4 °C at 35 mV and was blocked for 1 hour at room temperature using 1 % BSA (Sigma) in PBS with 0.05 % Tween-20. The membrane was washed twice for 5 minutes each with PBS with 0.05 % Tween-20 then incubated with streptavidin-peroxidase polymer,

ultrasensitive (Sigma) diluted 1:1000 in PBS with 0.05 % Tween-20 for 1 hour at room temperature. The membrane was washed 6 times at room temperature with PBS with 0.05 % Tween-20 for 5 minutes each and then incubated with SuperSignal West Dura Extended Duration Substrate (Thermo) for 1 minute at room temperature. The blot was visualized with chemiluminescent detection using the FluorChem HD2 imaging system (Protein Simple). The membrane was stripped by incubating in a mild stripping buffer (200 mM glycine, 3.5 mM SDS, 1 % Tween-20, pH = 2.2) for 10 minutes at room temperature. The stripping buffer was discarded, and fresh buffer was added and incubated at room temperature for an additional 10 minutes. The membrane was washed twice with PBS for 10 minutes at room temperature and then washed twice with TBST (50 mM Tris, 150 mM NaCl, 0.05 % Tween-20, pH = 7.6) for 5 minutes at room temperature. The membrane was then re-blocked using 5 % non-fat milk in PBS, probed for FASN expression (BD Biosciences) (1:1000 dilution) and β -actin (1:3000 dilution) and visualizing using HRP-conjugated anti-mouse IgG (1:3000 dilution) with chemiluminescent detection as described in section III E above.

G. Determination of Inhibition Mechanism of FASN TE by Lansoprazole

To determine the type of enzymatic inhibition that lansoprazole imparts on FASN TE, recombinant FASN TE was incubated with several lansoprazole concentrations (50, 25, 6.25 μ M) in the presence of a range of 4-MUH concentrations (160, 80, 40, 20, 10 μ M), as described in section II E. The fluorescence due to liberated 4-MU was measured and a Lineweaver-Burk plot was created by plotting $1/v$ vs. $1/[S]$ for each lansoprazole concentration [291].

H. PARP-1 Cleavage Apoptosis Assay

Apoptosis induction by lansoprazole was confirmed by measuring the amount of cleaved poly(ADP-ribose) polymerase-1 (PARP-1) in cells following lansoprazole treatment via Western Blot. 6-well tissue culture plates were seeded with BxPC-3 cells (212,000 cells/well, 2 mL growth media) and cultured for 24 hours as described previously. Cells were then treated by adding 10 μ L of lansoprazole (12, 25, 50 μ M) or DMSO control directly to the well and incubating for 8 hours in the tissue incubator. Cell lysate was isolated and 30 μ g of total protein from each sample was resolved using a 10 % SDS-PAGE gel, transferred to a PVDF membrane, blocked with 5 % non-fat milk, and probed with an antibody specific for the cleaved form of PARP (Cell Signaling) (1:1000 dilution), following the Western Blot protocol as described in section III E above. The blot was visualized using HRP-conjugated anti-mouse IgG (1:3000 dilution) followed by chemiluminescent detection with SuperSignal West Dura Extended Duration Substrate (Thermo).

I. Cell Death Detection Apoptosis Assay

BxPC-3 cells were seeded in 12-well plates (18,000 cells/well, 1 mL media) and cultured for 24 hours as described previously, followed by treatment in triplicate with 5 μ L of lansoprazole (12, 25, 50 μ M) or DMSO control added directly to each well. The plates were incubated in the tissue culture incubator for 72 hours, and apoptosis was measured with the Cell Death Detection ELISA assay kit (Roche), which was performed according to the instructions provided. Following the 72 hour treatment, cells from wells specifically prepared for cell counting were counted by adding 500 μ L of trypsin to each

well (250 μ L was added to the 50 μ M treatment well) and then determining the number of cells in each well as described previously. Following cell counting, the media was removed and cells were lysed directly in the treatment wells by adding lysis buffer from the kit into each well to yield a final cell concentration of 10^4 cells/200 μ L of lysis buffer and incubating for 30 minutes at room temperature. The lysate was centrifuged at 200g for 10 minutes and 20 μ L from each sample was transferred into the microplate provided by the kit. 80 μ L of the immunoreagent prepared from the kit were added to each test well, and the plate was covered with foil and incubated with shaking for 2 hours at room temperature. The solution was removed with vacuum aspiration and each well was washed three times with 220 μ L of incubation buffer from the kit and removed from the wells with aspiration. ABTS solution from the kit, which is highly light sensitive, was prepared in a dark area, such as in the tissue culture hood with no lights, in an opaque 15 mL centrifuge tube. ABTS solution (100 μ L) was placed into each well and incubated at room temperature with shaking for 20 minutes. Finally, 100 μ L of ABTS stop solution from the kit was pipetted into each well and the absorbance was measured at 405 nm, with a reference wavelength of 490 nm.

J. Extracellular and Intracellular pH Measurement

Extracellular pH was measured by plating BxPC-3 cells in 6-well plates (55,000 cells/well) and then incubating the cells in the presence of 100 μ M lansoprazole or DMSO control in 2 mL of growth media for 72 hours. The cellular media was collected, spun down and measured with a pH probe (Fisher Scientific). Intracellular pH was measured by plating BxPC-3 cells in 96-well plates (2,000 cells/well) and then incubating

the cells in the presence of lansoprazole (100-6.25 μM) or DMSO control for 72 hours. Four sets of cells were plated, each in triplicate. Media was removed, washed with 100 μL of live imaging cell solution (Life Technologies) and then all cells were incubated with 50 μL of pHrodo red intracellular pH dye (Molecular Probes) according to manufactures' instructions. Cells were again washed once with live imaging cell solution, and then 100 μL of fresh imaging solution was added to each well and fluorescence was measured with excitation and emission wavelengths of 560/590 nm. Intracellular pH was then quantified using the intracellular pH calibration kit (Molecular Probes) according to manufactures' instructions. Cells were again washed once with imaging solution and then each of the four sets of cells was incubated for 5 minutes at 37 $^{\circ}\text{C}$ with one of the four intracellular pH calibration buffers. Fluorescence was again measured and a standard curve plotting fluorescence units vs. known pH values was created for each lansoprazole concentration, and the intracellular pH of each well at each lansoprazole concentration was calculated using the standard curve to convert fluorescence units to intracellular pH.

K. Rescue with Palmitate Supplementation

BxPC-3 cells were plated and a standard assay treatment protocol was used as described in detail in section III B for MTT assays; section III C for colony formation assays; or section III I for apoptosis induction. For MTT assays, a stock solution of media with 3.75 μM of palmitic acid (Sigma) in DMSO (0.1 %) was prepared and after replacing the growth media, BxPC-3 cells were then treated with varying concentrations of lansoprazole (100-3.125 μM) or DMSO control in the presence or absence of palmitate for 72 hours, and then cellular proliferation was measured as described previously.

Palmitic acid, dissolved in DMSO (0.125 %) was then immediately added directly to the media to a final concentration of 3.75 μ M. For apoptosis assays, a stock solution of media with 3.75 μ M of palmitic acid in DMSO (0.1 %) was prepared and after replacing the growth media, BxPC-3 cells were then treated with 25 μ M lansoprazole or DMSO control in the presence or absence of palmitate for 72 hours, and then apoptosis induction was measured by the cell death detection assay as described previously.

L. IC₅₀ and Statistical Calculations

All IC₅₀ values and statistical calculations were performed using Prism5 (GraphPad). IC₅₀ values were calculated using the log(inhibitor) vs. normalized response regression equation. All statistics were calculated using a two-tailed Student's t-test.

Chapter 3: Aim I: Mechanism of Orlistat Hydrolysis by the Thioesterase of Human Fatty Acid Synthase

A. Background and Rationale

Orlistat (Fig. 1A), an FDA approved drug for obesity treatment that inhibits pancreatic lipases in the gastrointestinal tract, has been shown to inhibit TE of FASN [212]. Computational docking analysis shows that orlistat binds to the ligand binding site in TE [292], and the co-crystal structure of the TE of human FASN with orlistat (ID: 2PX6) shows that orlistat is indeed present in the active site of TE [213]. However, in the co-crystal structure, orlistat exists in the active site of TE both as a hydrolyzed product and as a covalently-bound intermediate (covalent-orlistat), in which the C1 carbon of the β -lactone cyclic ester moiety of orlistat forms a covalent bond with the active site Ser²³⁰⁸ (Fig. 1A). Interestingly, these two states are found in one single co-crystal structure as an asymmetric dimer of the TE-orlistat complex. In addition, the hexyl tail of orlistat appears to adopt two different conformations in covalent-orlistat and hydrolyzed product, and it was thought that the hexyl tail of covalent-orlistat may pack against His²⁴⁸¹. As discussed in Chapter 1, at the end of the fatty acid synthesis cycle, a water molecule is activated by forming a hydrogen bond with the catalytic nitrogen atom of the His²⁴⁸¹ residue and nucleophilically attacks the carbonyl carbon of the acyl-enzyme intermediate, releasing the fatty acid from Ser²³⁰⁸ and regenerating the Ser²³⁰⁸ and His²⁴⁸¹ residues [29,293]. Thus, the presence of hexyl tail of covalent-orlistat may prevent access and activation of a water molecule needed for hydrolysis of the covalent bond between

orlistat and Ser²³⁰⁸ [213]. However, it is unknown if the hexyl tail of covalent-orlistat can shift from one conformation to another, and if and how the shift contributes to catalysis.

The potential role of the hexyl tail in orlistat hydrolysis was examined using molecular dynamics (MD) simulations. MD simulations allow for the functional study of complex biomolecules, such as proteins, carbohydrates or nucleic acids, by using molecular mechanic force fields to virtually predict the motions of each component residue within the system. These force fields work to calculate the behavior of atoms in the system as a function of time by solving Newton's equations of motion for each atom [294]. MD simulations are especially useful for studying the properties of a biological system that would be very difficult to examine with experiments on the actual system [295]. In this case, the Assisted Model Building with Energy Refinement (AMBER) MD package was used to perform the MD simulations, which contains all the programs for the simulation, including the LeAP program for input file preparation; the sander program for performing the MD simulation; and the ptraj program for analyzing the simulated trajectory [296]. AMBER also contains classical molecular mechanic force fields and parameter sets that are used to describe various components of biological system such as amino acid residues, ions, and solvent molecules [297]. Although the system with FASN TE and orlistat is unusual, as orlistat has covalently modified one of the residues in the system, creating a non-natural residue, MD simulations of macromolecules with covalently bound adducts originating from x-ray crystal structure data have been successfully completed in previous studies [298,299].

All calculations for this study were performed using the Big Red supercomputer at Indiana University. At the time of its commission in 2006, Big Red was one of the 50

fastest supercomputers in the world and was one of the most powerful supercomputers owned by a university prior to its retirement in late 2013 [300]. Supercomputers are a powerful tool for highly complex computational calculations, such as those required for MD simulation, as they allow for mass parallel computing, in which a number of calculations are performed simultaneously by multiple processors, thus greatly shortening the amount of time needed to complete a set of calculations [301]. At its peak, Big Red was theoretically capable of nearly 40 teraFLOPS (**F**loating-point **O**perations **P**er **S**econd), or 40-trillion calculations per second. In contrast, the successor for Big Red, Big Red II, is theoretically capable of 1 petaFLOPS, or 1-quadrillion calculations per second [300].

In this study, three independent 35-nanosecond (ns) simulations showed that the hexyl tail of covalent-orlistat can shift from one conformation to another during the simulations. However, the shift of the hexyl tail does not increase the accessibility of water molecules to the active site. Instead, this shift destabilizes a hydrogen bond between the catalytic nitrogen atom of His²⁴⁸¹ and the hydroxyl moiety of covalent-orlistat, allowing a water molecule to be activated via hydrogen bonding with His²⁴⁸¹ in a proper orientation for catalysis, thus demonstrating the importance of hexyl tail in orlistat hydrolysis by TE. This study satisfies Specific Aim I because a potential molecular process involving the hexyl tail of orlistat, and the way in which the conformational change of the tail promotes orlistat hydrolysis, was elucidated by the MD simulations. The results provide new information on the way in which the flexibility of the orlistat hexyl tail limits its ability to inhibit FASN TE, and may be useful for the design of new irreversible inhibitors of FASN TE.

B. Results

B1. Covalent-Orlistat Molecular Mechanic Parameter Verification by Quantum Mechanics

Fig. 1A shows the structures of free, covalent-, and hydrolyzed orlistat. The two conformations adopted by the hexyl tails in covalent- and hydrolyzed orlistat in TE in the crystal structure were assigned as conformations I and II (Fig. 1B), respectively, which are defined by the ω angle of the hexyl tail (Fig. 1A and B). The hexyl tail in these two conformations interacts with two different groups of amino acid residues. The hexyl tail of covalent-orlistat with an ω angle of 337.97° is accommodated in pocket I, or “short-chain pocket,” defined by residues Gly²³³⁹, Thr²³⁴², Tyr²³⁴³ and Tyr²⁴⁶² of TE in conformation I, while the hexyl tail of hydrolyzed orlistat with an ω angle of 139.54° interacts with pocket II, or “shift pocket,” defined by residues Tyr²³⁰⁹, Tyr²³⁴² and Ala²⁴³⁰ in conformation II as previously described [213].

Within the active site of FASN TE, orlistat exerts its effects by covalently binding with Ser²³⁰⁸ of the catalytic triad. However, this covalent bond creates an irregular residue that cannot be recognized by the AMBER suite of programs (University of California, San Francisco), which are used to parameterize and derive charges for ligands and proteins for molecular mechanics (MM) calculations and molecular dynamics (MD) simulations. As such, this irregular covalently bound serine-orlistat residue (hereafter referred to as ‘covalent-orlistat’) must be manually parameterized for the MD simulation. The Ser²³⁰⁸ residue covalently-bound to orlistat was parameterized using the well-established procedure from the AMBER manual (see Chapter 2) [302]. Derived parameters for covalent-orlistat can be found in Appendix B. Then, it was determined if

the developed AMBER parameters could reproduce the ab initio energy profile for the ω dihedral angle of the hexyl tail that defines conformation I and II in the crystal structure by performing QM and MM dihedral angle scans of a 3-mer peptide containing covalent-orlistat attached to Ser²³⁰⁸. As shown in Fig. 2A, the MM method using the AMBER parameters yielded an energy profile that is very similar to the curve generated by the ab initio method, with both profiles showing two minima and two maxima each. The two maxima appeared at 8.2° and 248.2° in the ab initio curve and at 5.3° and 246.8° in the MM curve, indicating a good agreement. The two minima appeared at 158.2° and 308.2° in the ab initio curve and at 158.4° and 306.4° in the MM curve, which not only agree with each other very well, but are similar to the ω angles (139.54° and 337.97°) of the hexyl tail of covalent- and hydrolyzed orlistat in the crystal structure, respectively. Interestingly, the QM energy barrier separating the two hexyl tail conformations is 29.6 kcal/mol to shift from conformation I to II, and 28.35 kcal/mol to shift from conformation II to I, which is considerably high. Thus, covalent-orlistat was likely parameterized properly for MD simulations and the hexyl tail of covalent-orlistat may adopt both conformations as observed in the crystal structure without hydrolysis.

FIGURE 1:

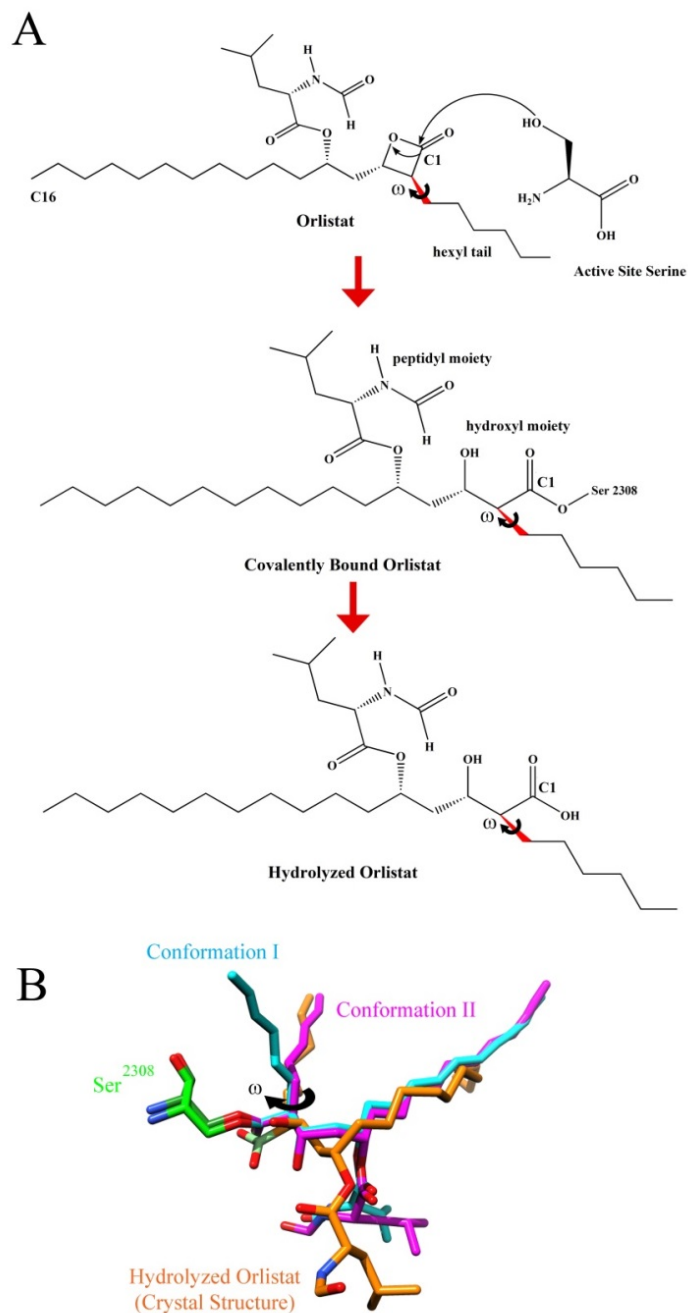


Figure 1. Catalytic mechanism of orlistat hydrolysis by FASN TE. (A) The active site Ser²³⁰⁸ of TE nucleophilically attacks the C¹ carbon of the β -lactone moiety of orlistat to form a covalent bond between Ser²³⁰⁸ and orlistat. Orlistat is then hydrolyzed and

inactivated by TE. The ω dihedral angle of the hexyl tail that defines conformations I and II is depicted in red. (B) Alignment of average structures of covalent-orlistat in conformations I (cyan) and II (magenta) from the first simulation and the hydrolyzed orlistat from the crystal structure (orange). Each conformation is defined by a distinct ω dihedral angle. The Ser²³⁰⁸ portion of covalent-orlistat is shown in green, and the hydrolyzed group in hydrolyzed orlistat is shown in light green.

B2. Two Distinct Conformations of the Hexyl Tail in Covalent-Orlistat

To show that the hexyl tail of covalent-orlistat can adopt both ω angle conformations observed in the crystal structure without influence from TE, and that these conformations are energetically-equivalent but independent conformations, a 100-ns MD simulation of the 3-mer peptide containing covalent-orlistat was performed. As shown in Fig. 2B, the ω dihedral angle begins at $303.79 \pm 8.90^\circ$ and changes to $178.53 \pm 14.59^\circ$ at 12.55 ns. It then flips back to $305.61 \pm 9.68^\circ$ at 52.09 ns. At 56.39 ns, the ω dihedral angle adopts an average angle of $174.48 \pm 15.44^\circ$ for the remainder of the simulation (Fig. 2B). The conformations of the hexyl tail of covalent-orlistat with these two major ω dihedral angles are similar to conformations I and II as observed in the co-crystal structure and, thus, covalent-orlistat without the TE protein may adopt the same two conformations prior to hydrolysis (Fig. 2B). The calculated total free energies of the 3-mer peptide in both conformations are nearly identical, with energies of -329.61 ± 7.55 kcal/mol in conformation I and -330.52 ± 7.81 kcal/mol in conformation II. In an independent duplicate simulation, a similar conformational transition and free energies were observed (data not shown). Thus, without influence from the surrounding amino

acid residues, the hexyl tail of covalent-orlistat can adopt two distinct but energetically equivalent and interchangeable conformations that are similar to the two different conformations seen in the co-crystal structure.

FIGURE 2

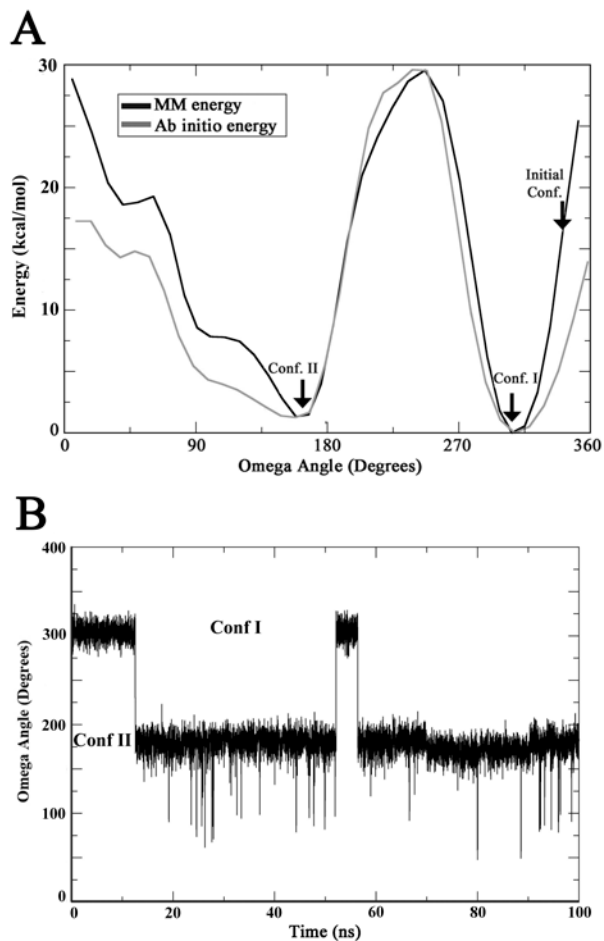


Figure 2. Potential energy of the 3-mer peptide containing covalent-orklistat and ω angle scan. (A) The energy curves calculated by QM and MM methods were scaled and overlaid. Conformations I and II of the hexyl tail are shown at two distinct energy minima. (B) ω dihedral angle scan of the 3-mer peptide containing covalent-orklistat.

B3. Compatibility of Covalent-Orlistat MM Parameters with AMBER Force Field

To further determine whether the developed AMBER parameters of covalent-orklistat are compatible with the AMBER force field, MM minimizations of the model system of TE in complex with covalent-orklistat in an explicit water environment were

examined. The developed parameters successfully minimized the initial structure with a convergence criterion of $1.0 \text{ kcal mol}^{-1}\text{\AA}^{-1}$. The equilibration period of 60 ps was confirmed to be adequate by examining the RMSD of the whole protein during the equilibration period, which was stable and remained less than 1.5 \AA . To confirm that the AMBER parameters of covalent-orlistat are suitable for MD simulation studies, various parameters were monitored during the 35-ns MD simulations. Both the temperature and energy remained constant with little deviation during equilibration and production MD runs of all three simulations (Table 1). The RMSD of the main chain atoms (RMSD^{TE}) is less than 2.0 \AA during the entire simulation process (Fig. 3A), which is consistently observed in all three simulations (Table 1). These findings indicate that the overall protein structure is not disrupted or distorted throughout the simulations. More importantly, the simulated B-factors of the protein ($\text{B-factor}^{\text{TE}}$) and covalent-orlistat ($\text{B-factor}^{\text{orlistat}}$) are comparable to the experimentally determined values [213] (Fig. 3B, Table 2). Thus, the parameterization is appropriate and compatible with the current AMBER force field.

TABLE 1. Summary of simulated trajectories and average RMSD, temperature, and energy.

	First Simulation	Second Simulation	Third Simulation
RMSD^{TE} (Å)	1.32 ± 0.22	1.29 ± 0.13	1.83 ± 0.33
T (Kelvin)	300.03 ± 1.51	300.24 ± 1.60	299.98 ± 1.60
E (kcal/mol)	-79207.9 ± 188.0	-79167.7 ± 205.2	-79271.5 ± 191.5
PE (kcal/mol)	-99984.4 ± 154.6	-99958.7 ± 162.8	-100044 ± 156.7
EK (kcal/mol)	20776.5 ± 104.6	20791.0 ± 110.6	20773.5 ± 111.0

B4. Conformational Transition of the Hexyl Tail in the FASN TE Domain

The above studies showed that, in the absence of the TE protein, the hexyl tail of covalent-orlistat in the 3-mer peptide is able to adopt two different conformations, defined by the ω dihedral angle, that are independent and can freely transit between the two conformations. To determine if a conformational transition of the hexyl tail of covalent-orlistat can occur within the binding pocket of the TE domain, and whether this transition has any effect on orlistat hydrolysis, the conformation of the hexyl tail was examined during three independent 35-ns simulations of the TE-covalent-orlistat complex.

To define the conformational transition of the hexyl tail within the TE protein and to determine if any observable change could potentially recapitulate the difference in hexyl tail conformation between covalent- and hydrolyzed orlistat as observed in the crystal structure, three criteria were considered: the RMSD of covalent-orlistat; the ω dihedral angle; and the distance of the hexyl tail to each pocket I and II in TE. First, the RMSD value of covalent-orlistat was monitored throughout each simulation. The hexyl tail remained in one conformation, as noted by a stable RMSD, during the initial 3,400 ps of the simulation until transitioning to a second conformation, which was completed at 18,250 ps when the RMSD of covalent-orlistat regained stability (Fig. 3A). Similar conformational transitions but at different times were also observed in two other independent simulations with the time-spans of each conformation shown in Table 1. The RMSD of orlistat ($\text{RMSD}^{\text{Orlistat}}$) in both stable states was calculated to be 0.6-1.94 Å before and 2.19-2.56 Å after the conformational transition (Table 2), indicating that the

hexyl tail adopts a conformation that is similar to the initial structure before the transition, but adopts a very different conformation after the transition.

Next, it was determined if the two conformations observed in these simulations are equivalent to and possibly represent conformations I and II observed in the crystal structure, by examining the ω dihedral angles throughout each simulation. There is a clear change in the ω angle between the two stable states of covalent-orlistat (Fig. 3C). In the three simulations, the average ω angles range from 304.89° to 309.73° in stable state I and 172.68° to 176.32° in stable state II (Table 2). Strikingly, the average ω angles in stable state I and II is respectively similar to the ω angles in conformation I (308.2°) and II (158.2°) determined by the ab initio method (see Fig. 2A). Furthermore, the average ω angles are also similar to the ω angles of the two conformations in the crystal structure (Table 2). These observations demonstrate that the two stable states of the ω angle of covalent-orlistat seen in the simulations could indeed correspond to conformations I and II, as determined by ab initio method and observed in the crystal structure. It is noteworthy that there is a brief reversion of the ω angle from conformation II back to I, which then again transitions to conformation II (at $\sim 11,440$ - $11,870$ ps) (Fig. 3C), which is consistent with the ω dihedral angle transition noted with the 3-mer peptide.

Next, the total free energy of covalent-orlistat within TE in conformations I and II was calculated, which are nearly equivalent, ranging from -131.60 ± 7.03 to -130.29 ± 6.21 kcal/mol in conformation I and -139.05 ± 6.26 to -135.25 ± 7.19 kcal/mol in conformation II, indicating that conformation II is unlikely a simple relaxation of conformation I. Together, these data show that the hexyl tail of covalent-orlistat in TE has shifted from conformation I to II during the simulations, which may resemble the

conformational transition during catalysis as suggested by the crystal structure, and suggests that the transition of the hexyl tail from conformation I to II likely occurs before the hydrolytic reaction, which may further indicate that the hexyl tail plays a role in dominating the hydrolytic catalysis reaction.

Finally, consistent with the crystal structure, the hexyl tail of covalent-orlistat in conformation I mainly interacts with pocket I, while the hexyl tail in conformation II mainly interacts with pocket II of TE. This is evident, as shown by the distance of the hexyl tail to the center of mass of each pocket in each simulation (Fig. 3D). As summarized in Table 3 for all three simulations, the average distance of the hexyl tail in conformation I is closer to pocket I, while the distance of the hexyl tail in conformation II is closer to pocket II, indicating that the hexyl tail has shifted from one pocket to the other.

FIGURE 3

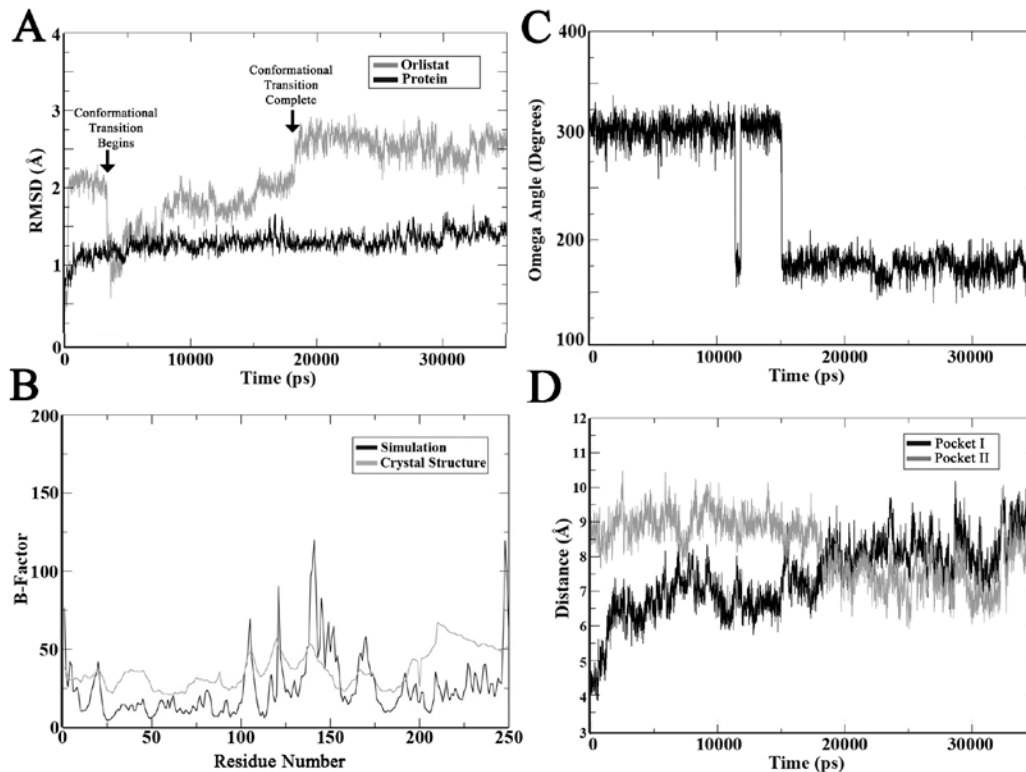


Figure 3. RMSD, B-Factor, ω dihedral angle, and distance of the hexyl tail of covalent-orlistat in the first simulation. (A) RMSD of TE and covalent-orlistat during the first simulation. Times when the conformational transition begins and completes are indicated. (B) Comparison of the B-factor values of each residue between the simulation (black) and the crystal structure (gray) of TE. (C) ω dihedral angle of the hexyl tail of covalent-orlistat in the orlistat-TE complex. (D) Distance of the hexyl tail of covalent-orlistat to the center of mass of pocket I and II in TE.

TABLE 2: Time span of conformation I and II, B factor, ω angles, hexyl tail RMSD and free energy for all three simulations.

	Conf.	First	Second	Third	Crystal Struct.
Time Span (ps)^a	I	0-3,400	0-600	0-4000	N/A
	II	18,250-35,000	4,000-35,000	11,400-35,000	N/A
B-factor^{TE}		43.8 ± 31.0	25.2 ± 19.4	38.64 ± 33.05	36.6
B-factor^{Orlistat}		77.1	69.2	83.4	60.2
RMSD^{Orlistat} (Å)	I	1.94 ± 0.42	0.61 ± 0.15	1.48 ± 0.33	N/A
	II	2.56 ± 0.14	2.19 ± 0.11	2.39 ± 0.31	N/A
ω Angles (°)	I	305.06 ± 11.14	309.73 ± 7.13	304.89 ± 8.90	337.97 ^b
	II	175.75 ± 9.91	175.63 ± 10.11	176.32 ± 8.93	139.54 ^b
$\Delta G^{\text{Covalent-Orlistat}}$ (kcal/mol)	I	-130.29 ± 6.21	-131.05 ± 6.92	-131.60 ± 7.03	N/A
	II	-136.75 ± 5.47	-139.05 ± 6.86	-135.25 ± 7.19	N/A

^aThe time span in which the hexyl tail adopted each conformation in each simulation was determined by examining the RMSD of orlistat in conjunction with the ω angle transition and the distance of the hexyl tail to pocket I and pocket II of the TE protein. The time during which the transition was taking place was not included in our calculations.

^bThe slight difference in the simulated ω angle from the crystal structure may come from crystal packing.

TABLE 3: Average distance of the hexyl tail to pocket I and pocket II within FASN TE.

Conf.	First Simulation		Second Simulation		Third Simulation	
	Pocket I	Pocket II	Pocket I	Pocket II	Pocket I	Pocket II
I (Å)	5.78 ± 0.91	8.79 ± 0.45	4.63 ± 0.52	8.68 ± 0.44	4.76 ± 0.27	8.87 ± 0.36
II (Å)	8.21 ± 0.61	7.45 ± 0.60	7.15 ± 0.30	7.45 ± 0.34	7.74 ± 0.40	7.35 ± 0.32

B5. Interactions of the Hexyl Tail with the Short-Chain and Shift Pockets

As discussed above, there are two pockets of residues that accommodate the hexyl tail of covalent-orlistat (conformation I) and hydrolyzed orlistat (conformation II): the short-chain pocket, consisting of residues Thr²³⁴², Tyr²³⁴³ and Tyr²⁴⁶² and the shift pocket consisting of residues Tyr²³⁰⁹, Tyr²³⁴³ and Ala²⁴³⁰. To examine if the hexyl tail of covalent-orlistat interacts with each set of residues during our simulations, and whether or not the pocket residues match their respective conformations seen in the crystal structure, the average structure of the protein with covalent-orlistat in conformation I and II from a representative simulation was aligned with the crystal structures of covalent-orlistat and hydrolyzed orlistat, respectively. As shown in Figure 4A, the crystal structure residues of covalent-orlistat defining the short-chain pocket were aligned with the short-chain pocket of the average structure of covalent-orlistat in conformation I. The hexyl tail of covalent-orlistat clearly interacts with the short-chain pocket in conformation I, with little interaction with the residues defining the shift pocket. Also, the conformations of residues from the crystal structure and the simulation are fairly similar. As shown in Figure 4B, the crystal structure residues of hydrolyzed orlistat defining the shift pocket were aligned with the shift pocket of the average structure of covalent-orlistat in conformation II, clearly demonstrating that the hexyl tail of covalent-orlistat interacts only with the shift pocket residues. In conformation II, it appears that the conformation of Thr²³⁴² changes drastically between the simulation and the crystal structure (Fig. 4B). This difference is likely the result of orlistat hydrolysis due to crystal packing after the orlistat molecule is hydrolyzed, explaining why this change is not seen during the simulation. In addition, in the crystal structure, Tyr²³⁴³ packs against the hexyl tail of

covalent-orlistat in conformation I, but not the hexyl tail of hydrolyzed orlistat in conformation II. This observation raised the possibility that a conformational change of Tyr²³⁴³ may promote shifting of the hexyl tail. In the simulations, however, the positioning of Tyr²³⁴³ changed very little and it continued to pack against the hexyl tail of covalent-orlistat in conformation II. It is possible that the change in conformation of Tyr²³⁴³ may be a result of the hydrolysis and therefore undergoes the conformational change after the covalent bond is cleaved. Thus, a different conformation of Tyr²³⁴³ is observed in the crystal structure with hydrolyzed orlistat than in the simulations, in which orlistat is covalently bound before hydrolysis. The finding that the hexyl tail of orlistat attached to a 3-mer peptide in the absence of TE, including Tyr²³⁴³, could freely transit between conformations I and II also supports the above conclusion that Tyr²³⁴³ does not promote conformational transition of the hexyl tail.

FIGURE 4

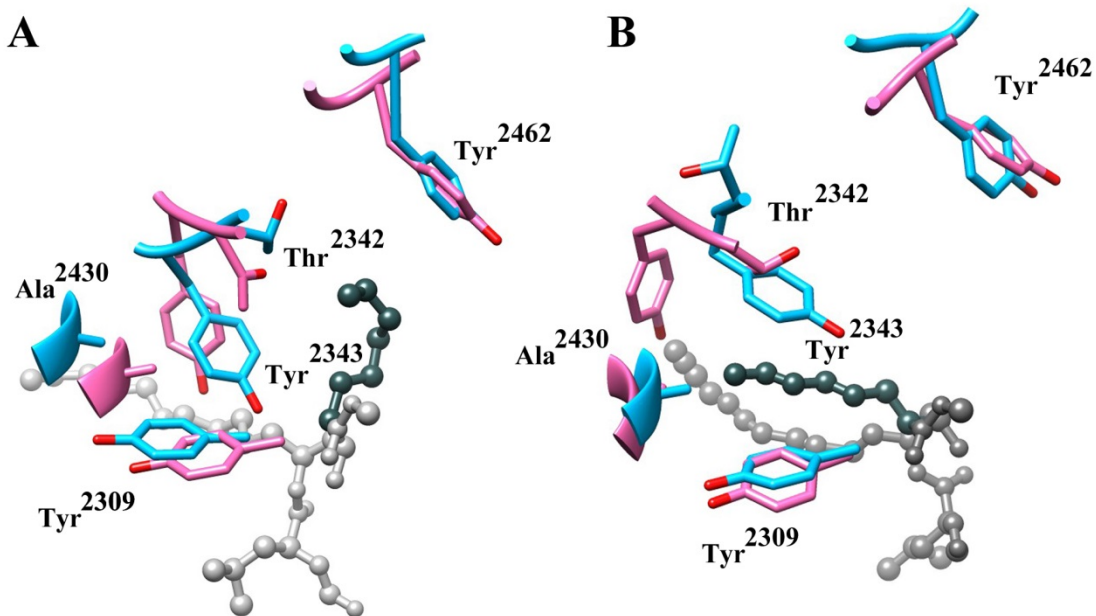


Figure 4. Hexyl tail interactions with short-chain and shift-pocket residues. (A) Short-chain (Thr²³⁴², Tyr²³⁴³ and Tyr²⁴⁶²) and shift pocket (Tyr²³⁰⁹, Tyr²³⁴³, Ala²⁴³⁰) residues when covalent-orlistat adopts conformation I. The crystal structure of covalent-orlistat (blue) is aligned with the average structure of conformation I (pink) in a representative simulation. Orlistat is shown in gray and the hexyl tail is shown in dark gray. (B) Short-chain and shift pocket residues when covalent-orlistat adopts conformation II. The crystal structure of hydrolyzed orlistat (blue) is aligned with the average structure of conformation II (pink) in a representative simulation. Orlistat is shown in gray and the hexyl tail is shown in dark gray.

B6. Crystal Packing Restrains the Covalent-Orlistat Hexyl Tail in Conformation I

The finding that orlistat exists in two different states in the complex structure solved by Pemble *et al.* is interesting because these structures are the result of co-crystallization of TE and orlistat, not a crystal soaking experiment. During the lengthy co-crystallization process, the protein and ligand are co-incubated in solution and can freely react with each other without crystal packing restraints that are present in a crystal soaking experiment. Yet in this condition, only a portion of orlistat is hydrolyzed, suggesting that the non-hydrolyzed covalent-orlistat cannot result solely from crystal packing. Rather, the crystal lattice may selectively pack TE with covalent-orlistat in conformation I from solution in one asymmetric unit and TE with hydrolyzed orlistat in conformation II from solution in another asymmetric unit. Once crystals are formed, the covalent-orlistat in conformation I may not be able to transit to conformation II due to crystal lattice restraint and therefore remains in non-hydrolyzed state. To test the above possibility, a 35-ns MD simulation of the crystal lattice involving chain A and B of FASN TE was performed and the RMSD and ω angle of each covalent-orlistat molecule was examined. Unlike our previous simulations containing only one FASN TE chain, the hexyl tail of the covalent-orlistat molecule appearing at the interface of the crystal lattice was contained in conformation I, as indicated by the ω angle of the hexyl tail (Fig. 5A), and a low and stable RMSD (Fig. 5B), indicating that the hexyl tail is contained in one position, conformation I, throughout the simulation. Interestingly, when examining the covalent-orlistat molecule in chain B, the molecule behaves much more similarly to the covalent-orlistat molecules from our FASN TE monomer simulations, with a transition

from conformation I to II, as noted by orlistat RMSD and single ω shift from conformation I to II.

We also sought to determine which crystal contacts are responsible for stabilizing covalent-orlistat in the crystal lattice. We found that Arg²³⁵², Thr²³⁵⁶, Pro²³⁵⁷, Gly²³⁵⁸, Cys²³⁵⁹, Glu²³⁶⁰, and Ala²³⁶¹ from chain B are likely the crystal contacts responsible for constraining the crystal lattice and the orlistat molecule in chain A. In addition, Tyr²³⁴⁷ and Thr²³⁴⁸ from chain B are responsible for stabilizing the short-chain pocket that accommodates the hexyl tail in conformation I in chain A.

FIGURE 5

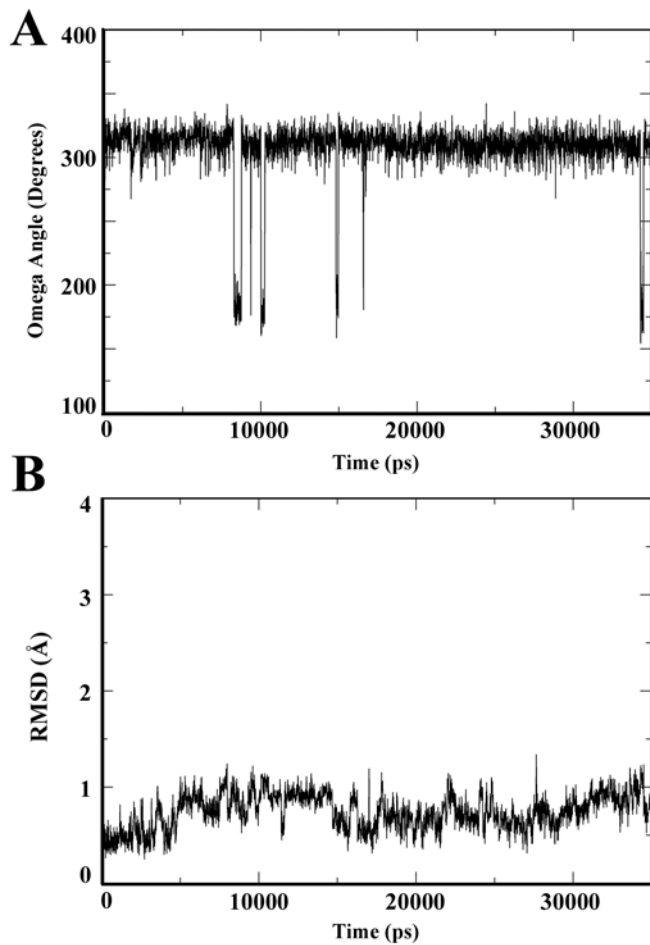


Figure 5. Crystal lattice simulation ω dihedral angle and RMSD. (A) ω dihedral angle of the hexyl tail of the covalent-orlistat molecule within the Chain A of the complex. (B) RMSD of this covalent-orlistat during this simulation.

B7. Accessibility of Water Molecules to the Active Site

Previously, it was proposed that the hexyl tail in covalent-orlistat packs against His²⁴⁸¹ of the catalytic triad, preventing access of a water molecule needed for hydrolysis of the covalent bond between orlistat and Ser²³⁰⁸. The shift of the hexyl tail may provide water molecules access to the TE active site for hydrolysis [213]. To test this hypothesis, water molecules in the active site were analyzed before and after the conformational transition of the hexyl tail. Because it has been shown previously that a water molecule can be potentially activated if the distance of the water molecule is ≤ 3.5 Å to the catalytic nitrogen of histidine and ≤ 4.0 Å to the carbonyl carbon atom of the covalent bond between orlistat and serine [303-305], only water molecules that satisfied these criteria were considered and were used to calculate the water occupancy in the active site with the hexyl tail in both conformations I and II during the simulations. Under this stringent condition, the average water occupancy of the three simulations (Table 4) in conformations I and II are 21.2 % and 30.6 % (Fig. 6B), respectively. Thus, it appears that in both conformations, the active site can be occupied by a water molecule for a significant amount of the time. The hexyl tail in conformation I does not block the active site and prevent water access. In addition, transition to conformation II does not significantly increase water access to the active site.

B8. Catalytically Critical Interactions at the Active Site

Next, it was determined whether the conformational transition of the hexyl tail might affect any catalytically important interactions in the active site by first examining the stability of the conserved salt bridge between Asp²³³⁸ and His²⁴⁸¹, which is

catalytically important because it orients His²⁴⁸¹ to deprotonate a water molecule for nucleophilic attack [293] (Fig. 6A). The average occupancy of this salt bridge (the oxygen atom of Asp²³³⁸ within 3.5 Å of the nitrogen atom of His²⁴⁸¹) in three simulations (Table 4) is 99.5 % in conformation I and 93.9 % in conformation II (Fig. 6B). These observations suggest that Asp²³³⁸ and His²⁴⁸¹ couple tightly both before and after conformational transition of the hexyl tail and that the conformational transition does not significantly affect the stability of this salt bridge.

In addition to the salt bridge, a hydrogen bond between the catalytic nitrogen of His²⁴⁸¹ and the hydroxyl moiety of covalent-orlistat was also identified (Fig. 6A). In contrast to the occupancy of the Asp²³³⁸-His²⁴⁸¹ salt bridge, the average occupancy of this hydrogen bond over all three simulations (Table 4) dropped significantly from 55.8 % in conformation I to 19.3 % in conformation II (Fig. 6B). This agrees with the distance between the catalytic nitrogen atom of His²⁴⁸¹ and the oxygen atom of the hydroxyl moiety in covalent-orlistat in each conformation, which increased from 2.91 ± 0.21 Å in conformation I to 4.63 ± 0.99 Å in conformation II in the first simulation (Table 4). A similar increase in this distance was also observed for the second and third simulations (Table 4). These results indicate that in each simulation, the potential for orlistat and His²⁴⁸¹ to form a strong hydrogen bond is diminished following the conformational transition. Therefore, the conformational transition of the hexyl tail does not appear to affect the salt bridge, but destabilizes the hydrogen bond between the catalytic nitrogen of His²⁴⁸¹ and the hydroxyl moiety of covalent-orlistat.

B9. Activation of Catalytic Water Molecules

To further understand how the conformational change of the hexyl tail affects catalysis, the presence of potentially activated water molecules in the active site of TE with orlistat in both conformations were investigated using the following criteria: A catalytically active water molecule (a) must strongly hydrogen bond with His²⁴⁸¹ (at a distance ≤ 3.0 Å); (b) must be ≤ 4.0 Å from the carbonyl carbon atom of covalent-orlistat for nucleophilic attack; and (c) must form an optimal catalytic orientation angle of $105^\circ \pm 5^\circ$ with the carbonyl carbon and the carbonyl oxygen (Fig. 6C) [306]. As shown in Fig. 6D, the average occupancy of water molecules that meet all three criteria is significantly increased from 0.1 % in conformation I to 4.6 % in conformation II (see also Table 4). This observation suggests that, when the hexyl tail adopts conformation I, a water molecule is unlikely to be catalytically activated, and the possibility of catalytic activation is significantly increased after the hexyl tail transitions to conformation II.

B10. Correlation of Interactions in the Active Site

To understand how the conformational transition may affect the potential activation of a water molecule for catalysis, the ability of water molecules to form strong hydrogen bonds (≤ 3.0 Å) with the catalytic nitrogen of His²⁴⁸¹ was examined before and after the conformational transition of the hexyl tail. As shown in Fig. 4B and Table 4, the average occupancy of water molecules that can strongly hydrogen bond with His²⁴⁸¹ is increased from 11 % in conformation I to 40 % in conformation II with a near significance ($p=0.051$).

Considering that there is a decrease in hydrogen bonding between His²⁴⁸¹ and the hydroxyl moiety of covalent-orlistat and an increase in hydrogen bonding between His²⁴⁸¹ and water (Fig. 6B), it is possible that these two events are correlated. To test this possibility, the occupancy of the hydrogen bond between His²⁴⁸¹ and covalent-orlistat when there is a water molecule in the active site that satisfies all catalytic criteria was calculated, which was 0.7 %, 0.8 % and 1.0 % in the first, second and third simulation, respectively. Then, a correlation analysis was performed comparing the occupancy of the hydrogen bond between His²⁴⁸¹ and covalent-orlistat and the occupancy of activated water molecules that satisfy all criteria for a catalytic interaction in both conformations I and II. As shown in Fig. 6E, there is a clear trend of linear correlation between these occupancies with a correlation coefficient of 0.94, indicating that a water molecule is more likely to catalytically interact with orlistat in the absence of the hydrogen bond between covalent-orlistat and His²⁴⁸¹. Together, the above findings suggest that the hydrogen bond between covalent-orlistat and His²⁴⁸¹ may need to be abrogated to successfully activate a catalytic water molecule.

FIGURE 6:

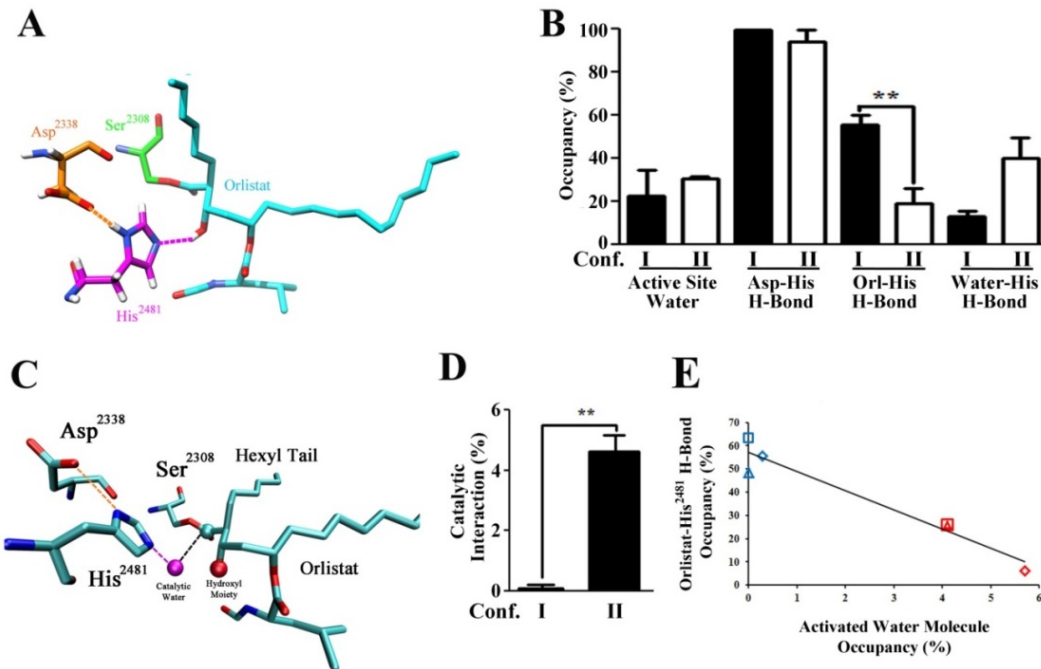


Figure 6. Catalytically important interactions at the active site. (A) Hydrogen bond between His²⁴⁸¹ and covalent-orlistat (magenta dashed line) and the salt bridge between His²⁴⁸¹ and Asp²³³⁸ (orange dashed line) in simulated conformation I of orlistat. Ser²³⁰⁸, Asp²³³⁸ and His²⁴⁸¹ residues of TE are depicted in green, orange and magenta, respectively. (B) Average occupancies of the active site water molecules and Asp²³³⁸-His²⁴⁸¹, orlistat-His²⁴⁸¹, and water-His²⁴⁸¹ hydrogen bonds in conformations I and II for all three simulations. (**p<0.01). (C) Activated water molecule in the active site of TE for nucleophilic attack of the covalent bond between orlistat and Ser²³⁰⁸ (black dashed line). The water molecule, the hydroxyl moiety oxygen and the carbonyl carbon are depicted as spheres. The salt bridge between Asp²³³⁸ and His²⁴⁸¹ is shown by the orange dashed line. (D) Average occupancy of activated water molecules in conformations I and II. (**p<0.01). (E) Correlation between the occupancy of the orlistat-His²⁴⁸¹ hydrogen

bond and the occupancy of activated water molecules in conformations I (blue points) and II (red points) of the first (\diamond), second (\square) and third (Δ) simulation.

TABLE 4: Catalytically important interactions at the active site.

	Conf.	First Simulation	Second Simulation	Third Simulation
Active Site Water Occupancy (%)	I	10.6	41.6	11.5
	II	31.4	28.9	31.5
Occupancy of Asp²³³⁸-His²⁴⁸¹ Salt Bridge (%)	I	100	98.4	100
	II	82.2	99.6	99.9
Occupancy of Orlistat-His²⁴⁸¹ H-Bond (%)	I	55.6	63.3	48.5
	II	6.0	25.9	25.9
Orlistat-His²⁴⁸¹ H-Bond Distance (Å)	I	2.91 ± 0.21	2.83 ± 0.13	2.90 ± 0.18
	II	4.63 ± 0.99	3.51 ± 0.65	3.53 ± 0.70
Occupancy of H₂O-His²⁴⁸¹ H-Bond (%)	I	14.1	8.3	17.0
	II	57.8	36.9	25.6
Occupancy of Activated H₂O Molecule (%)	I	0.3	0.0	0.0
	II	5.7	4.1	4.1

B11. Simulation of Truncated Orlistat Lacking the Hexyl Tail

The above findings suggest that the hexyl tail in conformation I may help to stabilize the hydrogen bond between His²⁴⁸¹ and covalent-orlistat. To test this possibility, an MD simulation analysis using a truncated covalent-orlistat lacking the hexyl tail was performed (Fig. 7A). For this purpose, the hexyl tail of covalent-orlistat in the crystal structure was virtually removed, parameterized, and simulated similarly as described above for the intact orlistat. Fig. 7B shows that the hydrogen bond between His²⁴⁸¹ and the hydroxyl group of truncated covalent-orlistat was spontaneously and quickly disrupted at 8,190 ps. It remained in a disrupted state and did not re-form for any significant amount of time during the remainder of the simulation. Interestingly, the occupancy of water molecules that can be potentially activated before and after disruption of the hydrogen bond is 0.9 % and 4.3 %, respectively (Fig. 7C), which is consistent with the observations made for intact covalent-orlistat (Fig. 6D). Taken together with the results for intact covalent-orlistat, it is likely that the hexyl tail in conformation I stabilizes the hydrogen bond between His²⁴⁸¹ and covalent-orlistat, which prevents His²⁴⁸¹ from hydrogen bonding with and properly orienting and activating a water molecule for catalysis in the active site.

FIGURE 7:

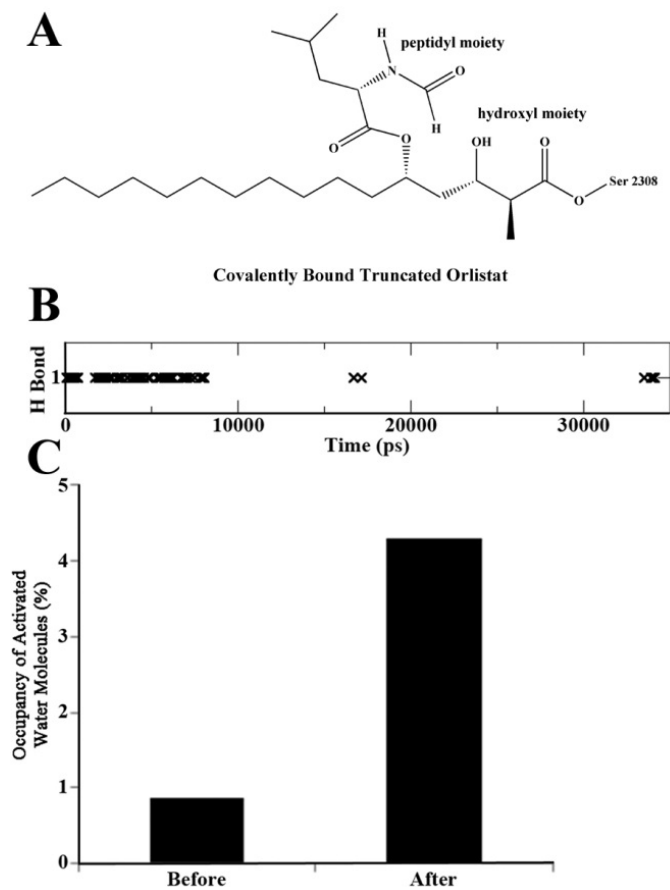


Figure 7. Simulation of truncated orlistat (A) lacking the hexyl tail in TE showing (B) the presence of the hydrogen bond between the truncated covalent-orlistat and His²⁴⁸¹ and (C) occupancy of activated water molecules in the active site of TE before and after the spontaneous disruption of the hydrogen bond between truncated covalent-orlistat and His²⁴⁸¹.

C. Conclusions and Discussion

The co-crystal structure of human FASN TE with orlistat (ID: 2PX6) shows that orlistat is present in the active site of TE in two states: as a covalently-bound intermediate and as a hydrolyzed product. The hexyl tail of orlistat in these two different states adopts two different conformations (I and II). Using MD simulations, I found that covalent-orlistat can adopt both conformations prior to hydrolysis. Further investigation shows that transition to conformation II is required for hydrolysis of covalent-orlistat, which destabilizes a hydrogen bond between the catalytic His²⁴⁸¹ of TE and the hydroxyl moiety of orlistat, leading to formation of a hydrogen bond between His²⁴⁸¹ and water molecules and allowing for the activation of a water molecule to hydrolyze the covalent bond between orlistat and Ser²³⁰⁸.

The finding that orlistat exists in two different states in the complex structure solved by Pemble *et al.* is informative and consistent with the findings of our simulations [213]. As these observed structures are from co-crystallization of TE and orlistat, not from crystal soaking, orlistat may have been hydrolyzed by TE during the crystallization process. Because the hexyl tail in covalent- and hydrolyzed orlistat adopts two different conformations with ω dihedral angles of $\sim 340^\circ$ (conformation I) and $\sim 140^\circ$ (conformation II), and because covalent-orlistat can also adopt conformation II during simulation analysis, the shift of the hexyl tail from conformation I to II likely contributes to the hydrolysis. It is also noteworthy that the un-hydrolyzed covalently-bound orlistat intermediate was found in the co-crystal structure despite the lengthy co-crystallization process involving co-incubation of TE and orlistat, suggesting that hydrolysis of orlistat by TE may be a slow process.

In all simulations, the hexyl tail of covalent-orlistat undergoes a conformational transition in which the RMSD of covalent-orlistat changed; the ω angle shifted from $\sim 310^\circ$ to $\sim 170^\circ$; and the hexyl tail shifted its interaction from TE pocket I to TE pocket II; which together recapitulate the two conformations observed in the crystal structure. The two ω angles coincide with the two local minima calculated during the dihedral energy scan and represent conformations I and II found in the crystal structure, albeit with a phase difference compared with the crystal structure, which is likely due to crystal packing. One limitation of this study is that the simulations are short, and therefore a complete reverse transition of the covalent-orlistat hexyl tail from conformation II back to conformation I is not observed, which might take place upon longer simulation. However, physiologically, such a reverse transition is unlikely, based on the finding that when the hexyl tail transitions to conformation II, water molecules could be readily activated to hydrolyze covalent-orlistat. It is tempting to speculate that the conformational transition of the hexyl tail may be a rate-limiting step of orlistat hydrolysis, after which the hydrolysis step occurs very quickly, and the hexyl tail is unlikely able to reverse back to conformation I following the hydrolysis. Consistent with these speculations, covalent-orlistat is not found in conformation II and hydrolyzed orlistat is not found in conformation I in the co-crystal structure. Most importantly, these simulations have demonstrated that a hydrogen bond exists between the catalytic His²⁴⁸¹ residue and covalent-orlistat, which may control orlistat hydrolysis. It appears that in conformation I, the strong interaction between the catalytic nitrogen atom of His²⁴⁸¹ and the hydroxyl moiety of covalent-orlistat greatly prevents water molecules from hydrogen bonding with the same atom of His²⁴⁸¹ and from adopting the proper orientation for

activation and catalysis. Upon transition of the hexyl tail from conformation I to II, the hydrogen bond between His²⁴⁸¹ and covalent-orlistat is disrupted, which frees and enables His²⁴⁸¹ to hydrogen bond with and activate water molecules to attack the carbonyl carbon of the orlistat-Ser²³⁰⁸ residue. In the co-crystal structure, the distance between the catalytic nitrogen atom of His²⁴⁸¹ and the hydroxyl moiety of covalent-orlistat is 3.9 Å in conformation I and 5.4 Å in conformation II. Although a distance of 3.9 Å in conformation I indicates a weak electrostatic interaction, it also indicates a good proximity for forming a potential hydrogen bond, considering that the crystal structure is a still snapshot of a protein, subjected to crystal packing, and may not capture the hydrogen bonding event. Nevertheless, both the crystal structure and simulation data suggest stronger interactions between the catalytic nitrogen atom of His²⁴⁸¹ and the oxygen atom of the hydroxyl group of covalent-orlistat in conformation I than in conformation II.

The stronger interaction between the catalytic nitrogen atom of His²⁴⁸¹ and the oxygen atom of the hydroxyl group of covalent-orlistat in conformation I may be due to the hexyl tail in conformation I creating restraints that favor this interaction. Simulation of TE-covalently-bound to a truncated orlistat lacking the long hexyl tail shows that the hydrogen bond between His²⁴⁸¹ and the hydroxyl moiety of truncated covalent-orlistat is quickly and spontaneously disrupted, accompanied with an increase in activated water molecules in the active site for hydrolysis. Thus, the truncated orlistat may be more easily hydrolyzed than the intact orlistat. Interestingly, it has been found previously that ebelactone B, a β -lactone compound containing an ethyl group in the same position as the hexyl tail of orlistat, was more effective in inhibiting FASN TE activity than ebelactone

A, which contains a methyl group [212], leading to the speculation that this moiety may be important for stabilizing the ligand in the TE active site and protecting it from hydrolysis [225,307]. We speculate that longer aliphatic carbon moieties in this position on the inhibitor may aid in the stabilization of the hydrogen bond that forms between His²⁴⁸¹ and the hydroxyl moiety of the compound, perhaps by preventing conformational changes in the core of the ligand that could potentially disrupt the hydrogen bond. The simulation data supports this hypothesis by demonstrating that the hexyl tail in conformation I is needed to stabilize the hydrogen bond that forms between His²⁴⁸¹ and the hydroxyl moiety of orlistat, which helps to prevent hydrolysis of the inhibitor. This stabilization is lost when the hexyl tail is virtually truncated, or undergoes transition, likely leading to rapid hydrolysis shortly thereafter.

Considering that FASN over-expression causes increased metastatic potential, poorer prognosis, and resistance toward cancer chemotherapeutics in a wide variety of human cancers [94,96,148,149,178,308-312], targeting the fatty acid synthesis pathway may be a useful strategy for the treatment of cancer. Previous studies have shown that orlistat is nearly 1000-fold more potent in inhibiting pancreatic lipases than the hydrolyzed orlistat [222,313], thus, it is likely that hydrolyzed orlistat is likely also a very poor inhibitor of FASN TE. Information from this study may aid in the rational design of TE inhibitors that are resistant to hydrolysis and inactivation, and are thus more potent for anticancer treatment. One possible strategy is to design compounds that use and stabilize the hydrogen bond between the drug and His²⁴⁸¹, therefore inhibiting the activation of a water molecule by His²⁴⁸¹ for catalysis. Another strategy for next generation compound design may be to use moieties that block the space in the active site

near His²⁴⁸¹ that water molecules must occupy for activation. This may be achievable, as it has previously been shown in a similar case of inhibitors of *E. coli* TEM-1 β -lactamase. Although β -lactamases have a different catalytic triad than that of TE, they contain an active site Ser, and inhibitors of β -lactamase, such as penicillanic acid, inhibit the enzyme by acetylation of this active site Ser [314]. A modified form of penicillanic acid, 6 α -(hydroxymethyl) penicillanate, created by incorporating a hydroxymethyl moiety designed to displace the catalytic water molecule in the active site, resulted in a retarded rate of hydrolysis of the acyl-enzyme intermediate [315]. The mechanism of action was later confirmed by x-ray crystallography [315].

Chapter 4: Aim II: Identification of FDA Approved Proton Pump Inhibitors as Inhibitors of Human Fatty Acid Synthase Thioesterase

A. Background and Rationale

In a majority of drug discovery research projects, lead compounds for a desired biological target are discovered by manually screening large libraries of compounds in a process known as high-throughput screening (HTS). An alternative strategy for drug discovery is to employ an *in-silico* screening method, in which virtual compound ligands are computationally matched to a receptor with known structure [316]. This technique was first envisioned in the 1970s, when investigators suggested that it may be possible to use computational simulations to predict the chemical interactions of ligands within receptors with elucidated structure [317,318]. A method for performing such screening was first described in the early 1980s, when the interaction between heme and myoglobin, as well as the binding of thyroid hormone analogs to prealbumin, was examined. The algorithms correctly predicted the binding of ligands to within 1 Å of x-ray crystallography results, and also predicted other binding modes with good steric fit to the receptors [319]. A number of studies have also demonstrated the utility of *in-silico* screening and validating its use as a drug discovery tool [320,321]. In particular, a study examining and comparing HTS and *in-silico* screening for new inhibitors of protein tyrosine phosphatase-1B, a target for type II diabetes, showed that *in-silico* screening is more advantageous than HTS. In this study, a virtual library of 235,000 compounds was docked into the receptor, resulting in 365 of the top-scoring compounds for further test, while 400,000 compounds were screened against the target using traditional HTS

methods. Of the 400,000 compounds tested, HTS yielded 85 compounds with IC₅₀ values less than 100 μM (6 with an IC₅₀ less than 10 μM) with a hit rate of 0.0021 %. Of the 365 compounds yielded from the *in-silico* screening, 127 compounds had IC₅₀ values less than 100 μM (18 with an IC₅₀ less than 10 μM), resulting in a hit rate of 34.8 %. Thus, *in-silico* screening enriched the potential hit rate by approximately 1700 fold [322]. The compounds suggested by *in-silico* screening were also more ‘drug-like’ in character, with a higher number of compounds adhering to Lipinski’s rule of five for drug-likeness, which are parameters used to estimate the solubility and membrane permeability of potential drug candidates. Poor absorption and bioavailability, or the amount of unchanged drug that reaches the systemic circulation, are likely when a drug candidate has more than 5 hydrogen bond donors; more than 10 hydrogen bond acceptors; a molecular weight of greater than 500 Da; and a calculated water/octanol partition coefficient (CLogP) of greater than 5 [323]. Interestingly, hit compounds yielded from HTS and *in-silico* screening were dissimilar, suggesting that the two methods could be complimentary and that using both may increase the success rate of finding a useful lead compound. Indeed, the usefulness of *in-silico* screening methods has been demonstrated, as there are several examples of drugs on the market that have arisen from *in-silico* screening, including Viracept, a human immunodeficiency virus (HIV) protease inhibitor, and Relenza, an anti-influenza drug [316,324,325].

In this study, *in-silico* ligand screening with virtual ligand libraries was used to search for novel inhibitors of FASN TE using the DOCK suite of programs. In previous studies, DOCK software has successfully produced potent hits with anti-tumor activity for various proteins implicated in cancer including BCR-ABL [326], protein kinase CK2

[327], and BCL2/BCL-XL [328]. DOCK screening works by first using the sphgen program within DOCK to generate a set of spheres that describe the active site, or desired binding pocket, of the receptor [282]. The spheres are used to approximate the positions of ligand atoms within the active site of the receptor. Then, scoring grids are generated using the grid program within DOCK. These grids evaluate the position of, and rapidly score, each ligand based on size and shape complementarity to the receptor active site, removing any ligands that have a high amount of steric interference with any active site residues. Ligands with the highest scores from the first round of docking were then subjected to AMBER scoring, which employs energy minimization and molecular dynamics simulations to evaluate the energy of the binding between each ligand and the receptor. The AMBER score is represented by electrostatic and van der Waals interactions, and the solvation energy of the ligand in complex with the receptor is calculated using the Generalized Born solvation model [329]. The final AMBER score is given as the $E(\text{Complex}) - [E(\text{Receptor}) + E(\text{Ligand})]$, with the solvated internal energies of each component approximated by the AMBER force field [281].

To fully investigate the FASN TE protein and to increase the probability of finding a novel inhibitor of TE activity, both *in silico* and HTS approaches were used. First, two compound libraries were virtually screened for this study: the ChemDiv library containing over 200,000 compounds and a library of FDA approved drugs containing approximately 2,000 compounds. Using a high-throughput fluorogenic assay with recombinant FASN TE protein to determine the ability of selected compound candidates to inhibit TE activity, a total of 81 compounds from the ChemDiv library and 34 compounds from the FDA approved library were tested. A novel compound from the

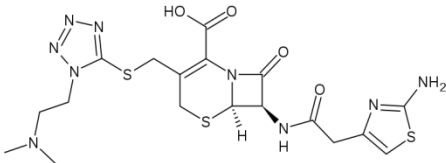
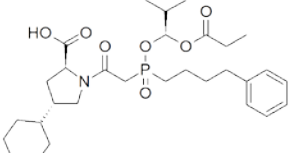
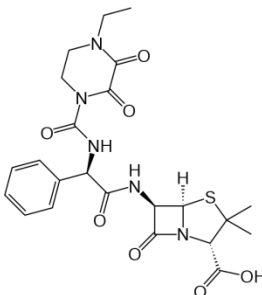
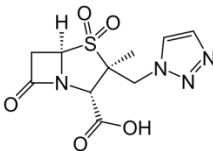
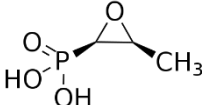
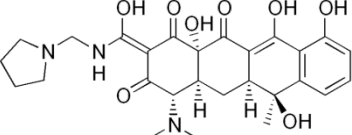
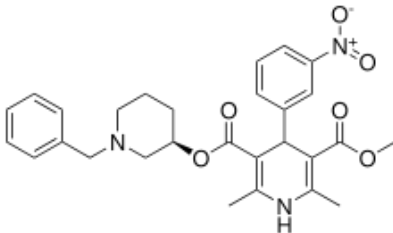
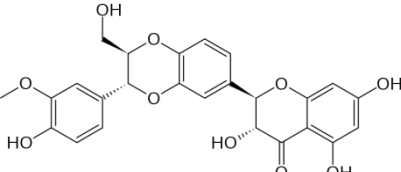
ChemDiv library, designated 13C, inhibited FASN TE activity and was found to inhibit cellular proliferation in subsequent *in vitro* assays, but was not investigated further because it failed to inhibit lipid synthesis *in vitro*. Results detailing this compound can be found in Appendix D. However, another top-scoring compound from the virtual screen, pantoprazole, a proton pump inhibitor from the FDA approved library, inhibited TE activity in a dose-dependent manner. It was determined that other PPIs from the class, omeprazole, esomeprazole, lansoprazole and rabeprazole, were also effective in inhibiting TE activity, demonstrating their potential utility for inhibiting FASN, and thus satisfying Specific Aim II of this project. As a number of studies have found that treatment with PPIs can inhibit cancer cell proliferation, these results provide a potential novel mechanism by which PPIs may be acting in cancer cells, thus warranting further investigation.

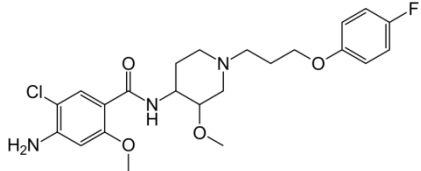
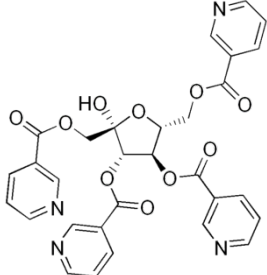
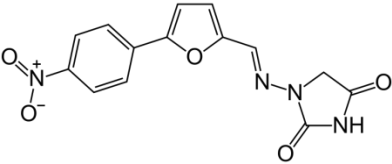
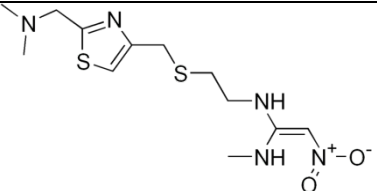
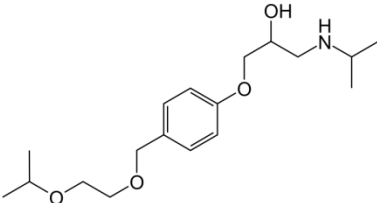
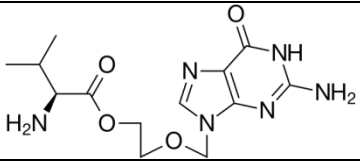
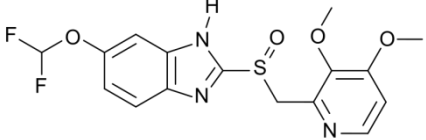
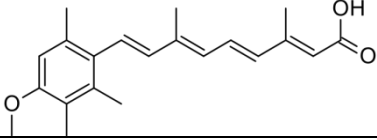
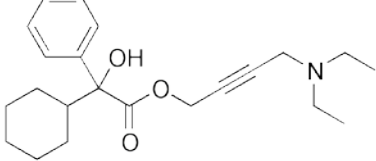
B. Results

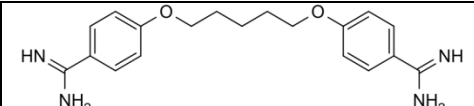
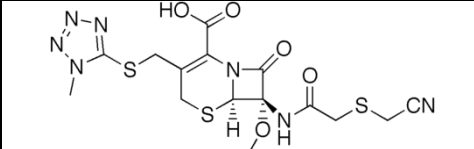
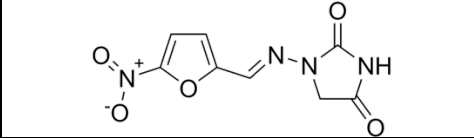
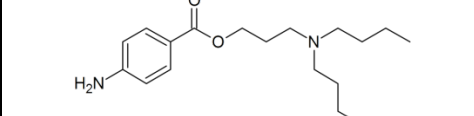
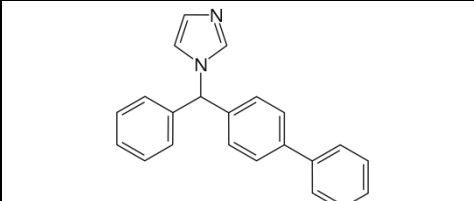
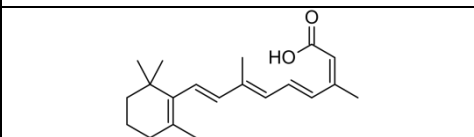
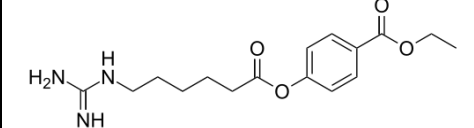
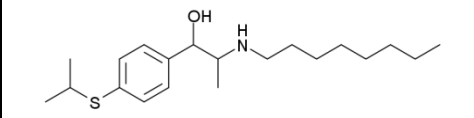
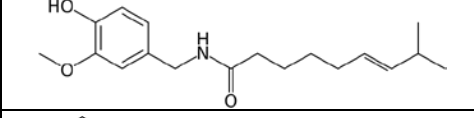
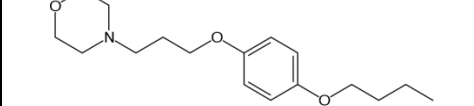
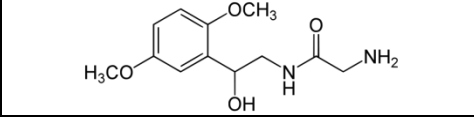
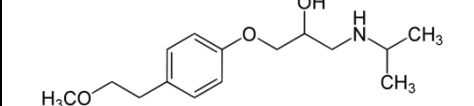
To search for novel inhibitors of the TE domain of human FASN, the highly-resolved FASN TE crystal structure with a polyunsaturated fatty acid adduct [280] was obtained from the RCSB protein data bank and was prepared for *in-silico* ligand screening using the DOCK suite of programs (see Chapter 2). This FASN TE crystal structure was chosen for *in-silico* screening because it is more highly resolved at 1.48 Å, instead of the previously published crystal structure of FASN TE with orlistat in the active site that was used for modeling experiments (see Chapter 3), which is resolved at 2.3 Å. A library containing approximately 2,000 FDA approved ligands was downloaded from the ZINC database. The grid program within DOCK was used to score each ligand

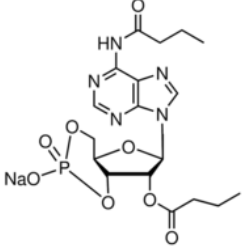
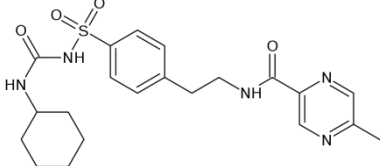
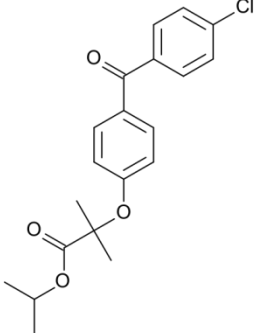
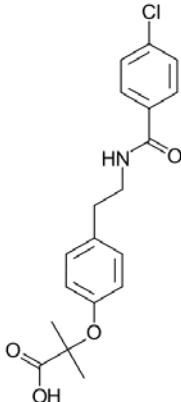
based on shape and size complementarity to the active site. The 200 top-scoring compounds were then subjected to AMBER scoring, which predicted the binding energy of each ligand in the active site. To select the group of compounds that would be further tested, all 200 ligands subjected to AMBER scoring were grouped based on chemical structure using the clustering tool Library MCS. Each cluster was visually examined within the TE active site using the Chimera visualization program to choose compounds that could potentially interact favorably with FASN TE residues through hydrogen bonding or other electrostatic interactions, such as hydrophobic interactions or pi-pi interactions. Any compound exhibiting a positive AMBER score was discarded. Representative compounds from each cluster were chosen based on AMBER score and the potential for favorable binding in the FASN TE active site. Ligands containing lactone or lactam moieties, or other moieties that could potentially be nucleophilically attacked by the active site serine to form a covalent bond, such as an epoxide ring, were given special preference, as were compounds containing long-chain hydrocarbon moieties. The final 34 compounds (Table 1), which met all above criteria, were selected for further examination.

TABLE 1: 34 selected FDA approved compounds from DOCK screening.

FDA Approved Compound Candidate	Structure	Use	
FDA1	Cefotiam	 <p>Chemical structure of Cefotiam, a cephalosporin antibiotic. It features a central beta-lactam ring fused to a six-membered dihydrothiazine ring, with a carboxylic acid group and a side chain containing a thiazolidine ring and a tetrazole ring.</p>	Cephalosporin antibiotic
FDA2	Fosinopril	 <p>Chemical structure of Fosinopril, an angiotensin converting enzyme inhibitor. It consists of a dihydrothiazine ring system with a phosphonic acid group and a side chain containing a cyclohexane ring and a benzyl group.</p>	Angiotensin converting enzyme inhibitor for hypertension
FDA3	Piperacillin	 <p>Chemical structure of Piperacillin, a beta-lactam antibiotic. It features a piperidine ring fused to a beta-lactam ring, with a side chain containing a phenyl ring and a carboxylic acid group.</p>	Beta-lactam antibiotic
FDA4	Tazobactam	 <p>Chemical structure of Tazobactam, a beta-lactamase inhibitor. It consists of a beta-lactam ring fused to a thiazolidine ring, with a side chain containing a carboxylic acid group and a thiazolidine ring.</p>	Beta-lactamase inhibitor
FDA5	Fosfomycin	 <p>Chemical structure of Fosfomycin, an antibiotic. It consists of a five-membered phosphonate ring with a methyl group and a hydroxyl group.</p>	Antibiotic
FDA6	Roli-tetracycline	 <p>Chemical structure of Roli-tetracycline, a tetracycline antibiotic. It features a tetracycline core with a piperidine ring and a methyl group.</p>	Tetracycline antibiotic
FDA7	Benidipine	 <p>Chemical structure of Benidipine, a calcium channel blocker. It features a piperidine ring with a side chain containing a benzene ring, a nitro group, and a methyl group.</p>	Ca ⁺ channel blocker for hypertension
FDA8	Silibinin	 <p>Chemical structure of Silibinin, a flavonoid. It consists of a flavone core with multiple hydroxyl groups and a methoxy group.</p>	Antihepatotoxic and has <i>in vitro</i> anti-cancer effects

FDA9	Cisapride		Gastroprokinetic agent
FDA 10	Nicofuranose		Hypolipidemic agent
FDA 11	Dantrolene		Muscle relaxant
FDA 12	Nizatidine		H ₂ receptor agonist for acid reflux treatment
FDA 13	Bisoprolol		Beta blocker
FDA 14	Valacyclovir		Antiviral for herpes treatment
FDA 15	Pantoprazole		Proton pump inhibitor for acid reflux treatment
FDA 17	Acitretin		Retinoid for psoriasis treatment
FDA 18	Oxybutynin		Anticholinergic for frequent urination

FDA 19	Pentamidine		Antimicrobial
FDA 20	Cefmetazole		Cephalosporin antibiotic
FDA 21	Furaltadone		Antibiotic
FDA 22	Butacaine		Local anesthetic
FDA 23	Bifonazole		Imidazole antifungal
FDA 24	13-cis-retinoic acid		Accutane, acne treatment
FDA 25	Gabexate		Serine protease inhibitor for treatment of pancreatitis
FDA 26	Sulcotidil		Vasodilator
FDA 27	Capsaicin		Active component of chili peppers
FDA 28	Pramoxine		Topical anesthetic
FDA 29	Midodrine		Vasopressor/ Antihypertensive
FDA 30	Metoprolol		Beta blocker

FDA 31	Dibutyryl-adenosine		cAMP analog
FDA 32	Glipizide		Anti-diabetic
FDA 33	Fenofibrate		Cholesterol lowering drug
FDA 34	Bezafibrate		Cholesterol lowering drug

These 34 compounds were then examined for their ability to inhibit TE activity using a fluorogenic assay with recombinant TE protein. The compound 4-methylumbelliferyl heptanoate (4-MUH), which contains an ester moiety, is not fluorescent. However, when the ester bond is cleaved by TE, the product, 4-methylumbelliferone (4-MU), fluoresces, providing a read-out for thioesterase activity. First, recombinant TE protein was expressed and purified, and confirmed by Western blot (Fig. 1A, also see Chapter 2), and the kinetic parameters of the protein were determined. The K_m of the protein, which is equivalent to the concentration required to achieve 50 % of the maximal velocity (v_{max}), was determined by incubating FASN TE with various concentrations of 4-MUH and obtaining the fluorescence readout. A standard curve using 4-MU was determined to quantify the product from TE catalysis (Fig. 1B), which was modeled into a Lineweaver-Burk plot (Fig. 1C) to ensure that a linear pattern of increasing fluorescence units vs. 4-MUH concentration was achieved [291]. The data were then fit using WinNonlin v2.0 software (Pharsight) with a 1 enzyme model with no weighing of the data (Fig. 1D). The K_m of the protein was determined to be 38.45 μ M.

FIGURE 1

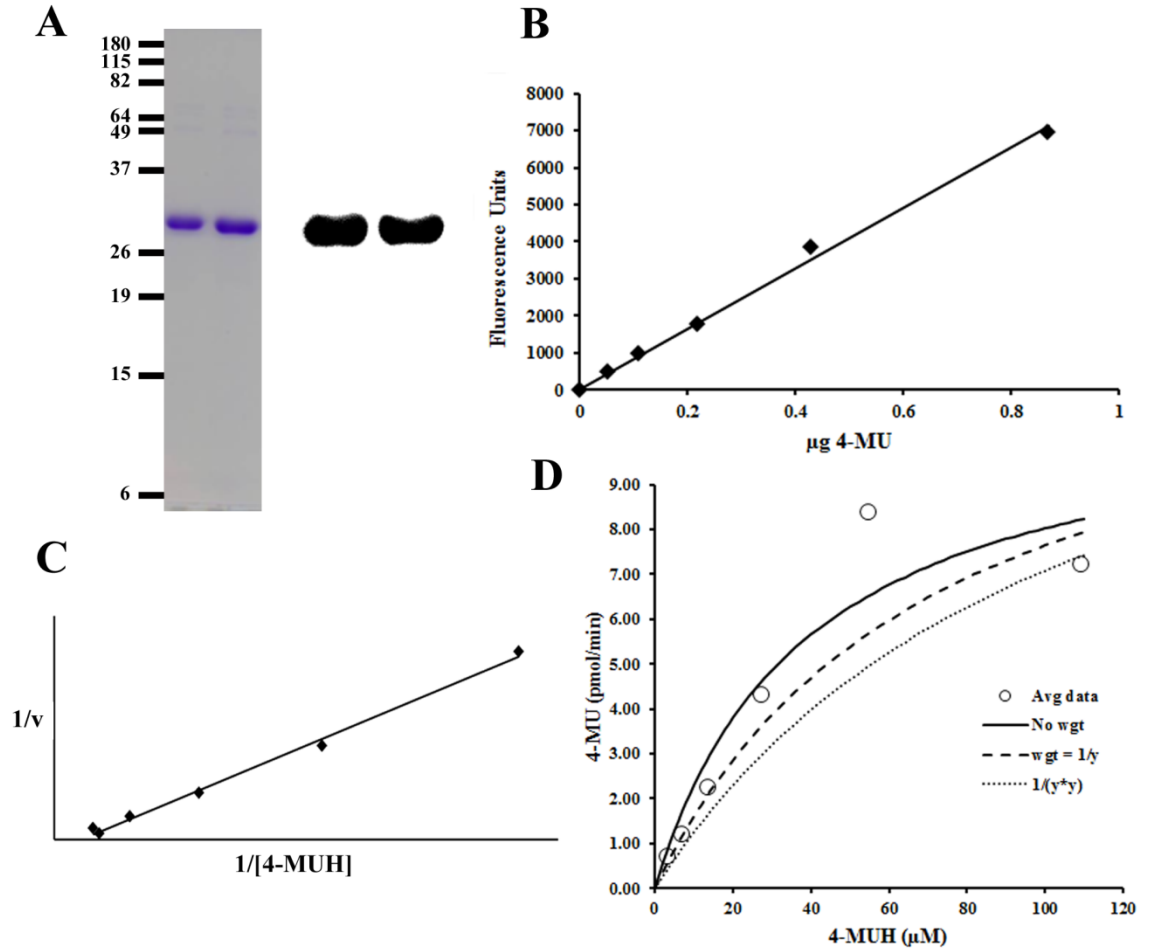


Figure 1: Determination of FASN TE kinetic parameters. (A) Recombinant FASN TE was expressed and purified. The purity of duplicate samples of the protein was confirmed with SDS-PAGE (left panel), and the presence of FASN TE was confirmed in duplicate samples via Western blot (right panel). (B) Standard curve plotting the fluorescence units yielded vs. μg of the fluorescent 4-MU. (C) Lineweaver-Burk plot of FASN TE activity. (D) The kinetic parameters of FASN TE were determined by plotting 4-MU product formed (pmol/min) vs. the substrate concentration (μM 4-MUH). The K_m of the protein was determined using a 1 enzyme model with no weighing of the data.

Next, to determine if any of the selected compounds were able to inhibit FASN TE, 100 μM of each compound candidate was incubated with TE and 4-MUH. Orlistat, a known inhibitor of FASN TE [212], was used as a positive control (Fig. 2A). Compounds FDA15, 24 and 26, which reduced $\geq 40\%$ of enzyme activity ($p < 0.001$), were selected for further investigation. Although FDA24, 13-*cis*-retinoic acid, and FDA26, sulcotidil, failed to inhibit FASN TE in a dose-dependent manner (data not shown), FDA15, pantoprazole, inhibited FASN TE activity in a dose-dependent manner (Fig. 2B) with an average IC_{50} value of 36.03 μM and a K_i value of 4.09 μM , which was calculated using the Cheng-Prusoff equation [288] (Table 2). Pantoprazole, as predicted by DOCK, is shown in the FASN TE active site (Fig. 2C).

FIGURE 2

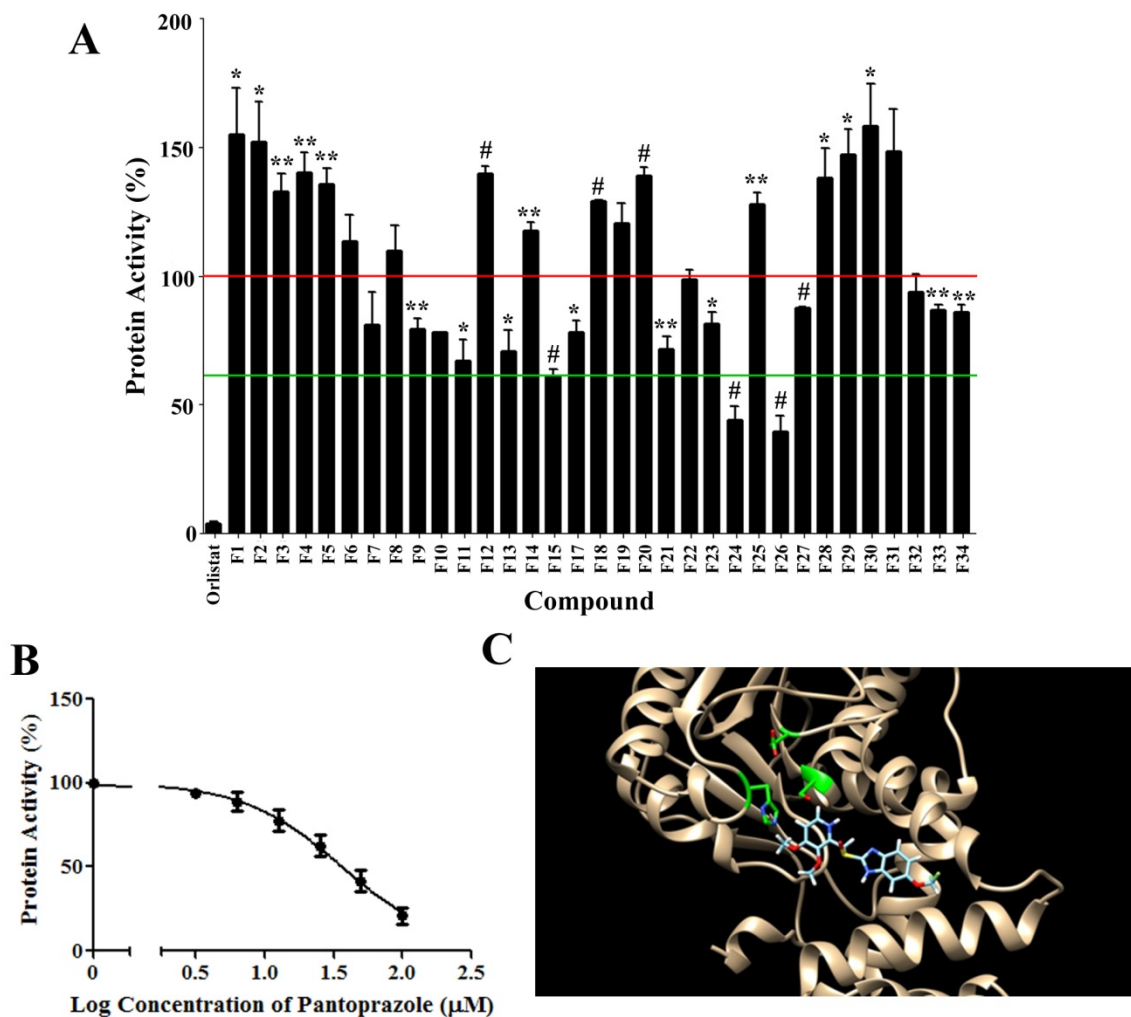


Figure 2: Pantoprazole inhibits FASN TE activity. (A) The ability of 34 FDA approved compounds to inhibit FASN TE activity was determined (100 % activity noted by red line). Compounds FDA15, 24 and 26 inhibited at least 40 % of protein activity (green line) (* $p < 0.05$, ** $p < 0.01$, # $p < 0.001$). (B) FDA15, pantoprazole, inhibited FASN TE activity in a dose-dependent manner. Each point is shown as the average \pm SEM. (C) Pantoprazole binds in the active site of FASN TE, as predicted by DOCK.

To determine if any other compounds from the same cluster as pantoprazole could also potentially inhibit FASN TE activity, the remaining compounds from the cluster were tested using the same assay as described above. Interestingly, all the remaining compounds in this cluster, which appeared in the list of 200 top-scoring compounds from *in-silico* docking, were PPIs including omeprazole, lansoprazole and rabeprazole. It should be noted that PPIs are chiral molecules and they are commercially formulated as racemic mixtures of their respective R- and S-enantiomers. The virtual FDA library contained only the S-enantiomer of each PPI. Esomeprazole, containing only the S-enantiomer of omeprazole, is also an FDA approved PPI that is commercially available. Esomeprazole, and racemic omeprazole, lansoprazole or rabeprazole were examined for their ability to inhibit FASN TE activity. As shown in Figure 3 and Table 2, except esomeprazole, all other racemic PPIs inhibited the esterase activity of FASN TE with K_i values of 3.4-5.9 μM . Based on these results, it is tempting to speculate that R-omeprazole may be more active than the S- enantiomer. However, it is difficult to compare with racemic omeprazole, as esomeprazole is commercially available as two molecules of S-omeprazole in a coordination complex with Mg^{2+} , which may affect its potency.

FIGURE 3

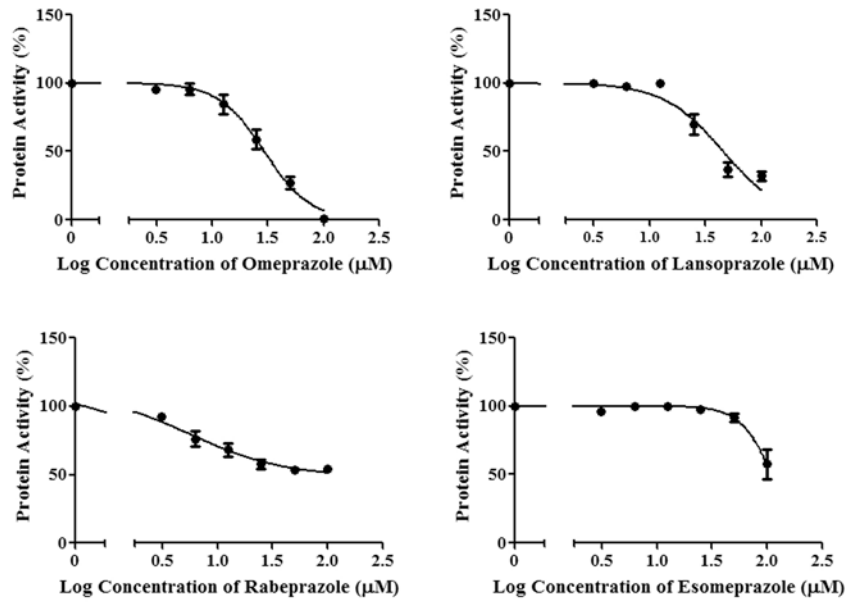
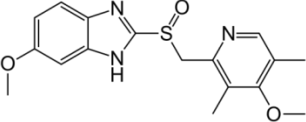
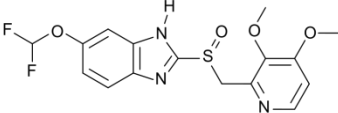
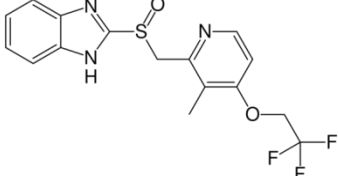
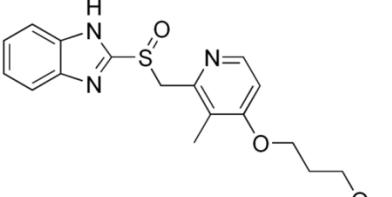
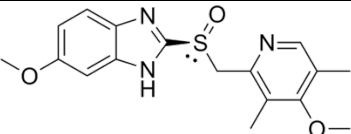


Figure 3: Dose-dependent inhibition of FASN TE by PPIs. Each point is shown as the average of three independent experiments \pm SEM.

TABLE 2: Chemical structure, IC₅₀ and K_i of PPIs.

PPI	Structure	IC ₅₀ ^a	K _i ^b
Omeprazole		29.52 ± 7.50	3.35 ± 0.85
Pantoprazole		36.03 ± 6.99	4.09 ± 0.79
Lansoprazole		46.47 ± 10.87	5.27 ± 1.23
Rabeprazole		51.95 ± 17.56	5.90 ± 1.99
Esomeprazole		117.84 ± 38.93	13.38 ± 4.42

^aThe IC₅₀ of each PPI is the concentration of drug required to inhibit 50 % of the recombinant FASN TE activity, as measured by the 4-MUH fluorescent assay.

^bThe inhibition constant of each PPI (K_i), defined as the concentration of compound required to inhibit 50 % of the TE enzyme receptors, was calculated from the IC₅₀ using the Cheng-Prusoff equation [288].

C. Conclusions and Discussion

In-silico screening is a promising method for the discovery of novel lead candidates that target a number of different proteins with known structure. Investigators have demonstrated the ability of *in-silico* screening methods to correctly predict the

binding modes of known ligand inhibitors within their targets, and when paired with high-throughput screening, *in-silico* screening can enrich the potential hit rate and provides a facile method to screen large libraries of compounds inexpensively and in a short amount of time [316,320,321]. Indeed, several drugs that are currently on the market were initially discovered with *in-silico* screening methods [324,325], and a number of lead compounds for various proteins implicated in cancer have been discovered using the DOCK method employed in this study [330]. DOCK software, which performs two rounds of *in-silico* screening to find ligands that could potentially bind in the active site of a protein target with size, shape and chemical complementarity, was paired with a high-throughput fluorescence assay that measured the relative activity of FASN TE. Using the highly-resolved crystal structure of FASN TE with a polyunsaturated fatty acyl adduct in the active site [280], a library of approximately 2,000 FDA approved drugs was screened. The top 200 scoring drugs were clustered into groups based on chemical structure. A total of 34 drugs to examine via HTS were chosen based on a number of criteria including predicted binding energy; chemical cluster; potential for favorable interaction in the FASN TE active site; presence of a lactone ring or other moiety that could covalently interact with the active site serine of FASN TE; and presence of aliphatic carbon chains. In this case, the integration of *in silico* screening and HTS was demonstrated to be particularly effective, because of the 34 drugs that were examined for their ability to disrupt the activity of a recombinant form of FASN TE, 10 compounds, or nearly 1/3, inhibited FASN TE activity in a statistically significant manner. These drugs include FDA9, cisapride; FDA11, dantrolene; FDA13, bisoprolol; FDA17, acitretin; FDA21, furaltadone; FDA23, bifonazole; and FDA27, capsaicin. These

drugs were not examined further because at a high concentration of 100 μ M, less than 40 % of FASN TE activity was inhibited. A number of compounds stimulated FASN TE activity in a significant manner including FDA2, fosinopril; FDA5, fosfomycin; FDA12, nizatidine; FDA14 valacyclovir; FDA18, oxybutynin; FDA25 gebaxate; FDA28, pramoxine; FDA29 midodrine; and FDA30, metoprolol. Several lactam-containing compounds were also tested as part of this screen, and interestingly, each one increased FASN TE activity in a statistically significant manner. The drugs included FDA1, cefotiam; FDA3, piperacillin; and FDA4, tazobactam; and FDA20, cefmetazole. Each of these drugs increased FASN TE by greater than 130 %. It is unknown how these compounds may be activating TE activity, but considering that nucleophilic attack by the active site serine is required for ester bond hydrolysis, it is possible that these drugs are somehow priming or activating serine and increasing its nucleophilic activity. Of the remaining top hits that failed to have an effect on FASN TE activity, there are several reasons why this could be the case. Drugs with a very low solubility in water may have been unable to inhibit FASN TE activity due to the aqueous conditions in which HTS was performed. Also, during DOCK screening, the chemical structure of the drug alone was evaluated, which may not correspond to the formulation in which the drug is commercially available, thus affecting its ability to inhibit FASN TE activity. Additionally, when *in-silico* screening was used, binding predictions for each of the top hits were made using coordinates of a protein that was obtained during crystallization with a polyunsaturated fatty acid adduct. Because the receptor is kept frozen during the virtual screening process, active site residues are kept in an optimal position for binding with the fatty acid adduct. Thus, the positions of residues of the active site of FASN TE

may adopt a vastly different conformation during the actual *in situ* screening process and drugs that were predicted to bind with a very favorable binding energy may not actually bind with FASN TE.

Several drugs inhibited at least 40 % of FASN TE activity, including FDA24, 13-*cis*-retinoic acid, and FDA26, sulcotidil, however, neither drug inhibited FASN TE activity in a dose-dependent manner. FDA15, pantoprazole, was able to inhibit FASN TE activity in a dose-dependent manner, with a K_i value in the low micromolar range. Pantoprazole is a member of the FDA approved class of compounds known as proton pump inhibitors. Interestingly, when the cluster of compounds containing pantoprazole was examined, other commercially available FDA approved PPIs omeprazole, lansoprazole and rabeprazole also appeared in the cluster from the top 200 scoring compounds from the FDA approved library. Like pantoprazole, each PPI inhibited the activity of FASN TE in a dose-dependent manner with K_i values in the low micromolar range. Esomeprazole was much less potent in inhibiting FASN TE activity, however, it was suspected that the formulation of commercially available esomeprazole, in which two esomeprazole molecules are chelated to a magnesium ion, may have been the cause of apparent decrease in potency of esomeprazole compared to other PPIs.

PPIs are known to block acid secretion into the gastrointestinal tract by covalently binding with a cysteine residue of hydrogen/potassium ATPase in gastric parietal cells and irreversibly inhibiting the secretion of protons into the gastric lumen [249]. PPIs are likely not inhibiting FASN TE in this manner, as there are no cysteine residues in the FASN TE active site. However, x-ray crystallography will be required to determine the exact way in which each PPI inhibits FASN activity. Crystal structure studies will also

confirm whether or not DOCK correctly predicted the binding mode of each PPI within the FASN TE active site.

Recently, a number of studies have shown that PPI treatment can sensitize cancer cells to chemotherapeutic agents. It has been proposed that PPI treatment causes a modulation of pH homeostasis by binding with vacuolar ATPases in the membranes of these cells (reviewed in [259,260]). However, it has been shown that acidic extracellular pH, which is common in a tumor microenvironment, causes an increase in FASN expression [76], indicating a close relationship between pH balance and lipid synthesis. Indeed, one study noted that PPI treatment altered the composition of cellular lipid metabolites in pancreatic cancer cells [270]. The results of this drug screening study are the first to demonstrate that PPIs may directly target FASN TE, and thus alter the fatty acid synthesis pathway, providing a new mechanism by which PPIs may exert anti-cancer effects in tumor cells. This study also shows that combining *in-silico* screening with HTS was a useful strategy in this study, and allowed us to quickly and successfully identify a new target and use for drugs that are already FDA approved. Applying such a strategy may allow for drug repurposing and fast-tracking of new treatment modalities.

Chapter 5: Aim III: Validation of Proton Pump Inhibitors as Inhibitors of Human Fatty Acid Synthase Thioesterase and Determination of their Therapeutic Potential as Anti-Cancer Agents in Pancreatic Cancer

A. Background and Rationale

Following lead compound discovery from high-throughput screening (HTS), the next phase in the drug discovery process is to test the therapeutic properties of lead compounds in appropriate cell lines and to determine if the selected compounds have the ability to inhibit the desired target *in vitro*. In this study, several cancer cell lines were used to examine the effects of PPIs on cancer cell growth, with BxPC-3 and PANC-1 pancreatic cancer cell lines being used as a model system. BxPC-3 cells were originally cultured from an adenocarcinoma resected via biopsy from the body of the pancreas of a 61-year-old woman, who died 6 months later even with chemotherapeutic and radiation treatment, although no metastasis was present. BxPC-3 cells have moderate to poor differentiation and when grown in mice, tumors from this cell line maintained the characteristics of the original primary adenocarcinoma [331]. PANC-1 cells were originally cultured from an adenocarcinoma resected from the head of the pancreas of a 56-year-old male that had invaded the duodenal wall. PANC-1 cells have poor differentiation and upon injection into mice, an anaplastic carcinoma formed that grew progressively [332]. In studies comparing these two cell lines, PANC-1 cells have been found to have greater migration capacity than BxPC-3 cells [333,334]. However, both cell lines appear to have similar invasive propensities when examined in matrigel [335,336]. BxPC-3 cells express higher levels of the pro-angiogenic factors

cyclooxygenase-2 (COX-2) [337], prostaglandin E2 [338] and vascular endothelial growth factor (VEGF) [339] than PANC-1 cells, indirectly indicating that BxPC-3 cells may have a greater angiogenic potential. Of the four most common mutations observed in pancreatic cancer (see chapter 1), BxPC-3 cells display wild-type KRAS; mutated p53; wild-type CDKN2A/p16 with a homozygous deletion; and a homozygous deletion of SMAD4/DPC4. PANC-1 cells display mutated KRAS; mutated p53; a homozygous deletion of CDKN2A/p16; and wild-type SMAD4/DPC4 (reviewed in [337]). In addition, our lab has observed that BxPC-3 and PANC-1 have varying amounts of FASN protein expression, with BxPC-3 expressing a lower amount of FASN protein and PANC-1 expressing a higher amount of FASN protein [149]. As BxPC-3 and PANC-1 cells display a number of widely different cellular characteristics, including a differential amount of FASN protein expression, these cell lines were chosen to represent the highly heterogeneous nature of tumor cells, reflecting differences that might be seen clinically.

In this study, the ability of PPIs to inhibit cancer cell growth and lipid synthesis was examined *in vitro*. All PPIs were effective in inhibiting tumor cell proliferation, colony forming ability and lipid synthesis in BxPC-3 and PANC-1 cells, with lansoprazole demonstrating the highest potency. Furthermore, lansoprazole likely directly binds to the active site of FASN TE, which was determined using a probe specific for serine hydrolase enzymes. Lansoprazole also induced apoptosis in pancreatic cancer cells, and cell lines with a higher fatty acid synthesis activity were more sensitive to lansoprazole treatment. Additionally, supplementing cells with exogenous palmitate partially rescued the effects of lansoprazole on tumor cell proliferation and apoptosis induction, indicating that lansoprazole is likely affecting the fatty acid synthesis pathway.

These results satisfy Specific Aim III by demonstrating that a novel class of FASN TE inhibitors, PPIs, can decrease cellular proliferation and lipid synthesis *in vitro*. FASN inhibition is an important mechanism by which PPIs are inducing cytotoxic effects in tumor cells, thus indicating the potential utility of PPIs, especially lansoprazole, in cancer chemotherapy in cancer types, including pancreatic cancer, that over-express FASN.

B. Results

B1. PPIs Inhibit Cellular Proliferation and Colony Forming Ability

To test the ability of each candidate PPI to inhibit cellular proliferation in cancer cells, human pancreatic cancer cell lines PANC-1 and BxPC-3 were treated with varying concentrations of the PPIs for 72 hours. Cellular proliferation was first examined using MTT assays. MTT assays allow for the estimation of the number of living cells in a sample by detecting the colorimetric change that occurs as the tetrazolium ring of the MTT dye is cleaved by dehydrogenase enzymes in the active mitochondria of living cells [340]. Each PPI exhibited a dose-dependent anti-proliferative effect in both PANC-1 (Fig. 1A) and BxPC-3 cells (Fig. 1B) (Table 1). Lansoprazole offered the most consistent potent effect in both cell lines, with an average IC_{50} value of 231.53 μ M in PANC-1 cells and 23.93 μ M in BxPC-3 cells. A known inhibitor of FASN, orlistat, was also examined (Fig. 1 A, B). Although orlistat was more potent than PPIs in PANC-1 cells with an average IC_{50} value of 136.21 μ M, its average IC_{50} value was 30.20 μ M in BxPC-3 cells, which was comparable to the effect induced by lansoprazole (Table 1).

FIGURE 1:

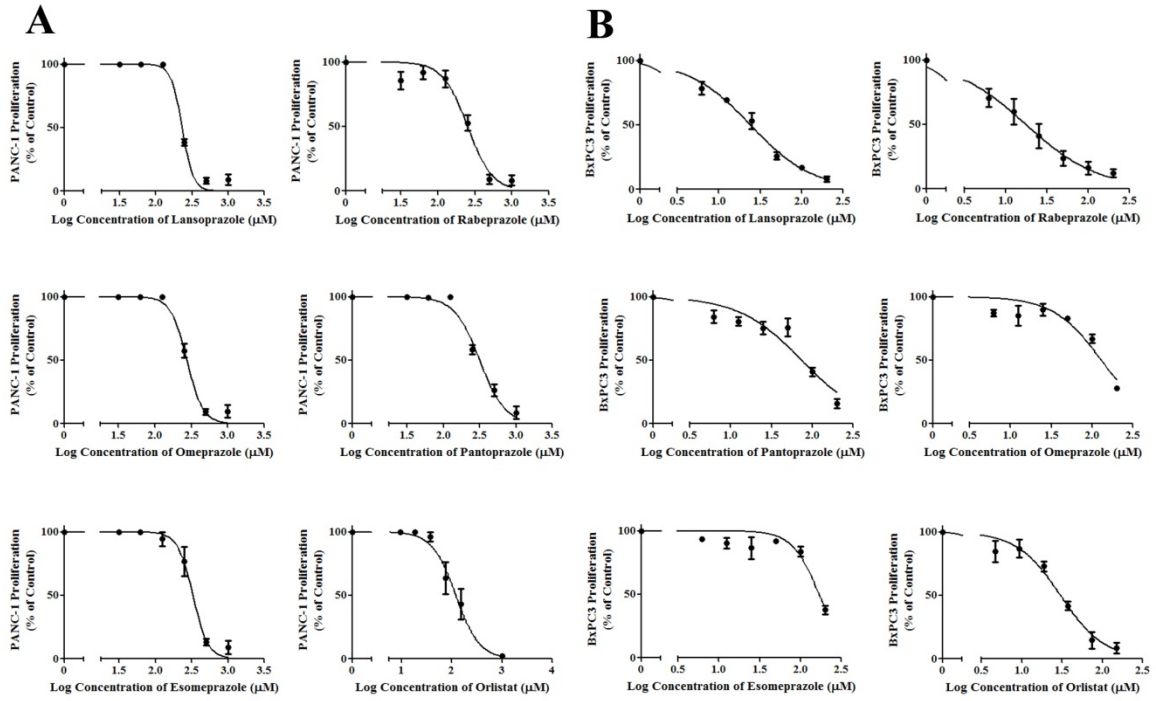


Figure 1: Dose-response curves of PPIs from MTT assays. The ability of each PPI, as well as orlistat, to inhibit cellular proliferation was measured by MTT assay in (A) PANC-1 cells and (B) BxPC-3 cells. Each point is shown as the average of three independent experiments \pm SEM.

TABLE 1: IC₅₀ values of PPIs from MTT assays.

PPI/Orlistat	PANC-1 IC ₅₀ (μ m)	PPI/Orlistat	BxPC-3 IC ₅₀ (μ m)
Lansoprazole	231.53 \pm 6.79	Rabeprazole	21.88 \pm 14.18
Rabeprazole	246.37 \pm 56.89	Lansoprazole	23.93 \pm 1.90
Omeprazole	276.87 \pm 31.31	Pantoprazole	76.13 \pm 17.61
Pantoprazole	322.37 \pm 7.21	Omeprazole	144.4 \pm 21.30
Esomeprazole	333.33 \pm 75.33	Esomeprazole	232.4 \pm 55.34
Orlistat	136.21 \pm 35.71	Orlistat	30.20 \pm 5.36

As MTT assays only allow for an estimation of living cells, and thus an estimation of IC_{50} , cell survival in the presence of each PPI was also examined using colony formation assays to confirm that PPIs could inhibit cell survival in a dose-dependent manner. Colony formation assays examine the ability of single cells to grow into colonies and to theoretically undergo unlimited division in the presence or absence of cytotoxic agents [341,342]. PANC-1 and BxPC-3 cells were treated with each PPI or orlistat for 10-14 days and their colony forming ability was inhibited in a dose-dependent manner (Fig. 2 A, B). Again, Lansoprazole was the most potent inhibitor of colony formation, with an average IC_{50} of 58.56 μ M in PANC-1 cells and 6.71 μ M in BxPC-3 cells (Table 2). Rabeprazole also appeared to be one of the most potent PPIs to affect both cellular proliferation and colony formation, however rabeprazole was one of least efficacious PPIs to inhibit FASN TE activity (see chapter 4), indicating that rabeprazole may be affecting cancerous cells through other pathways. Additionally, lansoprazole was more potent in inhibiting colony forming ability than orlistat in both cell lines (Table 2). Therefore, lansoprazole was selected as the lead candidate.

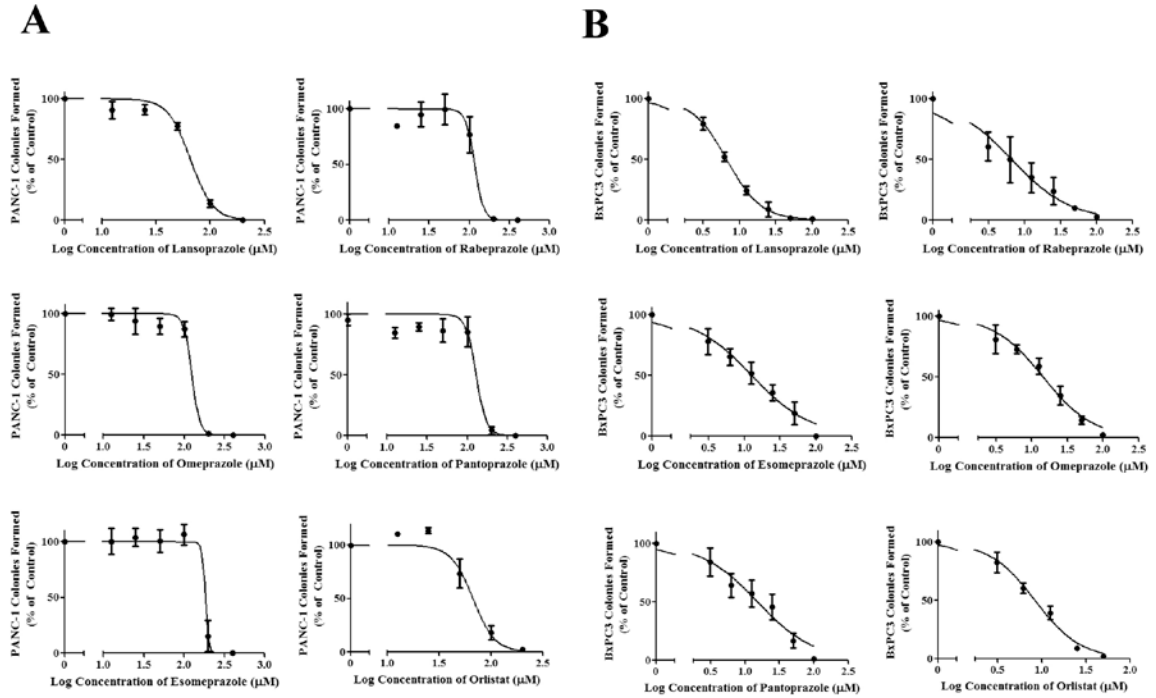
FIGURE 2

Figure 2: Dose-response curves of PPIs from colony formation assays. The ability of each PPI or orlistat to inhibit cellular proliferation was measured by colony formation assay in (A) PANC-1 cells and (B) BxPC-3 cells. Each point is shown as the average of three independent experiments \pm SEM.

TABLE 2: IC_{50} values of PPIs and orlistat from colony formation assays.

PPI	PANC-1 IC_{50} (μ m)	PPI	BxPC-3 IC_{50} (μ m)
Lansoprazole	58.56 ± 11.93	Lansoprazole	6.71 ± 0.84
Rabeprazole	117.36 ± 41.33	Rabeprazole	7.88 ± 4.92
Omeprazole	127.83 ± 16.12	Esomeprazole	13.33 ± 0.89
Pantoprazole	143.73 ± 27.78	Omeprazole	14.80 ± 2.24
Esomeprazole	166.47 ± 41.20	Pantoprazole	18.51 ± 14.32
Orlistat	68.02 ± 17.60	Orlistat	8.45 ± 1.83

To examine why lansoprazole is more effective to BxPC-3 than PANC-1 cells, the relative amount of FASN protein was determined using Western blot analysis and the amount of lipid synthesis by analyzing [¹⁴C]-acetate incorporation into lipids in each cell line (DPM/10⁵ cells). Although PANC-1 has a much higher level of FASN protein than BxPC-3 cells, the amount of [¹⁴C] incorporated into lipids extracted from BxPC-3 cells was approximately 1.75 fold higher than lipids extracted from PANC-1 cells, indicating that BxPC-3 has a higher amount of lipid synthesis (p<0.05) (Fig. 3 A, B). This is not unusual, as the rate limiting step of fatty acid synthesis is the conversion of acetyl-CoA to malonyl-CoA by acetyl-CoA carboxylase [6]. Because the reaction rate is being controlled by acetyl-CoA carboxylase, the rate of fatty acid synthesis does not necessarily correlate with the amount of FASN protein. These results indicate that because BxPC-3 cells have a higher rate of fatty acid synthesis and its survival may be more dependent on this higher rate of lipid synthesis, FASN blockade may be more detrimental to this cell line, especially due to the toxic accumulation of malonyl-CoA [196]. These results also indicate that the fatty acid synthesis pathway may be a target of PPIs.

FIGURE 3:

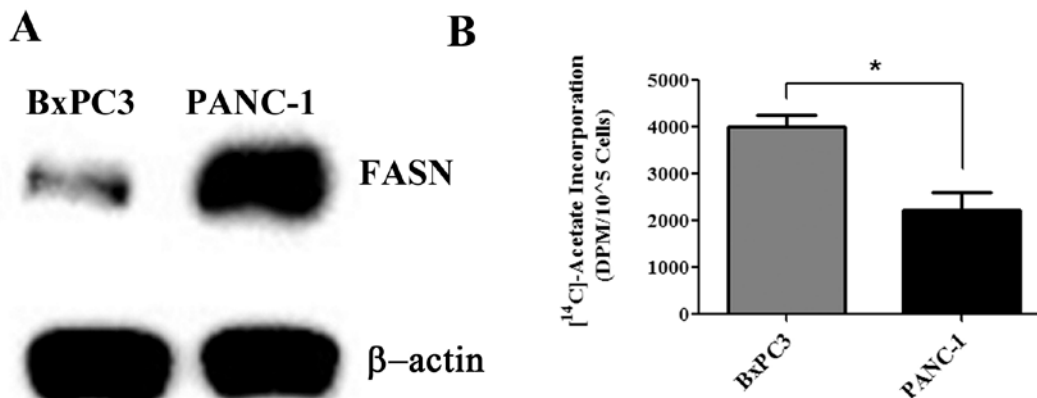


Figure 3: FASN protein expression and activity in PANC-1 and BxPC-3 cells. (A) PANC-1 cells have higher FASN protein expression than BxPC-3 cells, as measured by Western blot. A representative blot is shown. (B) The amount of lipid synthesis in BxPC-3 cells is about 1.75-fold higher ($n=3$, $*p<0.05$), as measured by the incorporation of [¹⁴C]-acetate into synthesized lipids.

B2. PPIs Inhibit Fatty Acid Synthesis in Whole Cells

Although the ability of PPIs to inhibit recombinant FASN TE activity had been shown, it was necessary to demonstrate that the fatty acid synthesis pathway is a target of lansoprazole in whole cells. In order to test this, PANC-1 and BxPC-3 cells were treated with lansoprazole for 4 hours followed by a 2 hour incubation with [¹⁴C]-acetate. The amount of radioactive carbon incorporated into newly synthesized lipids was determined by extracting lipids from the cells and measuring the radioactivity using scintillation counting. Lansoprazole inhibited the lipid production rate in both PANC-1 and BxPC-3 cell lines in a dose-dependent manner (Fig. 4 A, B). The average IC₅₀ of FASN synthesis

inhibition by lansoprazole was 134.55 μM in PANC-1 cells and 149.83 μM in BxPC-3 cells (Fig. 4C).

Rabeprazole, omeprazole, esomeprazole and pantoprazole were also examined in PANC-1 cells, with average IC_{50} values of 257.6, 532.7, 549.6 and 641.2 μM respectively (Fig. 5A, B), indicating that lansoprazole is clearly the most potent inhibitor of lipid synthesis by FASN. As a comparison, orlistat was also examined in PANC-1 cells, and inhibited fatty acid synthesis with an IC_{50} value of 208.5 μM (data not shown).

FIGURE 4

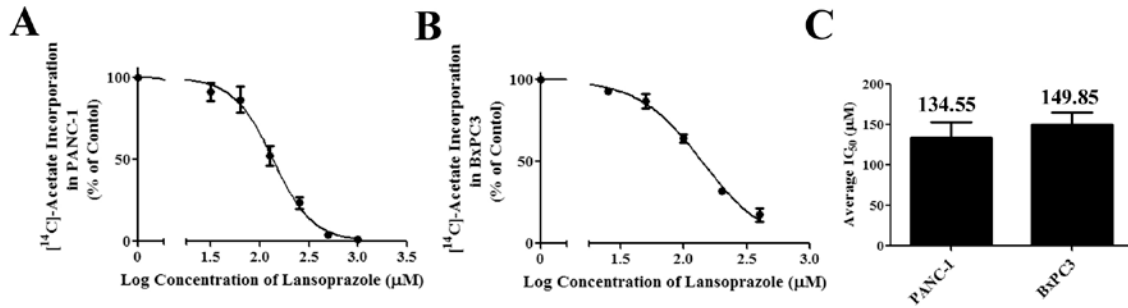


Figure 4: Lansoprazole inhibits FASN lipid synthesis. Lansoprazole decreased the incorporation of $[^{14}\text{C}]$ -acetate into lipids in a dose-dependent manner in (A) PANC-1 cells and (B) BxPC-3 cells. Each point is shown as the average of at least three independent experiments \pm SEM. (C) The IC_{50} values of lipid synthesis inhibition by lansoprazole is shown for both cell lines.

FIGURE 5

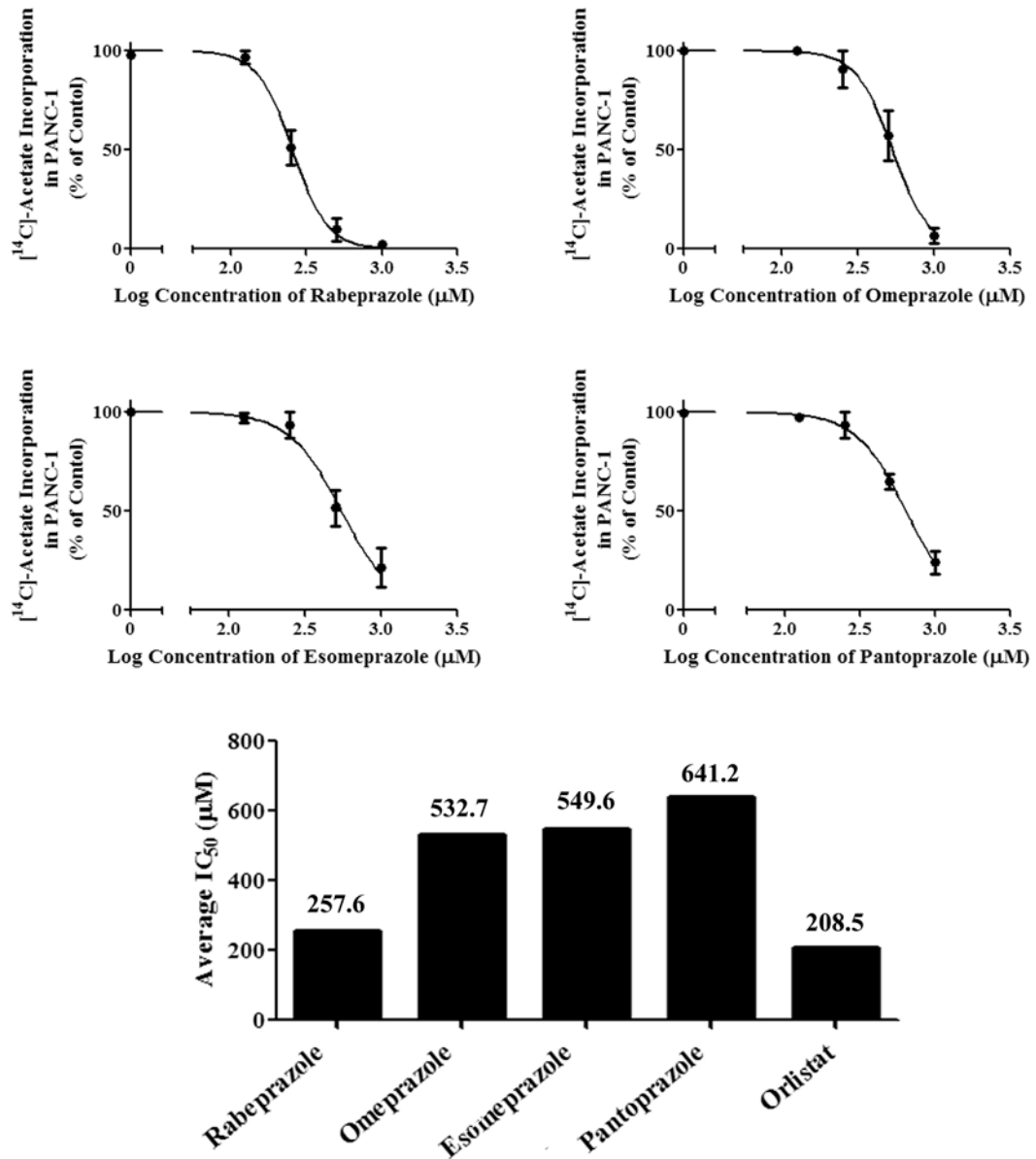


Figure 5: PPIs inhibit FASN lipid synthesis. (A) Rabeprazole, omeprazole, esomeprazole and pantoprazole each inhibit lipid synthesis in PANC-1 cells in a dose-dependent manner, but to a lesser degree than lansoprazole. Each point is shown as the average of two independent experiments. (B) The IC_{50} values of lipid synthesis inhibition by each PPI, and orlistat, is shown.

B3. Lansoprazole Competitively Inhibits the Active Site of FASN TE

To confirm that lansoprazole directly associates with the active site of FASN TE in full-length FASN, cell lysate was generated from PANC-1 cells. PANC-1 cells were chosen, as they have a higher amount of protein expression than BxPC-3 cells. The lysate was incubated with the ActivX Desthiobiotin-fluorophosphonate (FP) serine hydrolase probe in the presence and absence of lansoprazole. This probe irreversibly binds to and labels the active site serine of serine hydrolase enzymes, such as FASN TE, and can be detected using Western blot with HRP-conjugated streptavidin. As shown in Fig. 6A and 6B, labeling of FASN TE by the probe is inhibited by lansoprazole in a dose-dependent manner. However, lansoprazole had no effect on FASN expression, as determined using Western blot, or on the binding of the probe to other potential hydrolases (Fig. 6B). To determine the type of enzymatic inhibition that lansoprazole imparts on FASN TE, recombinant FASN TE was incubated with increasing concentrations of lansoprazole in the presence of a range of 4-MUH concentrations and the fluorescence yielded from hydrolyzed 4-MU was quantified. A Lineweaver-Burk plot was created by plotting $1/v$ vs. $1/[4\text{-MUH}]$ for each lansoprazole concentration. The slope of each line plotted increases with each increasing lansoprazole concentration; each line has a different x-intercept; and the lines intersect near the y-intercepts inside the plot, indicating that inhibition of FASN TE by lansoprazole is likely competitive in nature (Fig. 6C) [291].

FIGURE 6

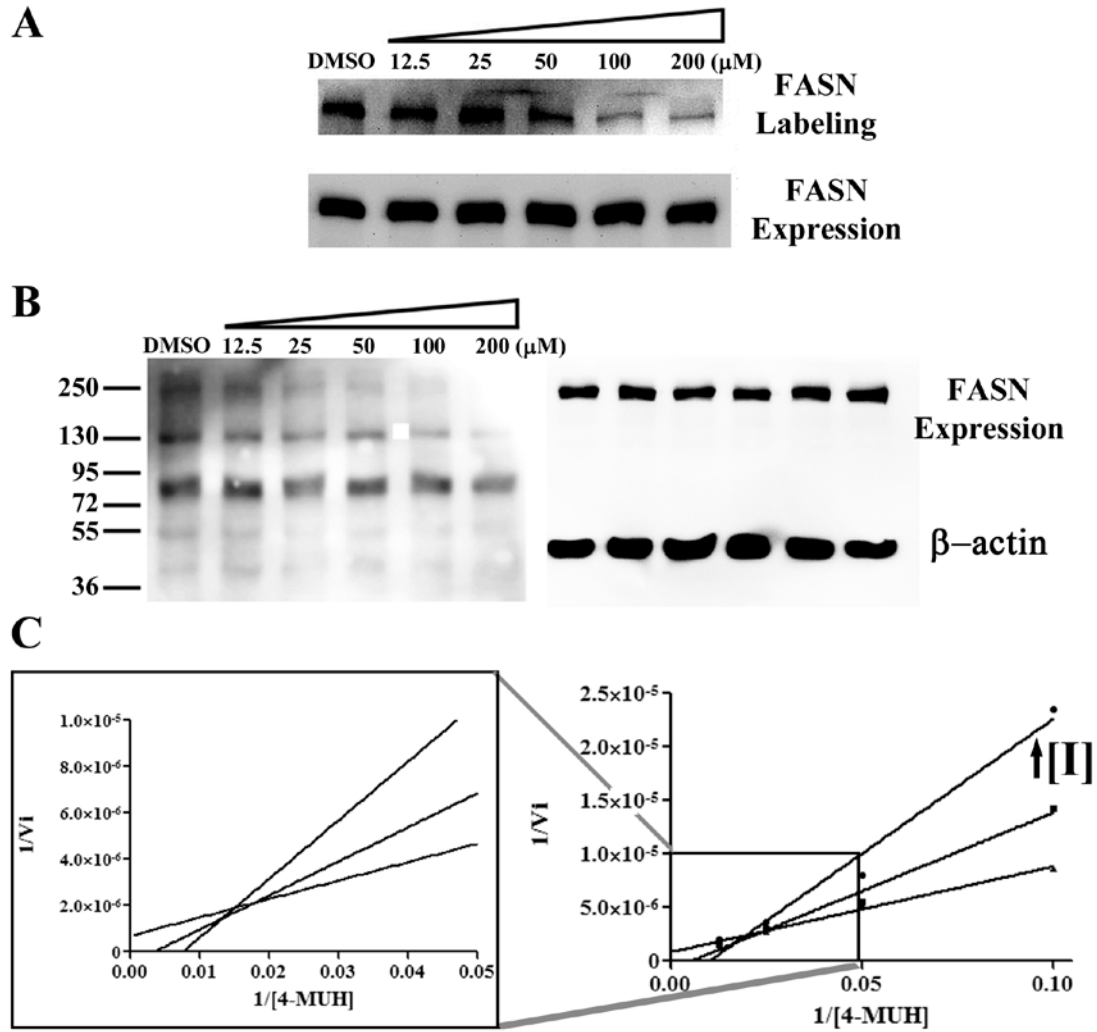


Figure 6: Direct inhibition of FASN TE by lansoprazole. (A) Incubating PANC-1 cell lysate with increasing concentrations of lansoprazole decreased the labeling of FASN TE by a serine hydrolase probe, indicating that lansoprazole is directly binding in the FASN TE active site. The expression of FASN remained unchanged. (B) Increasing concentrations of lansoprazole did not affect the labeling of other serine hydrolase proteins by the probe, indicating that lansoprazole inhibition is specific to FASN TE. Representative blots are shown for A and B. (C) Incubating recombinant FASN TE with

lansoprazole (50, 25, 6.25 μM) in the presence of various concentrations of 4-MUH yielded linear relationships with varying slopes and x-intercepts, when plotted via the Lineweaver-Burk method, indicating competitive inhibition. Representative plots are shown, and the left panel is a zoomed in view of the right panel.

B4. Lansoprazole Induces Cell Death In Vitro

Blockade of the fatty acid synthesis pathway has been shown to elicit apoptotic cell death, likely through toxic buildup of malonyl-CoA [196]. The ability of lansoprazole to elicit cell death was confirmed by two different methods to examine early and late stage apoptosis. First, apoptosis was examined in BxPC-3 cells by quantitating the amount of cytoplasmic histone-associated DNA-fragments formed following a 72 hour treatment with lansoprazole using the Cell Death Detection ELISA kit (Roche). DNA fragmentation leading to a release of nucleosomes from the nucleus into the cytoplasm is an early event in apoptosis, thus this test allows us to quantify cells in early apoptosis following lansoprazole treatment [343]. The induction of apoptosis was also confirmed by examining the cleavage of poly(ADP-ribose) polymerase (PARP) via Western blot following treatment with lansoprazole for 24 hours. The cleavage of PARP by executioner caspases is a hallmark of the execution phase of late stage apoptosis [344]. As the concentration of lansoprazole is increased, both DNA fragmentation (Fig. 7A) and formation of cleaved-PARP increased (Fig. 7B) in a dose-dependent manner, indicating that lansoprazole causes apoptosis in these cancer cells.

FIGURE 7

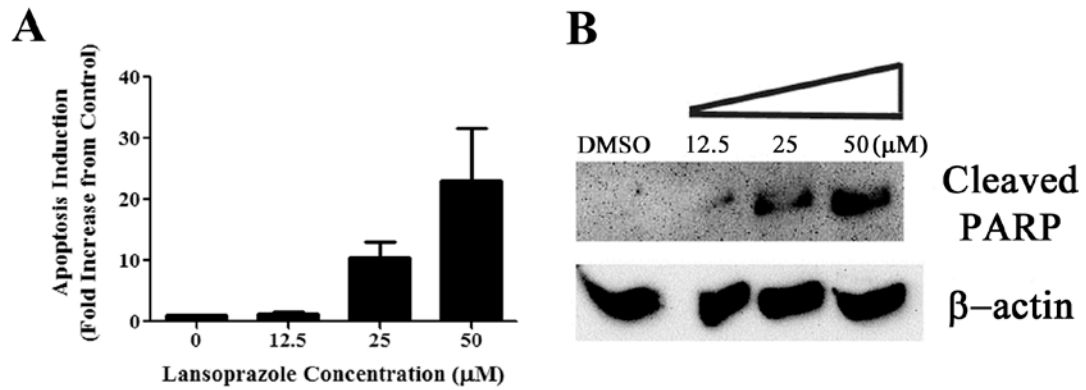


Figure 7: Initiation of apoptosis by lansoprazole. (A) Increasing concentrations of lansoprazole increase the induction of apoptosis in BxPC-3 cells in a dose-dependent manner, as measured by quantifying amount of cytoplasmic histone-associated DNA-fragments formed following lansoprazole treatment. Each point is shown as the average of three independent experiments \pm SEM. (B) Apoptosis induction was confirmed by examining the cleavage of PARP-1 via Western blot following treatment with increasing concentrations of lansoprazole. A representative blot is shown.

B5. Palmitate Supplementation Rescues the Effect of Lansoprazole on Cellular Proliferation and Apoptosis

To demonstrate that lansoprazole treatment is indeed affecting the fatty acid synthesis pathway, BxPC-3 cells were treated with varying concentrations of lansoprazole in the presence and absence of 3.75 μ M palmitic acid, and cellular proliferation was determined with MTT assay as described above. As palmitate is the main product of fatty acid synthesis by FASN, supplementing with exogenous palmitate following FASN inhibition should attenuate the effects of lansoprazole treatment by replenishing the cellular lipid supply, especially for the synthesis of phospholipids for membranes of proliferating cells, thus preventing cell death due to end product starvation (as reviewed in [345]). Palmitate supplementation alone did not enhance cellular proliferation, and in fact seemed to be slightly detrimental to cancer cell growth, however the difference was not statistically significant ($p=0.19$) (Fig. 8A). FASN expression also remained unchanged following supplementation with exogenous palmitate (Fig. 8B). The addition of palmitate partially rescued the cells from lansoprazole treatment, increasing the IC_{50} by approximately 1.7 fold ($p<0.001$) (Fig. 8C). As the addition of palmitate alone has no effect on cellular proliferation, but can rescue cells treated with lansoprazole, it is likely that lansoprazole is inhibiting the fatty acid synthesis pathway. The effect of exogenous palmitate supplementation on apoptosis induction by lansoprazole was also examined. BxPC-3 cells were treated in the presence and absence of 3.75 μ M palmitic acid with the addition of 25 μ M lansoprazole. Treatment with palmitic acid reduced apoptosis induction also by approximately 40 % ($p<0.001$) (Fig. 8D).

FIGURE 8

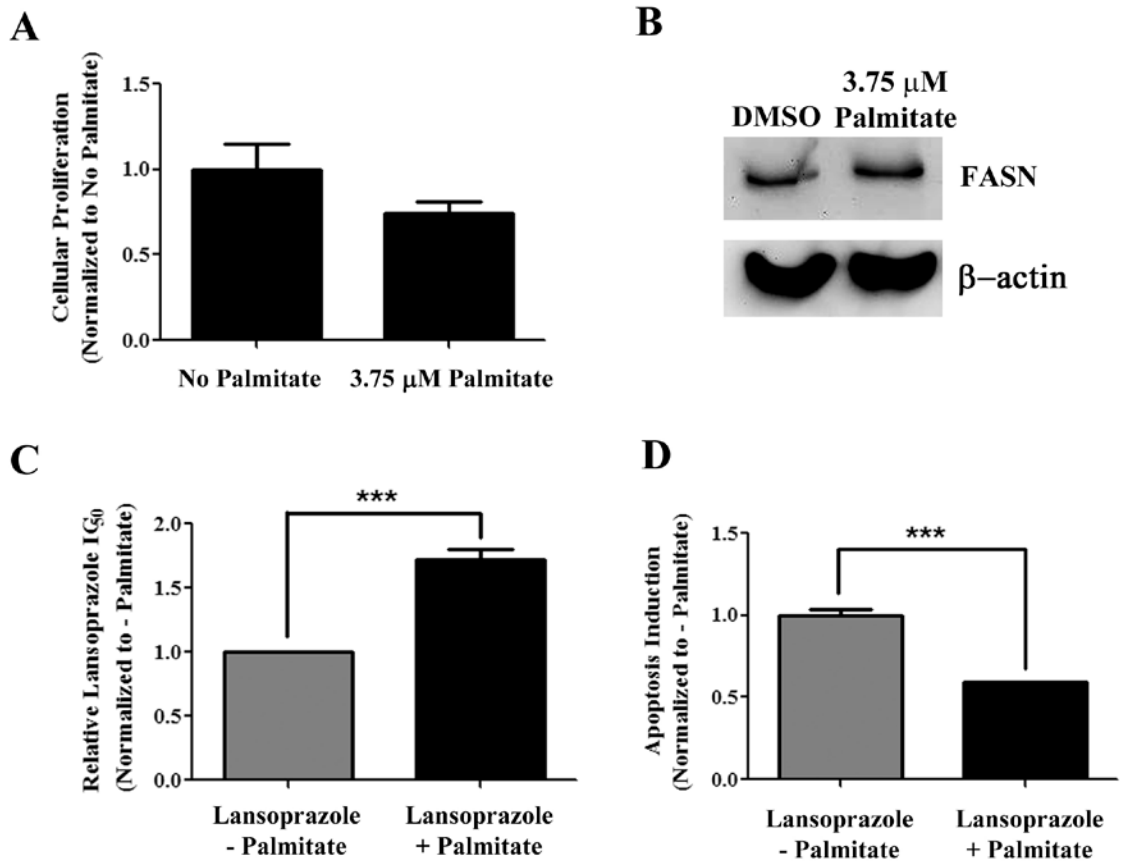


Figure 8: Palmitate supplementation rescues the effects of lansoprazole treatment. (A) The addition of 3.75 μ M palmitate has no statistically significant effect on cell growth compared to DMSO control, as measured by MTT assays (n=3, p=0.19). (B) The addition of 3.75 μ M palmitate has no effect on FASN protein expression, as measured by Western blot. (C) The effect of lansoprazole treatment on cellular proliferation, as measured by MTT assay, is mitigated by the addition of 3.75 μ M palmitate. The IC_{50} of lansoprazole is increased approximately 1.7-fold with the addition of palmitate (n=3, ***p<0.001). (D) The effect of apoptosis induced by treatment with 25 μ M lansoprazole, as measured by

cell death detection, is reduced with the addition of 3.75 μM palmitate by approximately 40 % (n=3, ***p<0.001).

B6. Effect of Lansoprazole on Extracellular and Intracellular pH

PPIs are known to inhibit H^+/K^+ ATPases and thus may also inhibit vacuolar ATPases in tumor cells. Therefore, lansoprazole may affect cellular proliferation by altering pH homeostasis, and the extracellular and intracellular pH in the presence and absence of lansoprazole was examined in BxPC-3 cells. Addition of lansoprazole did not affect the pH balance of the growth media, which was collected and measured by a pH meter following a 72 hour incubation, indicating that an alteration in extracellular pH was not a factor in affecting cellular growth (data not shown). The intracellular pH of BxPC-3 cells, treated in the presence or absence of various concentrations of lansoprazole for 72 hours, was measured by incubating the cells with the pHrodo red intracellular pH sensor, which exhibits a differential in fluorescence that is pH dependent. As shown in Figure 9A, intracellular pH was not affected by lansoprazole treatment in a statistically significant manner, indicating that alteration of pH homeostasis unlikely contributes to lansoprazole-induced cell death in BxPC-3 cells. These results are expected, as all cell lines used in this study were cultured in buffered media in order to minimize any effects caused by a change in cellular pH.

B7. Lansoprazole Treatment has a Greater Effect in Cells with Higher FASN Activity

To further demonstrate that the anti-proliferative and cell death inducing effect of lansoprazole is a direct result of FASN blockade, paired cells lines with varying amounts

of FASN activity was examined. First, FASN protein expression was evaluated in a PANC-1 vector control cell line PANC-1/V4 and a PANC-1 ectopic FASN over-expressing cell line, PANC-1/F7. These cell lines, created in our lab, have previously been used to show that cells with higher FASN protein expression are more intrinsically resistant to both radiation and gemcitabine treatment [149]. Western blot analysis confirmed that FASN protein expression is up-regulated in F7 over-expressing cells, and the [¹⁴C]-acetate lipid-incorporation assay showed that the FASN synthesis rate is 2-fold higher in the F7 over-expressing cells compared to the V4 vector-control cells (Fig. 9B). Conversely, when these cell lines were treated with lansoprazole, F7 over-expressing cells are 1.5-fold more sensitive to lansoprazole treatment than V4 cells (p<0.05) as determined using colony formation assay (Fig. 8C). As with BxPC-3 and PANC-1 cells, the paired cell lines that exhibited a higher rate of fatty acid synthesis were more sensitive to lansoprazole treatment. As conversion of acetyl-CoA to malonyl-CoA by acetyl-CoA carboxylase is the rate limiting step of fatty acid synthesis [6], inhibition of FASN is likely more harmful to cells that have a higher rate of fatty acid synthesis, due to the toxic accumulation of malonyl-CoA [196]. These results demonstrate the likelihood that lansoprazole is targeting FASN and indicating that lansoprazole may have utility in sensitizing cells to chemotherapeutic treatment.

FIGURE 9

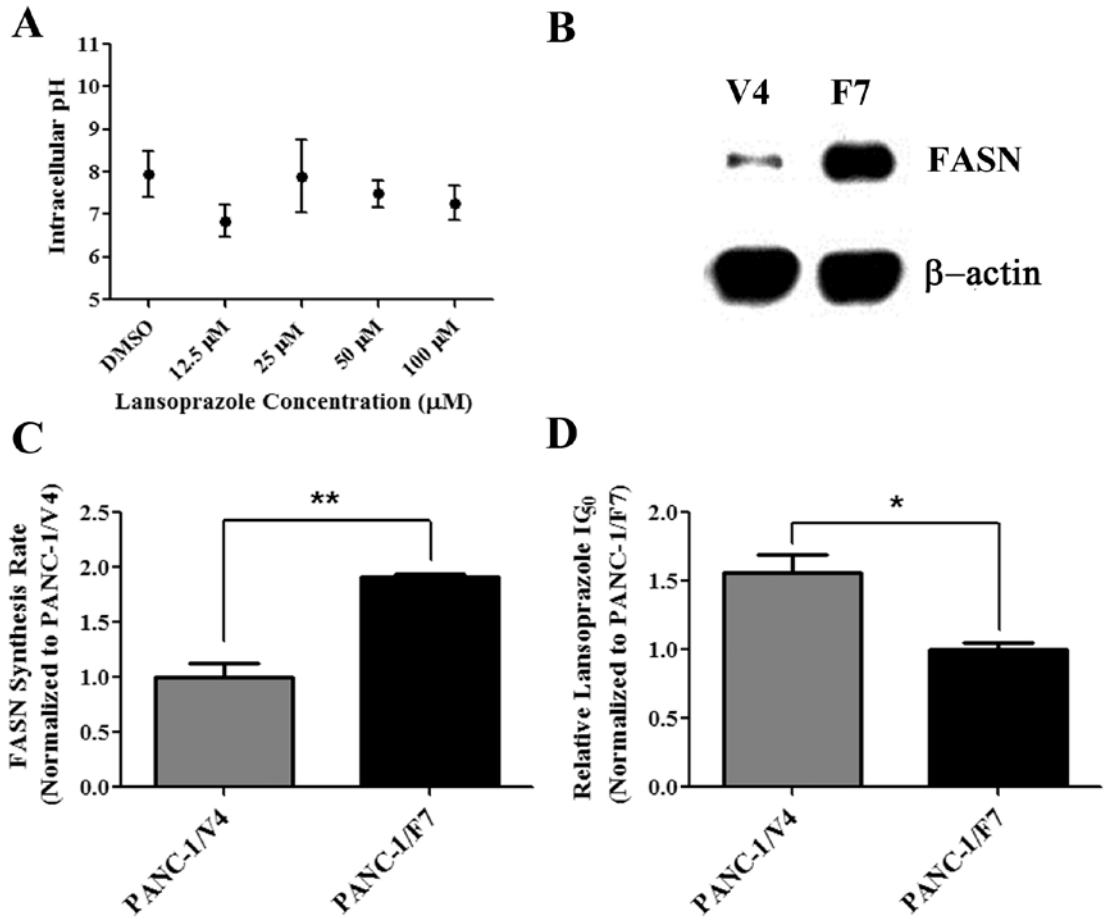


Figure 9: Effect of lansoprazole on intracellular pH and differential effects of lansoprazole in paired cells with varying FASN activity. (A) Treatment with varying concentrations of lansoprazole does not significantly affect intracellular pH, as measured in BxPC-3 cells. Each point is shown as the average of three independent experiments \pm SEM. $p > 0.05$ for all concentrations when compared to DMSO control. $p = 0.17$ when comparing DMSO to 12.5 μM lansoprazole. (B) FASN protein expression is increased in PANC-1/F7 FASN over-expressing cells, when compared to PANC-1/V4 vector control cells. A representative blot is shown. (C) Lipid synthesis in PANC-1/F7 over-expressing cells is 2-fold higher than in PANC-1/V4 cells ($n = 3$, $**p < 0.01$). (D) PANC-1/V4 cells

are 1.5-fold more resistant to lansoprazole treatment than PANC-1/F7 cells, as measured by colony formation assay (n=3, *p<0.05).

C. Conclusions and Discussion

In this study, the therapeutic potential of PPIs was evaluated in several pancreatic cancer cell lines, and fatty acid synthesis as a target of PPI treatment was also investigated. All PPIs investigated inhibited cellular proliferation, colony forming ability and lipid synthesis *in vitro*, with lansoprazole being the most potent inhibitor. Lansoprazole also induced dose-dependent apoptotic cell death. Interestingly, as noted in the previous chapter, lansoprazole was not the most potent PPI for inhibiting recombinant FASN TE activity, and the ability of each PPI to decrease cellular proliferation and fatty acid synthesis did not completely correspond with their ability to inhibit recombinant FASN TE. The most likely reason is that each drug may be differentially taken up by the cells, possibly due to drug formulation or the chemical differences of each compound, and lansoprazole may be the PPI that can enter the cells the most easily. Lansoprazole may also be the most stable PPI, thus it can exert its effects with greater potency. Another discrepancy that must be addressed is that the IC₅₀ of lansoprazole required to inhibit lipid synthesis was higher than the IC₅₀ required to inhibit cellular proliferation or colony formation. However, the time of treatment could explain this discrepancy, as cells were treated with lansoprazole for only 4 hours before measuring lipid synthesis, versus treatment for 72 hours and 10-14 days before measuring cellular proliferation or colony formation, respectively. It is also possible that there are other mechanisms by which PPIs are acting in cancer cells. Regardless, the involvement of the fatty acid synthesis pathway

as a mechanism by which lansoprazole exerts its effects against cancer cells was confirmed by demonstrating the ability of lansoprazole to directly block the FASN TE active site in full-length FASN protein in a competitive manner. Supplementation of exogenous palmitate partially rescued the effects of lansoprazole on cellular proliferation and apoptosis induction, and cells with a higher amount of lipid synthesis were more sensitive to lansoprazole treatment, indicating that the fatty acid synthesis pathway is likely a target by which lansoprazole is acting in cancer cells. As discussed previously, the modulation of pH homeostasis is an important mechanism by which PPIs interfere with cancer cell growth and increase the sensitivity of cancer cells to chemotherapeutic intervention [261]. In the cell lines and buffered culture conditions used in this particular study, pH deregulation was not likely a factor, as both the extracellular and intracellular the pH remained constant with increasing doses of lansoprazole treatment.

Recently, there has been considerable interest in PPIs as anti-cancer agents and PPI use in combination with other chemotherapeutic agents appears to be an attractive treatment regimen, as long-term and high-dose PPI treatment has been shown to be well tolerated in patients with few side effects [258,346], and both pantoprazole and lansoprazole are available in IV formulations. Indeed, a phase II clinical trial evaluating the combination of IV pantoprazole with doxorubicin in the treatment of solid tumors is currently underway [276]. In this study, high micromolar doses of lansoprazole were required to inhibit pancreatic cancer cell growth and lipid synthesis. These results might be of concern, however, in pharmacokinetic studies with lansoprazole, in which 30 mg oral lansoprazole was given daily in days 1-7, followed by 30 mg IV lansoprazole over 30 minutes daily in days 8-14, the maximal plasma concentration (C_{max}) of lansoprazole

reached 1705 (\pm 292) ng/mL, which is equivalent to a concentration of approximately 5 μ M [347]. Theoretically, a treatment regimen could be readily adapted for use in clinical trials with cancer patients that could reach the higher micromolar concentrations required for the therapeutic effects against cancer cells, by increasing the frequency and amount of drug administered in each dose.

FASN is an important protein to study and pursue the possibility of identifying and developing anticancer agents. The importance of the fatty acid synthesis pathway in the formation, maintenance, and progression of many types of cancer has been well documented, as has its involvement in the development resistance to chemotherapeutic treatment, thus, the development of a FASN inhibitor may have wide-reaching implications for patients with many types of tumors that over-express FASN (reviewed in [345]). Inhibiting FASN has been shown to be a highly selective way to target cancerous tissues without affecting normal tissue, as normal cells express very low levels of FASN [42,348]. Also, blocking cellular metabolism, which lies downstream of many of the pathways that are mutated in cancer, provides a strategy to target cancers of all types, regardless of the type or location of mutations up-stream [168]. Despite the apparent utility of blocking FASN for anti-cancer treatment, very little progress has been made in the development of potential FASN inhibitors. Although FDA approved, orlistat is unlikely to find use as an anti-cancer agent due to the side effect of weight loss, as well as its poor systemic availability. Several first-generation FASN inhibitors, such as C75 and cerulenin, have also induced severe side effects such as weight loss and anorexia in test animals, likely through stimulation of the fatty acid oxidation pathway. Other FASN inhibitors, such as the novel compound C93 and the natural product EGCG, do not

activate fatty acid oxidation or weight loss in test animals, but the current status of these compounds is unknown (reviewed in [349]). Clearly, more studies are needed to establish lansoprazole as a FASN inhibitor *in vivo* and to determine if lansoprazole administration can increase the efficacy and potency of current cytotoxic agents to increase cancer cell killing and tumor cell burden. Nevertheless, the results of this study provide further evidence that FASN inhibition and treatment with PPIs could potentially be a useful anti-cancer strategy for many types of cancer, including pancreatic cancer.

Chapter 6: Summary and Future Directions

A. Summary and Future Directions for Specific Aim I

In this dissertation study, molecular dynamics simulations were used to examine the mechanism of orlistat hydrolysis by the thioesterase domain of human FASN. Previously, crystal structure studies demonstrated that orlistat is present in the active site of TE both as covalent-orlistat, in which orlistat forms a covalent bond with the active site Ser²³⁰⁸ of TE, and hydrolyzed orlistat. In each orlistat state, the hexyl tail of orlistat adopts two different conformations, conformation I in covalent-orlistat and conformation II in hydrolyzed orlistat. Analysis of MD simulations demonstrated that the hexyl tail of covalent-orlistat can adopt both conformations I and II within TE. In conformation I, hydrogen bonding between the hydroxyl moiety of orlistat and His²⁴⁸¹ of the catalytic triad prevents the proper orientation of water molecules for catalysis of the covalent bond between orlistat and Ser²³⁰⁸. However, the hexyl tail can shift to conformation II while still covalently bound to TE, which then disrupted the hydrogen bond between orlistat and His²⁴⁸¹, allowing water molecules to be properly oriented for catalysis.

There are a number of proposed future studies that could build upon the results gained in this study. First, to experimentally confirm the role of the orlistat hexyl tail in hydrolysis and validate the MD simulation results, a recently described technique called temperature-scan cryocrystallography could be used. In conjunction with standard crystallography, this technique allows for the observation of reaction intermediates via cryotrapping, in which increasing temperature is used as a ‘mimic’ for time. As the temperature is increased, the structure of the protein crystal can relax, allowing for the

reaction to progress [350]. Theoretically, this technique could be used to observe the hydrolysis reaction within the TE active site, and confirm the role of the hexyl tail by capturing the position of the hexyl tail as the reaction proceeds. Following such a line of study would be highly feasible, as Dr. Jing-Yuan Liu, one of my mentors and committee members at IUSM, has extensive crystallography experience and is also acquainted with the authors of this study, indicating a high potential for collaboration.

Another future direction is to design orlistat derivatives that interact irreversibly with TE, and are resistant to hydrolysis. Based on the conclusions of this study, it could be speculated that hydrolysis resistance could be achieved with compounds that stabilize the hydrogen bond with His²⁴⁸¹. Hydrolysis resistance could also be achieved with compounds that contain moieties that block the area of the active site occupied by the catalytic water. Several collaborations within the IU community have been created in order to carry out the following future studies. We have designed several orlistat derivatives that contain bulky moieties that could potentially form hydrogen bonds with His²⁴⁸¹, while simultaneously blocking the active site from water molecules (Fig. 1). These derivatives are currently being synthesized in collaboration with Dr. Haibo Ge in the Department of Chemistry and Chemical Biology at IUPUI. In order to examine the hydrolysis potential of each derivative, we are collaborating with Dr. David Jones in the Division of Clinical Pharmacology at IUSM to create a method to separate parent orlistat from the hydrolyzed product and subsequently quantify the amount of hydrolyzed orlistat product that is created by recombinant FASN TE protein. Upon incubation with the synthesized orlistat derivatives, we expect to see a differential creation of hydrolyzed product compared to orlistat, indicating that the derivatives are more resistant to

hydrolysis by FASN TE. Additionally, it would be highly interesting to virtually modify orlistat within the FASN TE crystal structure to create the orlistat derivatives depicted in Figure 1 and repeat MD simulations to virtually predict the behavior of each derivative, to complement experimental studies.

FIGURE 1

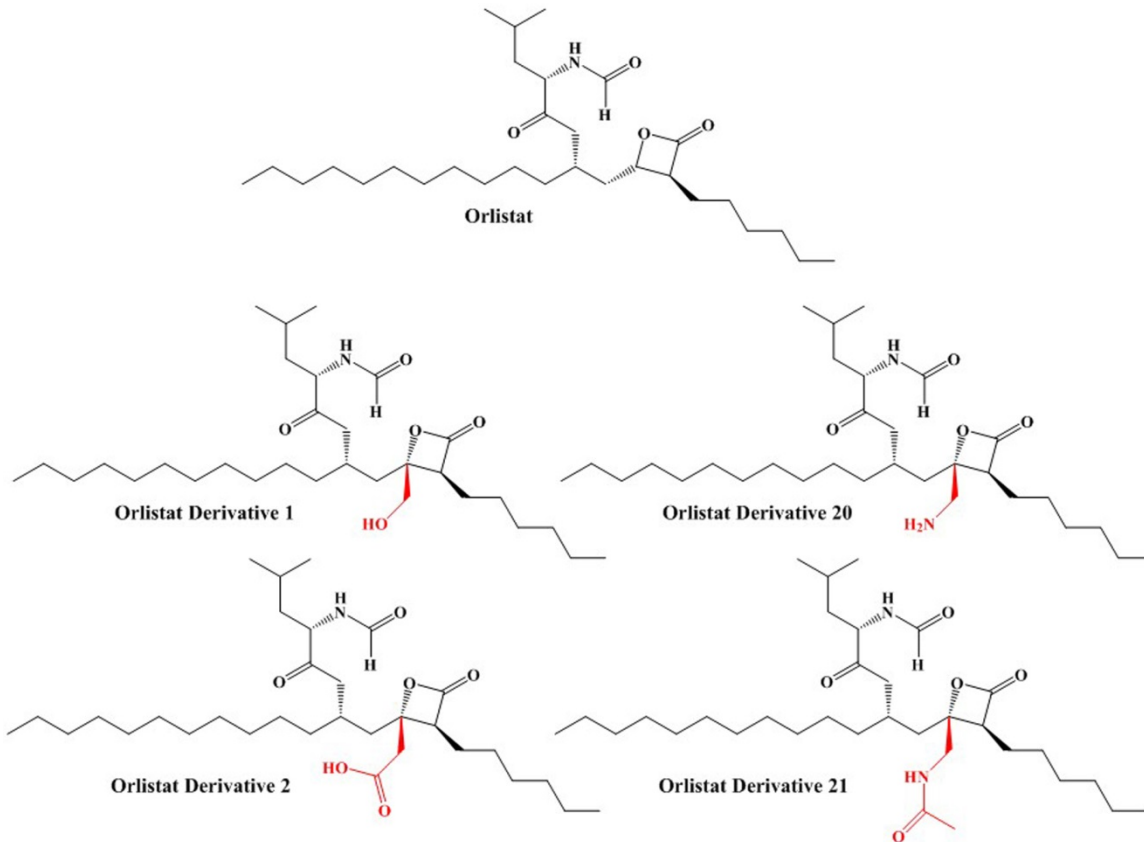


Figure 1: Orlistat derivatives. Orlistat derivatives 1, 2, 20 and 21 contain added moieties (depicted in red) that are designed to both form hydrogen bonds with His²⁴⁸¹ and block the space within the FASN TE active site that water must occupy to catalyze the hydrolysis of the covalent bond between orlistat and Ser²³⁰⁸.

B. Summary and Future Directions for Specific Aims II and III

The goal of the second part of this study was to search for novel inhibitors of FASN TE using *in-silico* ligand screening with DOCK. In total, a library of novel compounds containing approximately 200,000 ligands and a library of FDA approved drugs containing approximately 2,000 compounds were virtually screened. Of almost 200 compounds tested with a high-throughput method using recombinant FASN TE, it was found that one of the candidate ligands tested, FDA approved pantoprazole, could inhibit FASN TE activity in a dose-dependent manner. Pantoprazole is a member of a class of drugs called proton pump inhibitors, which inhibit gastric acid secretion by irreversibly binding to and inhibiting proton pumps in gastric parietal cells. Further examination determined that other PPIs, omeprazole/esomeprazole, lansoprazole and rabeprazole, also appeared among the highest scoring compounds from *in-silico* screening, and each inhibited FASN TE activity. All PPIs, especially lansoprazole, decreased tumor cell proliferation, colony forming ability and lipid synthesis in a dose-dependent manner in several pancreatic cancer cell lines. Further study determined that lansoprazole directly interacts with the active site of FASN TE in a competitive manner, inducing cell death in a dose-dependent manner. Supplementation with exogenous palmitate partially rescued the effects of lansoprazole, and cells with higher levels of FASN activity were more sensitive to lansoprazole treatment. As PPIs are currently under investigation as chemotherapeutic agents for use in combination therapy, the results of this study provide a mechanism by which PPIs, especially lansoprazole, are exerting their effects in cancer cells, and also demonstrate the utility of targeting FASN for anti-cancer treatment.

There are a number of studies that should be performed as a follow-up to the work presented here. In the immediate future, an imperative study would be to examine the effects of lansoprazole on fatty acid synthesis in tumor cells *in vivo*, to determine if the fatty acid synthesis pathway is indeed affected by lansoprazole treatment, confirming that this mechanism is an important pathway by which lansoprazole is acting *in vivo*. After implanting PANC-1 ectopic xenografts into mice, lansoprazole-mediated inhibition of FASN could be measured *in vivo* by administering lansoprazole or vehicle control intravenously to the tumor-bearing mice. Flank tumors would then be excised and FASN activity measured by the incorporation [¹⁴C]-acetate into lipids in the tumor tissue. A study to determine if lansoprazole treatment can synergize the effect of the first line chemotherapy drug for the treatment of pancreatic cancer, gemcitabine, or radiation treatment, or could potentially reduce the resistance of pancreatic cancer cells to either gemcitabine or radiation treatment, both *in vitro* and *in vivo* are also highly important and informative studies that should be conducted. As one of my thesis committee members, Dr. Karen Pollok, is the Director of the In Vivo Therapeutics Core at IUSM, it would be highly possible to perform *in vivo* studies with her assistance and expertise.

In addition, it is reasonable that the effect of lansoprazole treatment could be examined in other cancer types that are known to over-express FASN, and that combination therapies with lansoprazole could also be investigated. Performing x-ray crystallography with a protein crystal of FASN TE with lansoprazole would also provide invaluable information about the way in which lansoprazole interacts with the FASN TE active site, and could aid in the design of novel lansoprazole derivatives as FASN inhibitors. Further in the future, it is feasible that clinical trials with human patients could

be conducted, as lansoprazole is already FDA approved and is available in IV formulation, to determine if concurrent lansoprazole treatment is able to increase the efficacy of chemotherapeutic treatment. Lastly, it would be highly interesting to collaborate with an epidemiologist to examine medical data to determine the incidence of cancer in patients who have been subjected to long-term PPI therapy. Such a study may provide evidence that PPI therapy is useful as strategy for the prevention and treatment of cancer that should be further investigated.

C. Final Remarks

There are many ways that completing the work presented in this thesis shaped my development as a graduate student, but one of the greatest lessons I learned throughout my time as a graduate student researcher was the importance of alternative strategies. When trying to publish my results for Specific Aim I, we ran into a lot of trouble convincing reviewers that the hexyl tail conformational transition was not just a simple relaxation. We had to think outside the box to find new ways to demonstrate that two unique conformations of the hexyl tail existed. Although it certainly didn't seem like it at the time, I was very fortunate for this experience, because later in my graduate school career, I was sure to employ multiple strategies when examining the effects of lansoprazole for Specific Aim III. I wanted to be sure that the results I generated were harder to question or refute, and thus I tried to answer each question I was asking from at least two angles, especially when trying to demonstrate that the fatty acid synthesis pathway is affected by lansoprazole treatment. I also learned that new strategies may also drive the research in a new direction that wasn't originally envisioned. Following

multiple rounds of virtual screening and testing compounds with HTS, I found only one potential novel inhibitor of FASN TE with very moderate potency and although I was frustrated, I elected not to abandon the project. Instead, I decided to take the project in a different direction by virtually screening a new library of FDA compounds with a new, more highly resolved, FASN TE crystal structure. I never imagined that not only would I find a new inhibitor of FASN TE that was already FDA approved, but that I would find one from a class of drugs that has already garnered a high amount of interest in the cancer field, thus providing new information on how this drug may be affecting cancer cell growth. Although it is definitely the case that some projects must be abandoned, I fully realized the importance of exhausting alternative strategies before giving up on a project. I think that understanding the importance of troubleshooting and having the foresight to look at a question from multiple angles, as well as being able to more fully defend a position or actions, will serve any graduate student well in any career, not just scientific research.

It is possible that my research of orlistat within FASN TE may lead to the design of new inhibitors of TE for use in cancer treatment, or that my research with PPIs may provide a rationale for further investigating their use in cancer treatment. Knowing that I have contributed new information that may have an impact on clinical treatments and outcomes makes all of the sacrifices necessary to successfully complete graduate school seem extremely small in comparison. Focusing on the big picture is important advice for any graduate student—because in the end, when your graduate career comes to a close, the struggles are worth it.

Appendices

Appendix A: Gaussian and Molecular Dynamics Input Files

A. Input Files Used for Orlistat Parameterization

Detailed explanations of each value contained in the following files used for orlistat parameterization can be found in the Gaussian03 online user's manual (http://www.ict.jussieu.fr/manuels/Gaussian03/g_ur/keywords.htm).

The capped orlistat-serine complex was optimized by using the following .gau file:

```
%chk=orlistat_opt.chk
#P b3lyp/6-31G* Opt=modredundant

orlistat B3LYP geo out

0 1

C      9.61900    3.09900   35.26300
C     10.17400    2.55200   33.95500
O      9.46100    1.90700   33.19800
H     10.40300    3.64100   35.79300
H      8.79000    3.77400   35.05100
H      9.26600    2.27400   35.88100
N     11.33900    2.46400   33.47000
C     12.23400    1.83600   32.48900
C     11.68500    2.16800   31.08700
O     11.68900    3.34300   30.69900
C     12.26600    0.31900   32.73900
O     13.12100   -0.32000   31.76800
H     11.90800    3.11700   33.98900
H     13.23800    2.24600   32.59500
H     12.64900    0.12600   33.74100
H     11.25700   -0.08400   32.65400
N     10.90500    1.45800   30.37700
C     10.19400    1.81100   29.11500
H     10.74400    0.52100   30.71700
H      9.67700    0.93200   28.73100
```

H	10.91600	2.15900	28.37600
H	9.47000	2.60100	29.31500
C	16.33600	1.83200	30.27000
C	17.61800	1.02900	30.48300
C	17.45200	0.01400	31.61900
C	17.57700	-1.42200	31.08500
C	16.29100	-2.24400	31.29100
C	15.11100	-1.73000	30.42900
C	13.72400	-2.46300	30.55300
C	12.68800	-1.53900	31.29100
O	11.49200	-1.86700	31.40200
C	13.75800	-3.93200	31.09800
O	12.42200	-4.45400	31.24100
C	14.68200	-4.88700	30.26400
C	14.00800	-5.78100	29.14500
O	12.67200	-6.32400	29.46600
C	12.68100	-7.70200	29.52600
O	13.76100	-8.28100	29.37500
C	11.39400	-8.54800	29.78100
C	10.09300	-7.89000	29.26300
C	9.23700	-8.80400	28.35100
C	7.88200	-8.16000	28.05000
C	9.00500	-10.2130	28.90500
N	11.24900	-8.84900	31.22300
C	11.25000	-10.1060	31.68000
O	11.13300	-10.4270	32.86500
C	14.06000	-5.05800	27.77000
C	13.84800	-6.02500	26.60200
C	15.16600	-6.37500	25.89300
C	14.95500	-7.49200	24.86100
C	14.65500	-6.91200	23.47300
C	14.80600	-7.95500	22.36400
C	15.67100	-7.38900	21.23300
C	14.99400	-7.52800	19.86200
C	14.50100	-6.17700	19.33900
C	13.93800	-6.31100	17.92100
C	12.72700	-5.39300	17.69800
H	16.48300	2.54400	29.45800
H	15.52100	1.15400	30.01500
H	16.08800	2.37000	31.18500
H	18.42900	1.71300	30.73300
H	17.86600	0.50000	29.56300
H	18.22500	0.18600	32.36800

H	16.47100	0.14400	32.07700
H	18.39600	-1.91800	31.60600
H	17.80600	-1.38500	30.02000
H	16.49300	-3.28100	31.02300
H	16.00700	-2.19900	32.34200
H	15.42000	-1.79700	29.38600
H	14.95600	-0.67700	30.66600
H	13.35400	-2.54700	29.53100
H	14.18300	-3.88300	32.10100
H	11.94900	-3.94700	31.90600
H	15.17000	-5.56100	30.96700
H	15.45300	-4.28000	29.79000
H	14.65600	-6.65100	29.04000
H	11.51400	-9.49600	29.25700
H	10.36300	-6.99900	28.69600
H	9.49000	-7.58900	30.11900
H	9.76600	-8.90900	27.40400
H	8.03600	-7.15600	27.65500
H	7.29500	-8.10300	28.96700
H	7.34900	-8.76200	27.31400
H	9.96500	-10.6810	29.12300
H	8.41500	-10.1510	29.82000
H	8.46900	-10.8100	28.16700
H	11.14700	-8.08700	31.87800
H	11.36200	-10.9000	30.95700
H	13.27900	-4.29800	27.74300
H	15.03100	-4.57400	27.65900
H	13.17400	-5.56300	25.88100
H	13.39200	-6.94100	26.97800
H	15.89200	-6.70700	26.63500
H	15.54900	-5.48800	25.38800
H	15.85800	-8.10000	24.80500
H	14.12000	-8.11800	25.17600
H	13.63200	-6.53600	23.46400
H	15.33900	-6.08600	23.27800
H	13.82200	-8.21200	21.97300
H	15.27900	-8.84900	22.77000
H	16.61900	-7.92700	21.21300
H	15.86500	-6.33400	21.42800
H	14.14300	-8.20300	19.95400
H	15.70700	-7.94700	19.15200
H	13.71900	-5.80300	19.99900
H	15.33100	-5.47100	19.33000

H	14.71700	-6.04700	17.20600
H	13.63700	-7.34500	17.75400
H	12.35800	-5.51800	16.68000
H	11.93900	-5.65300	18.40500
H	13.02400	-4.35600	17.85100

1 2 7 8 F

#* * * * F (additional dihedrals to be frozen listed by atom number as above)

Opt=modredundant indicates to Gaussian that internal coordinates are to be used for the frozen dihedrals, and the line 0 1 is used to indicate to Gaussian that the charge on this particular molecule is 0.

To calculate the electrostatic potential (ESP) for the optimized orlistat ligand, the coordinates of the optimized orlistat-serine complex were input into Gaussian with a similar .gau file as above, but this time with this route card preceding the coordinates:

```
%chk=floB_hf.chk
#P HF/6-31G* Geom=check SCF=Tight Pop=MK IOp(6/33=2)
```

```
orlistat HF ESP
```

```
0 1
```

IOp(6/33=2) instructs Gaussian to write out potential points and potentials, and SCF=Tight indicates tight convergence.

The ESP data from Gaussian was converted into RESP format using the script esp.sh, which contained the following:

```
#!/bin/csh
xlf /usr/local/Amber/AMBER8/amber8/src/resp/readit.f
```



```
grep "Atomic Center " $1 > a
grep "ESP Fit" $1 > b
grep "Fit " $1 > c
./a.out
rm -f a b c a.out readit.o
```

To perform the RESP charge fitting, a two-step procedure was used. In the first step, the charges of the caps were specified as by Cornell *et al.* The resp.in file included the following information:

```
orlistat- resp run #1
```

```
&cntrl
ihfree=1,
qwt=0.0005,
iqopt=2,
/
```

```
1.0
orlistat
0 111
6 -1
6 -1
8 -1
1 -1
1 -1
1 -1
7 0
6 0
6 0
8 0
6 0
8 0
1 0
1 0
1 0
1 0
7 -1
6 -1
1 -1
1 -1
1 -1
1 -1
```

```
#Remaining atoms would continue to be defined below.
```

ihfree=1 indicated to RESP to weakly restrain only the heavy atoms, with a strength of 0.0005 AU (qwt=0.0005). iqopt=2 indicated that RESP should read in initial charges from a .qin file, where we defined and fixed the cap charges. In the resp.in file, each atom was defined by its atomic number (1 for hydrogen, 6 for carbon, 7 for nitrogen and 8 for oxygen) in the same order as in the Gaussian optimization and ESP coordinates. A designator of 0 indicated that the charge for the atom should be calculated freely, whereas a designator of -1 indicated that the charge is fixed and should be read-in from the qin file:

```
-0.366200 0.597200 -0.567900 0.112300 0.112300 0.112300 0.000000 0.000000
0.000000 0.000000 0.000000 0.000000 0.000000 0.000000 0.000000 0.000000
-0.415700 -0.149000 0.217900 0.097600 0.097600 0.097600 0.000000 0.000000
0.000000 0.000000 0.000000 0.000000 0.000000 0.000000 0.000000 0.000000
0.000000 0.000000 0.000000 0.000000 0.000000 0.000000 0.000000 0.000000
0.000000 0.000000 0.000000 0.000000 0.000000 0.000000 0.000000 0.000000
0.000000 0.000000 0.000000 0.000000 0.000000 0.000000 0.000000 0.000000
0.000000 0.000000 0.000000 0.000000 0.000000 0.000000 0.000000 0.000000
0.000000 0.000000 0.000000 0.000000 0.000000 0.000000 0.000000 0.000000
0.000000 0.000000 0.000000 0.000000 0.000000 0.000000 0.000000 0.000000
0.000000 0.000000 0.000000 0.000000 0.000000 0.000000 0.000000 0.000000
0.000000 0.000000 0.000000 0.000000 0.000000 0.000000 0.000000 0.000000
0.000000 0.000000 0.000000 0.000000 0.000000 0.000000 0.000000 0.000000
0.000000 0.000000 0.000000 0.000000 0.000000 0.000000 0.000000 0.000000
0.000000 0.000000 0.000000 0.000000 0.000000 0.000000 0.000000 0.000000
0.000000 0.000000 0.000000 0.000000 0.000000 0.000000 0.000000 0.000000
```

To perform the second step of RESP, a new input file is created, with the same RESP parameters as above, except qwt, which is upped to 0.001, that freezes all atoms except for methyl and methylene hydrogen atoms. This step is necessary to ensure that rotationally-degenerate atoms have the same charge. For frozen atoms, the charges calculated from the previous step are read-in from a new .qin file, with the charge on all methyl and methylene hydrogens listed as 0 in order to calculate a new charge. To

indicate in the resp.in file that a set of hydrogen atoms are to have an equivalent charge, the first hydrogen atom in the atom list is designated as 0, and the equivalent hydrogen atom(s) are designated as the atom number of the first hydrogen.

B. Input Files Used for the Validation of Covalent-Orlistat Parameterization

The QM package Gaussian03 was used to calculate the single point energy of each ω angle rotamer of the 3-mer covalent-orlistat peptide in order to create a potential energy surface of the ω angle. The ω angle is described by variable d25. The z-matrix input file for the rotamer at 338 degrees (orlistat_8A_338.gau) appeared as follows:

```
%chk=orlistat_338_SP.chk  
#HF/6-31G* SCF=Tight
```

```
_338_SP
```

```
O 1  
N  
H 1 r2  
H 1 r3 2 a3  
H 1 r4 2 a4 3 d4  
C 1 r5 2 a5 3 d5  
H 5 r6 1 a6 2 d6  
H 5 r7 1 a7 2 d7  
C 5 r8 1 a8 2 d8  
O 8 r9 5 a9 1 d9  
C 9 r10 8 a10 5 d10  
O 10 r11 9 a11 8 d11  
N 8 r12 5 a12 1 d12  
C 12 r13 8 a13 5 d13  
C 13 r14 12 a14 8 d14  
O 14 r15 13 a15 12 d15  
C 15 r16 14 a16 13 d16  
C 16 r17 15 a17 14 d17  
C 17 r18 16 a18 15 d18  
C 18 r19 17 a19 16 d19  
C 19 r20 18 a20 17 d20  
C 20 r21 19 a21 18 d21  
C 21 r22 20 a22 19 d22  
C 15 r23 14 a23 13 d23
```

O 23 r24 15 a24 14 d24
C 22 r25 21 a25 20 d25
O 25 r26 22 a26 21 d26
C 25 r27 22 a27 21 d27
C 27 r28 25 a28 22 d28
O 28 r29 27 a29 25 d29
C 29 r30 28 a30 27 d30
O 30 r31 29 a31 28 d31
C 30 r32 29 a32 28 d32
C 32 r33 30 a33 29 d33
C 33 r34 32 a34 30 d34
C 34 r35 33 a35 32 d35
C 34 r36 33 a36 32 d36
N 32 r37 30 a37 29 d37
C 37 r38 32 a38 30 d38
O 38 r39 37 a39 32 d39
C 28 r40 27 a40 25 d40
C 40 r41 28 a41 27 d41
C 41 r42 40 a42 28 d42
C 42 r43 41 a43 40 d43
C 43 r44 42 a44 41 d44
C 44 r45 43 a45 42 d45
C 45 r46 44 a46 43 d46
C 46 r47 45 a47 44 d47
C 47 r48 46 a48 45 d48
C 48 r49 47 a49 46 d49
C 49 r50 48 a50 47 d50
H 12 r51 8 a51 5 d51
H 13 r52 12 a52 8 d52
H 14 r53 13 a53 12 d53
H 14 r54 13 a54 12 d54
H 33 r55 32 a55 30 d55
H 33 r56 32 a56 30 d56
H 17 r57 16 a57 15 d57
H 17 r58 16 a58 15 d58
H 16 r59 15 a59 14 d59
H 16 r60 15 a60 14 d60
H 16 r61 15 a61 14 d61
H 22 r62 21 a62 20 d62
H 25 r63 22 a63 21 d63
H 27 r64 25 a64 22 d64
H 27 r65 25 a65 22 d65
H 28 r66 27 a66 25 d66
H 32 r67 30 a67 29 d67
H 37 r68 32 a68 30 d68
H 38 r69 37 a69 32 d69
H 34 r70 33 a70 32 d70
H 36 r71 34 a71 33 d71

H 36 r72 34 a72 33 d72
H 36 r73 34 a73 33 d73
H 35 r74 34 a74 33 d74
H 35 r75 34 a75 33 d75
H 35 r76 34 a76 33 d76
H 40 r77 28 a77 27 d77
H 40 r78 28 a78 27 d78
H 41 r79 40 a79 28 d79
H 41 r80 40 a80 28 d80
H 42 r81 41 a81 40 d81
H 42 r82 41 a82 40 d82
H 43 r83 42 a83 41 d83
H 43 r84 42 a84 41 d84
H 44 r85 43 a85 42 d85
H 44 r86 43 a86 42 d86
H 45 r87 44 a87 43 d87
H 45 r88 44 a88 43 d88
H 46 r89 45 a89 44 d89
H 46 r90 45 a90 44 d90
H 47 r91 46 a91 45 d91
H 47 r92 46 a92 45 d92
H 48 r93 47 a93 46 d93
H 48 r94 47 a94 46 d94
H 49 r95 48 a95 47 d95
H 49 r96 48 a96 47 d96
H 50 r97 49 a97 48 d97
H 50 r98 49 a98 48 d98
H 50 r99 49 a99 48 d99
H 26 r100 25 a100 22 d100
H 21 r101 20 a101 19 d101
H 21 r102 20 a102 19 d102
H 20 r103 19 a103 18 d103
H 20 r104 19 a104 18 d104
H 19 r105 18 a105 17 d105
H 19 r106 18 a106 17 d106
H 18 r107 17 a107 16 d107
H 18 r108 17 a108 16 d108
N 10 r109 9 a109 8 d109
H 109 r110 10 a110 9 d110
C 109 r111 10 a111 9 d111
H 111 r112 109 a112 10 d112
H 111 r113 109 a113 10 d113
C 111 r114 109 a114 10 d114
O 114 r115 111 a115 109 d115
O 114 r116 111 a116 109 d116

Variables:

r2= 1.0104

#Each subsequent variable would be listed below

The mini.in file, used to execute the minimization and energy calculation of each dihedral rotamer within the Big Red Supercomputer environment, contained the following:

```
minimize structure
&cntrl
imin=1,maxcyc=1000,ncyc=500,
cut=1000,ntb=0,
ntc=1,ntf=1,
ntpr=100,igb=6,
ntr=1,restraintmask=':1-3',
restraint_wt=25.0
/
```

C. Input Files Used for Molecular Modeling and MD Simulations

Detailed explanations of each value contained in the following files used for the MD simulations can be found in the AMBER11 user's manual (<http://ambermd.org/doc11/Amber11.pdf>). Each step of the MD simulation was performed using the Big Red supercomputer.

The tleap script used to prepare the topology and coordinate files of the FASN TE system with covalent-orlistat for AMBER simulation contained the following:

```
source leaprc.ff03
source leaprc.gaff
loadoff unk_new_definitions.lib
loadAmberParams unk.frcmod
x=loadpdb orlistat_new_definitions_for_MD_HID.pdb
charge x
addions x Na+ 0
solvatebox x TIP3PBOX 8
savepdb x orlistat_HID_solvate.pdb
saveamberparm x orlistat_HID_solvate.top orlistat_HID_solvate.crd
charge x
check x
quit
```

The first step of the system equilibration, which minimized the energy of the water molecules and the counter ions in the system, used the following input file:

```
minimize structure
&cntrl
imin=1,maxcyc=1000,ncyc=500,
cut=8.0,ntb=1,
ntc=2,ntf=2,
ntpr=100,
ntr=1, restraintmask=':1-281',
restraint_wt=500.0
/
```

The second step of the system equilibration, which removed the restraints and minimized the energy of the whole system, used the following input file:

```
minimize structure
&cntrl
imin=1,maxcyc=25000,ncyc=10000,
cut=8.0,ntb=1,
ntc=2,ntf=2,
ntpr=100,
ntr=0,
/
```

The third step of the system equilibration, which heated the system from 0 to 300 K, used the following input file:

```
heat structure
&cntrl
imin=0,irest=0,ntx=1,
nstlim=25000,dt=0.002,
ntc=2,ntf=2,
cut=8.0,ntb=1,
ntpr=500,ntwx=500,
ntt=3,gamma_ln=2.0,
tempi=0.0,temp0=300.0,
ntr=1, restraintmask=':1-281',
restraint_wt=10.0,
nmropt=1
/
&wt TYPE='TEMPO', istep1=0, istep2=25000,
```

```
value1=0.1, value2=300.0, /  
&wt TYPE='END' /
```

The fourth step of the equilibration, which equilibrated the system with a constant pressure dynamics simulation, used the following input file:

```
heat structure  
&cntrl  
  imin=0, irest=1, ntx=5,  
  nstlim=25000, dt=0.002,  
  ntb=2, pres0=1.0, ntp=1, taup=1.0,  
  ntc=2, ntf=2,  
  cut=8.0,  
  ntp=100, ntwx=100, ntwr = 1000  
  ntt=3, gamma_ln=2.0,  
  tempi=300, temp0=300.0,  
  ntr=1, restraintmask=':1-281',  
  restraint_wt=10.0  
/
```

The final step of the equilibration and beginning of the MD simulation used the following input file:

```
heat structure  
&cntrl  
  imin=0, irest=1, ntx=5,  
  nstlim=2500000, dt=0.002,  
  ntc=2, ntf=2,  
  cut=8.0, ntb=2, ntp=1, taup=2.0,  
  ntp=1000, ntwx=1000,  
  ntt=3, gamma_ln=2.0,  
  temp0=300.0  
/
```

The production steps of the MD simulation used a series of input files to perform the MD simulation within the Big Red Supercomputer environment. Each production step simulated 10 ns of the total simulation, building upon each previous portion of the simulation. An example prod input file contained the following:

```
production MD  
&cntrl
```



```
imin=0,irest=1,ntx=5,  
nstim=5000000,dt=0.002,  
ntc=2,ntf=2,  
cut=8.0,ntb=2,ntp=1,taup=2.0,  
ntpr=5000,ntwx=5000,  
ntt=3,gamma_ln=2.0,  
temp0=300.0,  
/  

```

D. Input Files for MD Simulation Trajectory Analysis

The ptraj module of AMBER was used to process each simulation, and was then used to extract a variety of information from the simulations. First, to process the simulation, each production output .mdcrd coordinate file was combined into one file using the image_equil_prod.ptraj input file. In addition, the first 60 ps from the equilibration step were excluded from the trajectory by indicating the frame number in which the trajectory should begin:

```
trajin equil.mdcrd 301 2500 5  
trajin prod.mdcrd  
trajin prod2.mdcrd  
trajin prod3.mdcrd  
trajin prod4.mdcrd  
center :1-281  
image familiar  
trajout extended_equil_prod_orlistat_HID_imaged.mdcrd
```

Desired information could then be extracted from the trajectory by using the newly written mdcrd file in conjunction with the ptraj module. Instructions on how to request specific trajectory information with ptraj can be found in the AMBER manual.

RMSD:

```
trajin ../equil_prod_orlistat_HID_extended_imaged.mdcrd  
center :1-281  
image familiar
```

```
rms first mass out rmsd_equil_prod_whole_structure :1-281@CA,C,N
rms first mass out rmsd_equil_prod_catalytic_triad_ser2308 :88
rms first mass out rmsd_equil_prod_whole_structure_without_loops :1-105,109-123,141-
229,241-281@CA,C,N
go
```

RMSF:

```
trajin ../extended_equil_prod_orlistat_HID_imaged.mdcrd
strip @H*
strip @?H*
rms out rmsd_noH :1-281@CA,C,N
atomicfluct out orlistat_equil_prod_noH_byres :1-281 byres
atomicfluct out orlistat_equil_prod_noH_byres_bfactor :1-281 byres bfactor
atomicfluct out orlistat_equil_prod_noH_byatom_bfactor :1-281 byatom bfactor
atomicfluct out orlistat_equil_prod_noH_byatom :1-281 byatom
atomicfluct out orlistat_equil_prod_noH_residue_byres_bfactor :88 byres bfactor
atomicfluct out orlistat_equil_prod_noH_residue_byres :88 byres
atomicfluct out orlistat_equil_prod_noH_residue_byatom_bfactor :88 byatom bfactor
atomicfluct out orlistat_equil_prod_noH_residue_byatom :88 byatom
go
```

Hexyl tail-pocket distance:

```
trajin ../extended_equil_prod_orlistat_HID_imaged.mdcrd
distance a :88@C7,C8,C9,C10,C11,C12,C13 :119,122,123,242 mass out distance_pocket1
distance b :88@C7,C8,C9,C10,C11,C12,C13 :89,123,212 mass out distance_pocket2
```

Dihedral angle:

```
trajin ../extended_equil_prod_orlistat_HID_imaged.mdcrd
dihedral tail_shift :88@C15 :88@C13 :88@C12 :88@C11 out tail_shift
```

Some of the dihedral angle information is output as negative numbers. To correct this, the following .awk script is used:

```
{
  if ($2 ~ /-/) {
    print $1 "\t" $2+360
  } else {
    print $1 "\t" $2
  }
}
```

E. Free Energy Calculations

To calculate the free energy of orlistat, either in the 3-mer complex or within TE, during each MD simulation, snapshots were first extracted from the trajectory and then the free energy was calculated using the MM_PBSA module of AMBER. An explanation of each value contained in the files can be found in the AMBER manual. First, a topology file containing only orlistat with all solvent removed was prepared by Tleap. Snapshots from each simulation were extracted using an extraction.in file, as shown below for the 3-mer peptide containing orlistat:

```
@GENERAL
PREFIX                snapshot_confl
PATH                  ./
COMPLEX               0
RECEPTOR            1
LIGAND                0
RECPT                 ../orlistat_rec.top
GC                   1
AS                   0
DC                   0
MM                   0
GB                   0
PB                   0
MS                   0
NM                   0
@MAKECRD
```

```

BOX                YES
NTOTAL             10370
NSTART             1547
NSTOP              1947
NFREQ              8
NUMBER_LIG_GROUPS 0
NUMBER_REC_GROUPS 1
RSTART             1
RSTOP              116
@TRAJECTORY
TRAJECTORY         ../../equil_prod_three_mer_imaged.mdcrd
@PROGRAMS

```

Where NTotal is the total number of atoms in the simulation, including solvent atoms; NStart and NStop indicate the desired frame numbers of the simulation that the snapshots will be extracted from; NFreq indicates the frequency in which a frame snapshot will be extracted; and RStart and RStop indicate the first and last atom number of the 3-mer orlistat peptide.

Following frame extraction, free energy calculations were performed using the Big Red Supercomputer using the following input file:

```

@GENERAL
PREFIX            snapshot_conf1
PATH               ../extract_snapshots_conf1/
COMPLEX            0
RECEPTOR         1
LIGAND             0
RECPT              ../orlistat_rec.top
GC                 0
AS                 0
DC                 0
MM                 1
GB                 1
PB                 1
MS                 1
NM                 0
@PB

```

PROC	2
REFE	0
INDI	1
EXDI	80
FILLRATIO	2
SCALE	2
LINIT	1000
PRBRAD	1.4
ISTRNG	0
RADIOPT	0
NPOPT	1
CAVITY_SURFTEN	0.0072
CAVITY_OFFSET	0
SURFTEN	0.0072
SURFOFF	0
@MM	
DIELC	1
@GB	
IGB	2
GBSA	1
SALTCON	0
EXTDIEL	80
INTDIEL	1
SURFTEN	0.0072
SURFOFF	0
@MS	
PROBE	0
@PROGRAMS	

Appendix B: Covalent-Orlistat AMBER Parameters

To manually parameterize covalent-orlistat, all atoms of the molecule were assigned using AMBER Parm99 atom types. Assigning atoms types to orlistat was relatively straightforward. As all the carbon atoms in covalent-orlistat are single-bonded, straight-chain carbons, all carbon atoms were assigned as either aliphatic carbons (CT) or carbonyl carbons (C). All oxygen atoms were assigned as carbonyl oxygen (O), ester oxygen (OS), or hydroxyl oxygen (OH). Both nitrogen atoms in the molecule were assigned as amide/amino nitrogen (N). Assigning most hydrogen atoms was also straightforward. Any hydrogen atom bound to nitrogen was assigned AMBER atom type H, the designator for any hydrogen atom bound to nitrogen, and the hydrogen atom of the hydroxyl group was assigned atom type HO. Assigning the hydrogen atoms bonded to carbon atoms proved to be a little more difficult. All remaining hydrogen atoms were assigned HC, indicating a hydrogen atom bonded to an aliphatic carbon atom that is not bonded to any electron withdrawing groups, or H1, indicating a hydrogen atom bonded to an aliphatic carbon that is bonded to an electron withdrawing group, such as a carbonyl oxygen or an ester group. Using tleap also gave us a clue as to how to assign some of the hydrogen atoms. For example, when the hydrogen atom bonded to the carbon atom that was bonded to the ester oxygen or hydroxyl oxygen was named as HC, the angle information was not recognized by AMBER, but was recognized when the hydrogen atom was assigned as H1, indicating that H1 is likely the correct designation. All atom type information is shown in Figure 1 and Table 1.

FIGURE 1

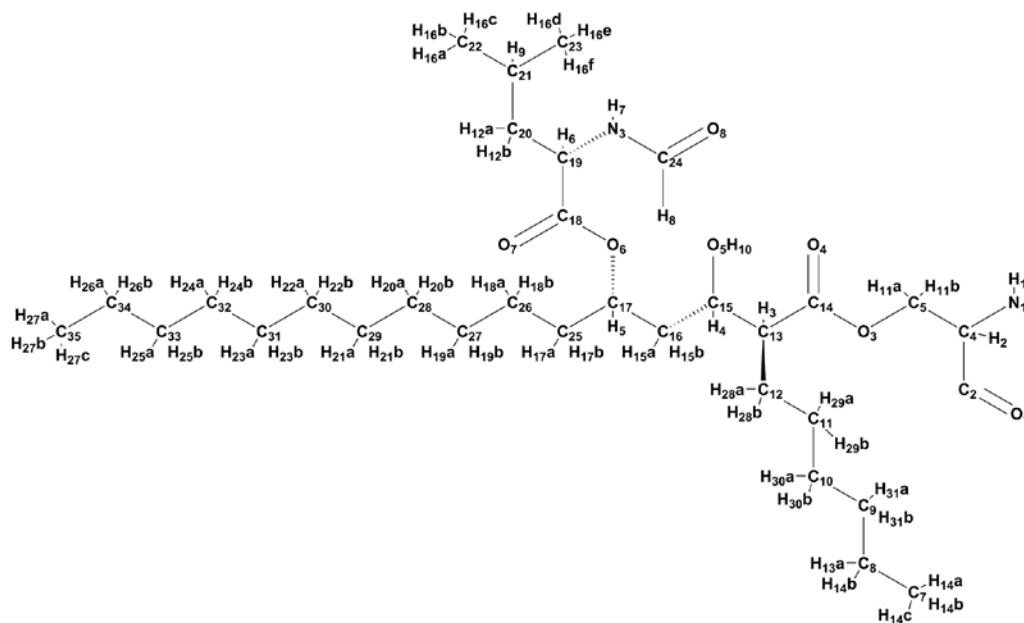


Figure 1: Orlistat atom type and charge indicator. All charge and atom type information for each labeled atom is shown in Table 1. Note: some atom names are skipped (e.g. N2) because they were part of the caps that were deleted after charge information was calculated. All atoms were designated with typical AMBER parameters.

TABLE 1: Charge and AMBER atom type for each covalent-orlistat atom.

Atom Name	Atom Type	Charge
C2	C	0.5973
C4	CT	-0.0249
C5	CT	0.96957
C7	CT	-0.21391
C8	CT	0.154356
C9	CT	-0.0384
C10	CT	-0.22333
C11	CT	-0.0256
C12	CT	0.289982
C13	CT	-0.21377
C14	C	0.64416
C15	CT	0.487977
C16	CT	-0.21933
C17	CT	0.375761
C18	C	0.734028
C19	CT	-0.09274
C20	CT	-0.18998
C21	CT	0.486037
C22	CT	-0.60515
C23	CT	-0.60515
C24	C	0.497094
C25	CT	-0.47223
C26	CT	0.095986
C27	CT	0.089067
C28	CT	-0.18191
C29	CT	-0.02542
C30	CT	-0.04101
C31	CT	-0.03524
C32	CT	-0.03744
C33	CT	0.015044
C34	CT	0.176255
C35	CT	-0.23118
O1	O	-0.5679
O3	OS	-0.70774
O4	O	-0.50997
O5	OH	-0.7108
O6	OS	-0.32649
O7	O	-0.58682
O8	O	-0.56608
N1	N	-0.4157
N3	N	-0.45928
H1	H	0.2179

H2	H1	0.0843
H3	HC	0.048444
H4	H1	-0.04318
H5	H1	0.040469
H6	H1	0.109389
H7	H	0.342667
H8	H1	0.056854
H9	HC	-0.04794
H10	HO	0.388459
H11a (Named 1H11 in AMBER)	H1	-0.1563
H11b (Named 2H11 in AMBER)	H1	-0.1563
H12a (1H12)	HC	0.065465
H12b (2H12)	HC	0.065465
H13a (1H13)	HC	-0.0192
H13b (2H13)	HC	-0.0192
H14a (1H14)	HC	0.036318
H14b (2H14)	HC	0.036318
H14c (3H14)	HC	0.036318
H15a (1H15)	HC	0.050923
H15b (2H15)	HC	0.050923
H16a (1H16)	HC	0.148555
H16b (2H16)	HC	0.148555
H16c (3H16)	HC	0.148555
H16d (4H16)	HC	0.148555
H16e (5H16)	HC	0.148555
H16f (6H16)	HC	0.148555
H17a (1H17)	HC	0.125201
H17b (2H17)	HC	0.125201
H18a (1H18)	HC	-0.00748
H18b (2H18)	HC	-0.00748
H19a (1H19)	HC	-0.00836
H19b (2H19)	HC	-0.00836
H20a (1H20)	HC	0.051187
H20b (2H20)	HC	0.051187
H21a (1H21)	HC	0.026561
H21b (2H21)	HC	0.026561
H22a (1H22)	HC	0.026055
H22b (2H22)	HC	0.026055
H23a (1H23)	HC	0.018544
H23b (2H23)	HC	0.018544
H24a (1H24)	HC	0.006275
H24b (2H24)	HC	0.006275
H25a (1H25)	HC	-0.01062

H25b (2H25)	HC	-0.01062
H26a (1H26)	HC	-0.03437
H26b (2H26)	HC	-0.03437
H27a (1H27)	HC	0.049487
H27b (2H27)	HC	0.049487
H27c (3H27)	HC	0.049487
H28a (1H28)	HC	-0.05
H28b (2H28)	HC	-0.05
H29a (1H29)	HC	0.007992
H29b (2H29)	HC	0.007992
H30a (1H30)	HC	0.066143
H30b (2H30)	HC	0.066143
H31a (1H31)	HC	0.026347
H31b (2H31)	HC	0.026347

Appendix C: DOCK Input Files

Explanations of each value contained in the following files used for *in-silico* ligand screening can be found in the DOCK user's manual (http://dock.compbio.ucsf.edu/DOCK_6/dock6_manual.htm) or the DOCK6.0 tutorial.

A. Input Files Used for Receptor and Ligand Preparation

Spheres were generated using the program sphgen_cpp, along with the input file INSPH. INSPH contained the following:

```
rec.ms  
R  
X  
0.0  
4.0  
1.4  
rec.sph
```

The box for grid generation was created using the DOCK command showbox, along with the input file box.in. Box.in contained the following:

```
Y  
5  
selected_spheres_reduced.sph  
1  
rec_box.pdb
```

The grid input file, grid.in, contained the following:

```
compute_grids      Yes  
grid_spacing       0.3  
output_molecule   No  
contact_score      No  
energy_score       Yes  
energy_cutoff_distance 9999  
atom_model         A  
attractive_exponent 6
```

repulsive_exponent	12
distance_dielectric	Yes
dielectric_factor	4
bump_filter	Yes
bump_overlap	0.75
receptor_file	rec_charged.mol2
box_file	rec_box.pdb
vdw_definition_file	../parameters/vdw_AMBER_parm99.defn
score_grid_prefix	Grid

B. Input Files Used in DOCK Ligand Screening

The input file (dock.in) for the first round of DOCK, grid scoring, contained the following:

ligand_atom_file	zinc.mol2
ligand_outfile_prefix	FASN
limit_max_ligands	no
read_mol_solvation	no
write_orientations	no
write_conformations	no
skip_molecule	no
calculate_rmsd	no
rank_ligands	yes
max_ranked_ligands	200
scored_conformer_output_override	no
orient_ligand	yes
automated_matching	yes
receptor_site_file	../grid/selected_spheres_reduced.sph
max_orientations	1000
critical_points	yes
chemical_matching	no
use_ligand_spheres	no
flexible_ligand	no
bump_filter	no
score_molecules	yes
contact_score_primary	no
contact_score_secondary	no
grid_score_primary	yes
grid_score_secondary	yes
grid_score_vdw_scale	1

grid_score_es_scale	1
grid_score_grid_prefix	../grid/grid
minimize_ligand	yes
simplex_max_iterations	1000
simplex_max_cycles	1
simplex_score_converge	0.1
simplex_cycle_converge	1
simplex_trans_step	1
simplex_rot_step	0.1
simplex_tors_step	10
simplex_final_min_add_internal	no
simplex_secondary_minimize_pose	no
simplex_random_seed	0
atom_model	all
vdw_defn_file	../parameters/vdw_AMBER_parm99.defn
flex_defn_file	../parameters/flex.defn
flex_drive_file	../parameters/flex_drive.tbl

The input file (dock.in) for AMBER scoring contained the following:

ligand_atom_file	lig.amber_score.mol2
ligand_outfile_prefix	output
limit_max_ligands	no
read_mol_solvation	no
write_orientations	no
write_conformations	no
num_scored_conformers_written	1
skip_molecule	no
calculate_rmsd	no
rank_ligands	yes
max_ranked_ligands	200
scored_conformer_output_override	no
orient_ligand	no
flexible_ligand	no
bump_filter	no
score_molecules	yes
contact_score_primary	no
contact_score_secondary	no
grid_score_primary	no
grid_score_secondary	no
dock3.5_score_primary	no
dock3.5_score_secondary	no

continuous_score_primary	no
continuous_score_secondary	no
gbsa_zou_score_primary	no
gbsa_zou_score_secondary	no
gbsa_hawkins_score_primary	no
gbsa_hawkins_score_secondary	no
amber_score_primary	yes
amber_score_secondary	no
amber_score_receptor_file_prefix	FASN
amber_score_movable_region	ligand
amber_score_before_md_minimization_cycles	100
amber_score_after_md_minimization_cycles	100
amber_score_gb_model	5
amber_score_md_steps	3000
amber_score_minimization_cycles	100
amber_score_nonbonded_cutoff	18
amber_score_temperature	300

Appendix D: Novel Compound 13C

To search for novel inhibitors of the TE domain of human FASN, the FASN TE crystal structure with orlistat [213] was obtained from the RCSB protein data bank and was prepared for *in-silico* ligand screening using the DOCK suite of programs (see Chapter 2). A virtual library, ChemDiv, containing over 200,000 total ligands, was scored using DOCK. The 2000 top scoring compounds were scored by AMBER and clustered into groups based on chemical structure using Library MCS (ChemAxon). Any compound with a positive AMBER score, indicating unfavorable binding energy, was discarded and the Lipinski parameters for drug-likeness were calculated for remaining compounds [323]. Any compound violating more than one parameter was discarded. All remaining compounds were visually examined within the TE active site using the Chimera visualization program, and a total of 81 compounds were chosen to examine further, ensuring that each chemical cluster, as determined by Library MCS, was represented.

Compound 13C (Fig. 1A) was initially chosen from the screen because it contains a lactone moiety. Unlike the lactone of orlistat, which could be readily opened upon nucleophilic attack because its 4-membered ring is sterically hindered and therefore unstable, 13C contains a 6-membered ring with double bonds, which is more stable. However, the DOCK program predicted that 13C would bind in the active site of FASN TE with the lactone moiety in close proximity to the active site serine, demonstrating the possibility that 13C may have the potential to be nucleophilically attacked by the active site serine, covalently modifying the enzyme (Fig. 1B). Indeed, chosen compounds were examined for their ability to inhibit TE activity using a fluorogenic assay with

recombinant TE protein, and 13C inhibited FASN TE activity in a dose-dependent manner, with an IC_{50} of 19.18 μ M and a K_i of 2.18 μ M (Fig. 1C). 13 C also inhibited cellular proliferation in PANC-1 cells, with an IC_{50} of 101.5 μ M (Fig. 1D). However, studies with 13C were discontinued when 13C was unable to inhibit FASN activity, as measured by the incorporation of [14 C]-acetate into lipids, *in vitro* (Fig. 1E).

FIGURE 1

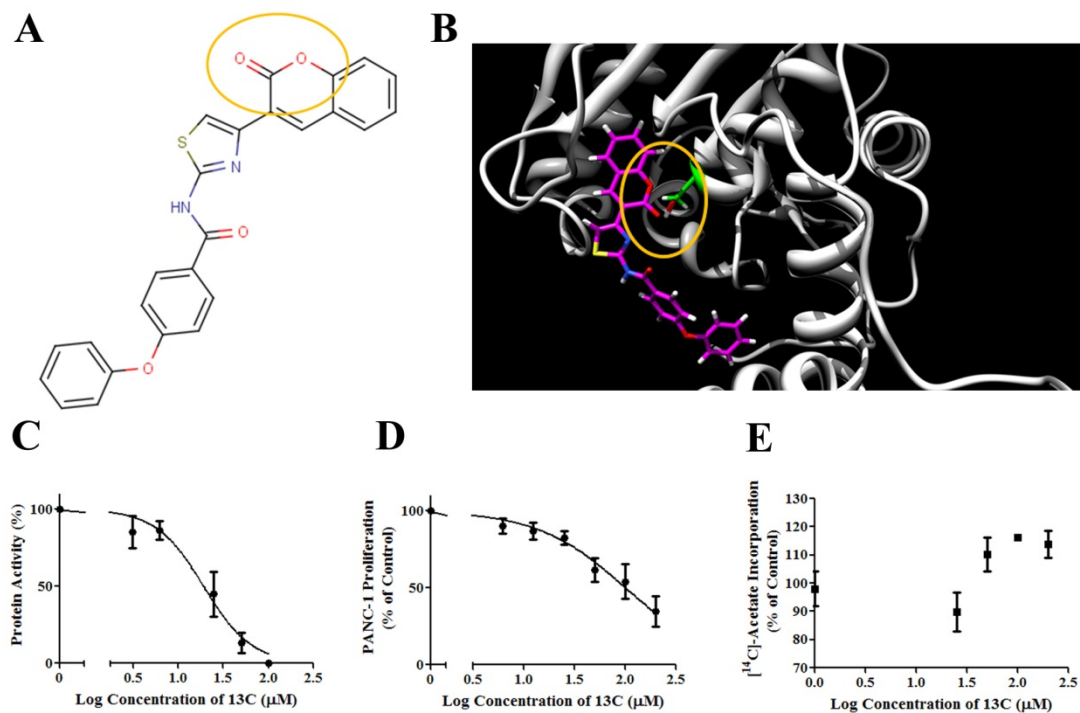


Figure 1: Novel compound 13C inhibits recombinant FASN TE activity and inhibits tumor cell proliferation. (A) Compound 13C from the ChemDiv library was chosen due to the presence of a lactone moiety (circled in yellow). (B) The binding mode of 13C predicted by DOCK indicates that the lactone moiety may be in close proximity to the active site serine of FASN TE (circled in yellow). 13C inhibited (C) the activity of recombinant FASN TE and (D) PANC-1 cellular proliferation in a dose-dependent manner, but did not inhibit (E) the incorporation of [^{14}C]-acetate into lipids.

References

1. Hellerstein MK, Schwarz JM, Neese RA (1996) Regulation of hepatic de novo lipogenesis in humans. *Annual Review of Nutrition* 16: 523-557.
2. Hellerstein MK (1999) De novo lipogenesis in humans: metabolic and regulatory aspects. *European Journal of Clinical Nutrition* 53 Suppl 1: S53-65.
3. Hillgartner FB, Salati LM, Goodridge AG (1995) Physiological and molecular mechanisms involved in nutritional regulation of fatty acid synthesis. *Physiological Reviews* 75: 47-76.
4. Girard J, Ferre P, Fougere F (1997) Mechanisms by which carbohydrates regulate expression of genes for glycolytic and lipogenic enzymes. *Annual Review of Nutrition* 17: 325-352.
5. Kersten S (2001) Mechanisms of nutritional and hormonal regulation of lipogenesis. *EMBO Reports* 2: 282-286.
6. Wakil SJ, Stoops JK, Joshi VC (1983) Fatty acid synthesis and its regulation. *Annual Review of Biochemistry* 52: 537-579.
7. Wakil SJ (1989) Fatty acid synthase, a proficient multifunctional enzyme. *Biochemistry* 28: 4523-4530.
8. Smith S (1994) The animal fatty acid synthase: one gene, one polypeptide, seven enzymes. *FASEB Journal* 8: 1248-1259.
9. Maier T, Jenni S, Ban N (2006) Architecture of mammalian fatty acid synthase at 4.5 Å resolution. *Science* 311: 1258-1262.
10. Maier T, Leibundgut M, Ban N (2008) The crystal structure of a mammalian fatty acid synthase. *Science* 321: 1315-1322.
11. Jayakumar A, Chirala SS, Chinault AC, Baldini A, Abu-Elheiga L, et al. (1994) Isolation and chromosomal mapping of genomic clones encoding the human fatty acid synthase gene. *Genomics* 23: 420-424.
12. Foretz M, Guichard C, Ferre P, Fougere F (1999) Sterol regulatory element binding protein-1c is a major mediator of insulin action on the hepatic expression of glucokinase and lipogenesis-related genes. *Proceedings of the National Academy of Sciences of the United States of America* 96: 12737-12742.
13. Shimomura I, Bashmakov Y, Ikemoto S, Horton JD, Brown MS, et al. (1999) Insulin selectively increases SREBP-1c mRNA in the livers of rats with streptozotocin-induced diabetes. *Proceedings of the National Academy of Sciences of the United States of America* 96: 13656-13661.
14. Foretz M, Pacot C, Dugail I, Lemarchand P, Guichard C, et al. (1999) ADD1/SREBP-1c is required in the activation of hepatic lipogenic gene expression by glucose. *Molecular and Cellular Biology* 19: 3760-3768.
15. Shimomura I, Matsuda M, Hammer RE, Bashmakov Y, Brown MS, et al. (2000) Decreased IRS-2 and increased SREBP-1c lead to mixed insulin resistance and sensitivity in livers of lipodystrophic and ob/ob mice. *Molecular Cell* 6: 77-86.
16. Brown MS, Goldstein JL (1999) A proteolytic pathway that controls the cholesterol content of membranes, cells, and blood. *Proceedings of the National Academy of Sciences of the United States of America* 96: 11041-11048.
17. Matsuda M, Korn BS, Hammer RE, Moon YA, Komuro R, et al. (2001) SREBP cleavage-activating protein (SCAP) is required for increased lipid synthesis in

- liver induced by cholesterol deprivation and insulin elevation. *Genes and Development* 15: 1206-1216.
18. Yang T, Espenshade PJ, Wright ME, Yabe D, Gong Y, et al. (2002) Crucial step in cholesterol homeostasis: sterols promote binding of SCAP to INSIG-1, a membrane protein that facilitates retention of SREBPs in ER. *Cell* 110: 489-500.
 19. Yabe D, Brown MS, Goldstein JL (2002) Insig-2, a second endoplasmic reticulum protein that binds SCAP and blocks export of sterol regulatory element-binding proteins. *Proceedings of the National Academy of Sciences of the United States of America* 99: 12753-12758.
 20. Brown MS, Goldstein JL (1997) The SREBP pathway: regulation of cholesterol metabolism by proteolysis of a membrane-bound transcription factor. *Cell* 89: 331-340.
 21. Goldstein JL, DeBose-Boyd RA, Brown MS (2006) Protein sensors for membrane sterols. *Cell* 124: 35-46.
 22. Horton JD, Shimomura I (1999) Sterol regulatory element-binding proteins: activators of cholesterol and fatty acid biosynthesis. *Current Opinion in Lipidology* 10: 143-150.
 23. Horton JD, Goldstein JL, Brown MS (2002) SREBPs: activators of the complete program of cholesterol and fatty acid synthesis in the liver. *Journal of Clinical Investigation* 109: 1125-1131.
 24. Horton JD, Shah NA, Warrington JA, Anderson NN, Park SW, et al. (2003) Combined analysis of oligonucleotide microarray data from transgenic and knockout mice identifies direct SREBP target genes. *Proceedings of the National Academy of Sciences of the United States of America* 100: 12027-12032.
 25. Tong L (2005) Acetyl-coenzyme A carboxylase: crucial metabolic enzyme and attractive target for drug discovery. *Cellular and Molecular Life Sciences* 62: 1784-1803.
 26. Wakil SJ, Titchener EB, Gibson DM (1958) Evidence for the participation of biotin in the enzymic synthesis of fatty acids. *Biochimica et Biophysica Acta* 29: 225-226.
 27. Munday MR (2002) Regulation of mammalian acetyl-CoA carboxylase. *Biochemical Society Transactions* 30: 1059-1064.
 28. Brownsey RW, Boone AN, Elliott JE, Kulpa JE, Lee WM (2006) Regulation of acetyl-CoA carboxylase. *Biochemical Society Transactions* 34: 223-227.
 29. Dodson G, Wlodawer A (1998) Catalytic triads and their relatives. *Trends in Biochemical Sciences* 23: 347-352.
 30. White SW, Zheng J, Zhang YM, Rock (2005) The structural biology of type II fatty acid biosynthesis. *Annual Review in Biochemistry* 74: 791-831.
 31. Jenni S, Leibundgut M, Boehringer D, Frick C, Mikolasek B, et al. (2007) Structure of fungal fatty acid synthase and implications for iterative substrate shuttling. *Science* 316: 254-261.
 32. Smith S, Tsai SC (2007) The type I fatty acid and polyketide synthases: a tale of two megasynthases. *Natural Product Reports* 24: 1041-1072.
 33. Camp LA, Hofmann SL (1993) Purification and properties of a palmitoyl-protein thioesterase that cleaves palmitate from H-Ras. *Journal of Biological Chemistry* 268: 22566-22574.

34. Hudgins LC, Hellerstein M, Seidman C, Neese R, Diakun J, et al. (1996) Human fatty acid synthesis is stimulated by a eucaloric low fat, high carbohydrate diet. *Journal of Clinical Investigation* 97: 2081-2091.
35. Linder ME, Deschenes RJ (2007) Palmitoylation: policing protein stability and traffic. *Nature Reviews Molecular Cell Biology* 8: 74-84.
36. Sprecher H, Luthria DL, Mohammed BS, Baykousheva SP (1995) Reevaluation of the pathways for the biosynthesis of polyunsaturated fatty acids. *Journal of Lipid Research* 36: 2471-2477.
37. Leonard AE, Pereira SL, Sprecher H, Huang YS (2004) Elongation of long-chain fatty acids. *Progress in Lipid Research* 43: 36-54.
38. Aarsland A, Chinkes D, Wolfe RR (1997) Hepatic and whole-body fat synthesis in humans during carbohydrate overfeeding. *American Journal of Clinical Nutrition* 65: 1774-1782.
39. Chascione C, Elwyn DH, Davila M, Gil KM, Askanazi J, et al. (1987) Effect of carbohydrate intake on de novo lipogenesis in human adipose tissue. *American Journal of Physiology* 253: E664-669.
40. Anderson SM, Rudolph MC, McManaman JL, Neville MC (2007) Key stages in mammary gland development. Secretory activation in the mammary gland: it's not just about milk protein synthesis! *Breast Cancer Res* 9: 204.
41. Pizer ES, Kurman RJ, Pasternack GR, Kuhajda FP (1997) Expression of fatty acid synthase is closely linked to proliferation and stromal decidualization in cycling endometrium. *International Journal of Gynecological Pathology* 16: 45-51.
42. Weiss L, Hoffmann GE, Schreiber R, Andres H, Fuchs E, et al. (1986) Fatty-acid biosynthesis in man, a pathway of minor importance. Purification, optimal assay conditions, and organ distribution of fatty-acid synthase. *Biological Chemistry Hoppe-Seyler* 367: 905-912.
43. Warburg O (1956) On the origin of cancer cells. *Science* 123: 309-314.
44. Shaw RJ (2006) Glucose metabolism and cancer. *Current Opinion in Cell Biology* 18: 598-608.
45. Szutowicz A, Kwiatkowski J, Angielski S (1979) Lipogenetic and glycolytic enzyme activities in carcinoma and nonmalignant diseases of the human breast. *British Journal of Cancer* 39: 681-687.
46. Medes G, Thomas A, Weinhouse S (1953) Metabolism of neoplastic tissue. IV. A study of lipid synthesis in neoplastic tissue slices in vitro. *Cancer Research* 13: 27-29.
47. Ookhtens M, Kannan R, Lyon I, Baker N (1984) Liver and adipose tissue contributions to newly formed fatty acids in an ascites tumor. *American Journal of Physiology* 247: R146-153.
48. Kuhajda FP, Jenner K, Wood FD, Hennigar RA, Jacobs LB, et al. (1994) Fatty acid synthesis: a potential selective target for antineoplastic therapy. *Proceedings of the National Academy of Sciences of the United States of America* 91: 6379-6383.
49. Swinnen JV, Van Veldhoven PP, Timmermans L, De Schrijver E, Brusselmans K, et al. (2003) Fatty acid synthase drives the synthesis of phospholipids partitioning into detergent-resistant membrane microdomains. *Biochemical and Biophysical Research Communications* 302: 898-903.

50. Swinnen JV, Heemers H, Deboel L, Foufelle F, Heyns W, et al. (2000) Stimulation of tumor-associated fatty acid synthase expression by growth factor activation of the sterol regulatory element-binding protein pathway. *Oncogene* 19: 5173-5181.
51. Van de Sande T, De Schrijver E, Heyns W, Verhoeven G, Swinnen JV (2002) Role of the phosphatidylinositol 3'-kinase/PTEN/Akt kinase pathway in the overexpression of fatty acid synthase in LNCaP prostate cancer cells. *Cancer Research* 62: 642-646.
52. Yang YA, Han WF, Morin PJ, Chrest FJ, Pizer ES (2002) Activation of fatty acid synthesis during neoplastic transformation: Role of mitogen-activated protein kinase and phosphatidylinositol 3-kinase. *Experimental Cell Research* 279: 80-90.
53. Bandyopadhyay S, Pai SK, Watabe M, Gross SC, Hirota S, et al. (2005) FAS expression inversely correlates with PTEN level in prostate cancer and a PI 3-kinase inhibitor synergizes with FAS siRNA to induce apoptosis. *Oncogene* 24: 5389-5395.
54. Wang HQ, Altomare DA, Skele KL, Poulikakos PI, Kuhajda FP, et al. (2005) Positive feedback regulation between AKT activation and fatty acid synthase expression in ovarian carcinoma cells. *Oncogene* 24: 3574-3582.
55. Kumar-Sinha C, Ignatoski KW, Lippman ME, Ethier SP, Chinnaiyan AM (2003) Transcriptome analysis of HER2 reveals a molecular connection to fatty acid synthesis. *Cancer Research* 63: 132-139.
56. Menendez JA, Mehmi I, Verma VA, Teng PK, Lupu R (2004) Pharmacological inhibition of fatty acid synthase (FAS): a novel therapeutic approach for breast cancer chemoprevention through its ability to suppress Her-2/neu (erbB-2) oncogene-induced malignant transformation. *Molecular Carcinogenesis* 41: 164-178.
57. Menendez JA, Vellon L, Mehmi I, Oza BP, Ropero S, et al. (2004) Inhibition of fatty acid synthase (FAS) suppresses HER2/neu (erbB-2) oncogene overexpression in cancer cells. *Proceedings of the National Academy of Sciences of the United States of America* 101: 10715-10720.
58. Chalbos D, Chambon M, Ailhaud G, Rochefort H (1987) Fatty acid synthetase and its mRNA are induced by progestins in breast cancer cells. *Journal of Biological Chemistry* 262: 9923-9926.
59. Swinnen JV, Esquenet M, Goossens K, Heyns W, Verhoeven G (1997) Androgens stimulate fatty acid synthase in the human prostate cancer cell line LNCaP. *Cancer Research* 57: 1086-1090.
60. Menendez JA, Oza BP, Colomer R, Lupu R (2005) The estrogenic activity of synthetic progestins used in oral contraceptives enhances fatty acid synthase-dependent breast cancer cell proliferation and survival. *International Journal of Oncology* 26: 1507-1515.
61. Santolla MF, Lappano R, De Marco P, Pupo M, Vivacqua A, et al. (2012) G protein-coupled estrogen receptor mediates the up-regulation of fatty acid synthase induced by 17beta-estradiol in cancer cells and cancer-associated fibroblasts. *Journal of Biological Chemistry* 287: 43234-43245.
62. Swinnen JV, Ulrix W, Heyns W, Verhoeven G (1997) Coordinate regulation of lipogenic gene expression by androgens: evidence for a cascade mechanism

- involving sterol regulatory element binding proteins. *Proceedings of the National Academy of Sciences of the United States of America* 94: 12975-12980.
63. Heemers H, Maes B, Fougelle F, Heyns W, Verhoeven G, et al. (2001) Androgens stimulate lipogenic gene expression in prostate cancer cells by activation of the sterol regulatory element-binding protein cleavage activating protein/sterol regulatory element-binding protein pathway. *Molecular Endocrinology* 15: 1817-1828.
 64. Yang Y, Morin PJ, Han WF, Chen T, Bornman DM, et al. (2003) Regulation of fatty acid synthase expression in breast cancer by sterol regulatory element binding protein-1c. *Experimental Cell Research* 282: 132-137.
 65. Ettinger SL, Sobel R, Whitmore TG, Akbari M, Bradley DR, et al. (2004) Dysregulation of sterol response element-binding proteins and downstream effectors in prostate cancer during progression to androgen independence. *Cancer Research* 64: 2212-2221.
 66. Rossi S, Graner E, Febbo P, Weinstein L, Bhattacharya N, et al. (2003) Fatty acid synthase expression defines distinct molecular signatures in prostate cancer. *Molecular Cancer Research* 1: 707-715.
 67. Shah US, Dhir R, Gollin SM, Chandran UR, Lewis D, et al. (2006) Fatty acid synthase gene overexpression and copy number gain in prostate adenocarcinoma. *Human Pathology* 37: 401-409.
 68. Kovacs P, Harper I, Hanson RL, Infante AM, Bogardus C, et al. (2004) A novel missense substitution (Val1483Ile) in the fatty acid synthase gene (FAS) is associated with percentage of body fat and substrate oxidation rates in nondiabetic Pima Indians. *Diabetes* 53: 1915-1919.
 69. Korner A, Ma L, Franks PW, Kiess W, Baier LJ, et al. (2007) Sex-specific effect of the Val1483Ile polymorphism in the fatty acid synthase gene (FAS) on body mass index and lipid profile in caucasian children. *International Journal of Obesity (London)* 31: 353-358.
 70. Campa D, McKay J, Sinilnikova O, Husing A, Vogel U, et al. (2009) Genetic variation in genes of the fatty acid synthesis pathway and breast cancer risk. *Breast Cancer Research and Treatment* 118: 565-574.
 71. Nguyen PL, Ma J, Chavarro JE, Freedman ML, Lis R, et al. (2010) Fatty acid synthase polymorphisms, tumor expression, body mass index, prostate cancer risk, and survival. *Journal of Clinical Oncology* 28: 3958-3964.
 72. Jin Q, Yuan LX, Boulbes D, Baek JM, Wang YN, et al. (2010) Fatty acid synthase phosphorylation: a novel therapeutic target in HER2-overexpressing breast cancer cells. *Breast Cancer Research* 12: R96.
 73. Graner E, Tang D, Rossi S, Baron A, Migita T, et al. (2004) The isopeptidase USP2a regulates the stability of fatty acid synthase in prostate cancer. *Cancer Cell* 5: 253-261.
 74. Priolo C, Tang D, Brahmamandan M, Benassi B, Sicinska E, et al. (2006) The isopeptidase USP2a protects human prostate cancer from apoptosis. *Cancer Research* 66: 8625-8632.
 75. Furuta E, Pai SK, Zhan R, Bandyopadhyay S, Watabe M, et al. (2008) Fatty acid synthase gene is up-regulated by hypoxia via activation of Akt and sterol regulatory element binding protein-1. *Cancer Research* 68: 1003-1011.

76. Menendez JA, Decker JP, Lupu R (2005) In support of fatty acid synthase (FAS) as a metabolic oncogene: extracellular acidosis acts in an epigenetic fashion activating FAS gene expression in cancer cells. *Journal of Cellular Biochemistry* 94: 1-4.
77. Pizer ES, Lax SF, Kuhajda FP, Pasternack GR, Kurman RJ (1998) Fatty acid synthase expression in endometrial carcinoma: correlation with cell proliferation and hormone receptors. *Cancer* 83: 528-537.
78. Rahman MT, Nakayama K, Ishikawa M, Rahman M, Katagiri H, et al. (2013) Fatty acid synthase is a potential therapeutic target in estrogen receptor-/progesterone receptor-positive endometrioid endometrial cancer. *Oncology* 84: 166-173.
79. Innocenzi D, Alo PL, Balzani A, Sebastiani V, Silipo V, et al. (2003) Fatty acid synthase expression in melanoma. *Journal of Cutaneous Pathology* 30: 23-28.
80. Nemoto T, Terashima S, Kogure M, Hoshino Y, Kusakabe T, et al. (2001) Overexpression of fatty acid synthase in oesophageal squamous cell dysplasia and carcinoma. *Pathobiology* 69: 297-303.
81. Zhou Y, Niu C, Li Y, Gao B, Zheng J, et al. (2012) Fatty acid synthase expression and esophageal cancer. *Molecular Biology Reports* 39: 9733-9739.
82. Orita H, Coulter J, Tully E, Abe M, Montgomery E, et al. (2010) High levels of fatty acid synthase expression in esophageal cancers represent a potential target for therapy. *Cancer Biology and Therapy* 10: 549-554.
83. Gabrielson EW, Pinn ML, Testa JR, Kuhajda FP (2001) Increased fatty acid synthase is a therapeutic target in mesothelioma. *Clinical Cancer Research* 7: 153-157.
84. Rossi S, Ou W, Tang D, Bhattacharya N, Dei Tos AP, et al. (2006) Gastrointestinal stromal tumours overexpress fatty acid synthase. *Journal of Pathology* 209: 369-375.
85. Alo PL, Galati GM, Sebastiani V, Ricci F, Visca P, et al. (2005) Fatty acid synthase expression in Paget's disease of the vulva. *International Journal of Gynecological Pathology* 24: 404-408.
86. Agostini M, Silva SD, Zecchin KG, Coletta RD, Jorge J, et al. (2004) Fatty acid synthase is required for the proliferation of human oral squamous carcinoma cells. *Oral Oncology* 40: 728-735.
87. Silva SD, Agostini M, Nishimoto IN, Coletta RD, Alves FA, et al. (2004) Expression of fatty acid synthase, ErbB2 and Ki-67 in head and neck squamous cell carcinoma. A clinicopathological study. *Oral Oncology* 40: 688-696.
88. Bhatt AP, Jacobs SR, Freemerman AJ, Makowski L, Rathmell JC, et al. (2012) Dysregulation of fatty acid synthesis and glycolysis in non-Hodgkin lymphoma. *Proceedings of the National Academy of Sciences of the United States of America* 109: 11818-11823.
89. de Andrade BA, Leon JE, Carlos R, Delgado-Azanero W, Mosqueda-Taylor A, et al. (2011) Expression of fatty acid synthase (FASN) in oral nevi and melanoma. *Oral Diseases* 17: 808-812.
90. Haase D, Schmidl S, Ewald C, Kalff R, Huebner C, et al. (2010) Fatty acid synthase as a novel target for meningioma therapy. *Neuro-Oncology* 12: 844-854.
91. Olsen AM, Eisenberg BL, Kuemmerle NB, Flanagan AJ, Morganelli PM, et al. (2010) Fatty acid synthesis is a therapeutic target in human liposarcoma. *International Journal of Oncology* 36: 1309-1314.

92. Okawa Y, Hideshima T, Ikeda H, Raje N, Vallet S, et al. (2008) Fatty acid synthase is a novel therapeutic target in multiple myeloma. *British Journal of Haematology* 141: 659-671.
93. Zhao W, Kridel S, Thorburn A, Kooshki M, Little J, et al. (2006) Fatty acid synthase: a novel target for antiglioma therapy. *British Journal of Cancer* 95: 869-878.
94. Epstein JI, Carmichael M, Partin AW (1995) OA-519 (fatty acid synthase) as an independent predictor of pathologic state in adenocarcinoma of the prostate. *Urology* 45: 81-86.
95. Shurbaji MS, Kalbfleisch JH, Thurmond TS (1996) Immunohistochemical detection of a fatty acid synthase (OA-519) as a predictor of progression of prostate cancer. *Human Pathology* 27: 917-921.
96. Alo PL, Visca P, Marci A, Mangoni A, Botti C, et al. (1996) Expression of fatty acid synthase (FAS) as a predictor of recurrence in stage I breast carcinoma patients. *Cancer* 77: 474-482.
97. Alo PL, Visca P, Trombetta G, Mangoni A, Lenti L, et al. (1999) Fatty acid synthase (FAS) predictive strength in poorly differentiated early breast carcinomas. *Tumori* 85: 35-40.
98. Gansler TS, Hardman W, 3rd, Hunt DA, Schaffel S, Hennigar RA (1997) Increased expression of fatty acid synthase (OA-519) in ovarian neoplasms predicts shorter survival. *Human Pathology* 28: 686-692.
99. Alo PL, Visca P, Framarino ML, Botti C, Monaco S, et al. (2000) Immunohistochemical study of fatty acid synthase in ovarian neoplasms. *Oncology Reports* 7: 1383-1388.
100. Krontiras H, Roye GD, Beenken SE, Myers RB, Mayo MS, et al. (1999) Fatty acid synthase expression is increased in neoplastic lesions of the oral tongue. *Head & Neck* 21: 325-329.
101. Silva SD, Perez DE, Alves FA, Nishimoto IN, Pinto CA, et al. (2008) ErbB2 and fatty acid synthase (FAS) expression in 102 squamous cell carcinomas of the tongue: correlation with clinical outcomes. *Oral Oncology* 44: 484-490.
102. Takahiro T, Shinichi K, Toshimitsu S (2003) Expression of fatty acid synthase as a prognostic indicator in soft tissue sarcomas. *Clinical Cancer Research* 9: 2204-2212.
103. Tsuji T, Yoshinaga M, Togami S, Douchi T, Nagata Y (2004) Fatty acid synthase expression and clinicopathological findings in endometrial cancer. *Acta Obstetrica et Gynecologica Scandinavica* 83: 586-590.
104. Sebastiani V, Visca P, Botti C, Santeusano G, Galati GM, et al. (2004) Fatty acid synthase is a marker of increased risk of recurrence in endometrial carcinoma. *Gynecologic Oncology* 92: 101-105.
105. Visca P, Sebastiani V, Botti C, Diodoro MG, Lasagni RP, et al. (2004) Fatty acid synthase (FAS) is a marker of increased risk of recurrence in lung carcinoma. *Anticancer Research* 24: 4169-4173.
106. Alo PL, Amini M, Piro F, Pizzuti L, Sebastiani V, et al. (2007) Immunohistochemical expression and prognostic significance of fatty acid synthase in pancreatic carcinoma. *Anticancer Research* 27: 2523-2527.

107. Horiguchi A, Asano T, Asano T, Ito K, Sumitomo M, et al. (2008) Fatty acid synthase over expression is an indicator of tumor aggressiveness and poor prognosis in renal cell carcinoma. *Journal of Urology* 180: 1137-1140.
108. De Vincentiis M, Di Cello P, Censi F, Leopizzi M, Natalizi S, et al. (2008) Immunohistochemical expression of fatty acid synthase, Ki-67 and p53 in squamous cell carcinomas of the larynx. *International Journal of Biological Markers* 23: 176-181.
109. Silva SD, Cunha IW, Younes RN, Soares FA, Kowalski LP, et al. (2010) ErbB receptors and fatty acid synthase expression in aggressive head and neck squamous cell carcinomas. *Oral Diseases* 16: 774-780.
110. Sugino T, Baba K, Hoshi N, Aikawa K, Yamaguchi O, et al. (2011) Overexpression of fatty acid synthase in human urinary bladder cancer and combined expression of the synthase and Ki-67 as a predictor of prognosis of cancer patients. *Medical Molecular Morphology* 44: 146-150.
111. Wu D, Xu J, Yu G, Zhang B, Wang H, et al. (2013) Expression status of fatty acid synthase (FAS) but not HER2 is correlated with the differentiation grade and prognosis of esophageal carcinoma. *Hepatogastroenterology* 60: 99-106.
112. Kapur P, Rakheja D, Roy LC, Hoang MP (2005) Fatty acid synthase expression in cutaneous melanocytic neoplasms. *Modern Pathology* 18: 1107-1112.
113. Camassei FD, Cozza R, Acquaviva A, Jenkner A, Rava L, et al. (2003) Expression of the lipogenic enzyme fatty acid synthase (FAS) in retinoblastoma and its correlation with tumor aggressiveness. *Investigative Ophthalmology & Visual Science* 44: 2399-2403.
114. Vandhana S, Deepa PR, Jayanthi U, Biswas J, Krishnakumar S (2011) Clinico-pathological correlations of fatty acid synthase expression in retinoblastoma: an Indian cohort study. *Experimental and Molecular Pathology* 90: 29-37.
115. Camassei FD, Jenkner A, Rava L, Bosman C, Francalanci P, et al. (2003) Expression of the lipogenic enzyme fatty acid synthase (FAS) as a predictor of poor outcome in nephroblastoma: an interinstitutional study. *Medical and Pediatric Oncology* 40: 302-308.
116. Liu ZL, Wang G, Peng AF, Luo QF, Zhou Y, et al. (2012) Fatty acid synthase expression in osteosarcoma and its correlation with pulmonary metastasis. *Oncology Letters* 4: 878-882.
117. Makino K, Nakamura H, Hide T, Yano S, Kuroda J, et al. (2012) Fatty acid synthase is a predictive marker for aggressiveness in meningiomas. *Journal of Neuro-Oncology* 109: 399-404.
118. Jiang J, Lin C, Liu N, Zhang Z, Sun Y, et al. (2013) The expression of fatty acid metabolism-associated proteins is correlated with the prognosis of meningiomas. *APMIS* 121: 997-1003.
119. Tao BB, He H, Shi XH, Wang CL, Li WQ, et al. (2013) Up-regulation of USP2a and FASN in gliomas correlates strongly with glioma grade. *Journal of Clinical Neuroscience* 20: 717-720.
120. Pflug BR, Pecher SM, Brink AW, Nelson JB, Foster BA (2003) Increased fatty acid synthase expression and activity during progression of prostate cancer in the TRAMP model. *Prostate* 57: 245-254.

121. Wang YY, Kuhajda FP, Li J, Finch TT, Cheng P, et al. (2004) Fatty acid synthase as a tumor marker: its extracellular expression in human breast cancer. *Journal of Experimental Therapeutics and Oncology* 4: 101-110.
122. Walter K, Hong SM, Nyhan S, Canto M, Fedarko N, et al. (2009) Serum fatty acid synthase as a marker of pancreatic neoplasia. *Cancer Epidemiology, Biomarkers & Prevention* 18: 2380-2385.
123. Notarnicola M, Tutino V, Calvani M, Lorusso D, Guerra V, et al. (2012) Serum levels of fatty acid synthase in colorectal cancer patients are associated with tumor stage. *Journal of Gastrointestinal Cancer* 43: 508-511.
124. Milgraum LZ, Witters LA, Pasternack GR, Kuhajda FP (1997) Enzymes of the fatty acid synthesis pathway are highly expressed in in situ breast carcinoma. *Clinical Cancer Research* 3: 2115-2120.
125. Esslimani-Sahla M, Thezenas S, Simony-Lafontaine J, Kramar A, Lavail R, et al. (2007) Increased expression of fatty acid synthase and progesterone receptor in early steps of human mammary carcinogenesis. *International Journal of Cancer* 120: 224-229.
126. Rashid A, Pizer ES, Moga M, Milgraum LZ, Zahurak M, et al. (1997) Elevated expression of fatty acid synthase and fatty acid synthetic activity in colorectal neoplasia. *American Journal of Pathology* 150: 201-208.
127. Piyathilake CJ, Frost AR, Manne U, Bell WC, Weiss H, et al. (2000) The expression of fatty acid synthase (FASE) is an early event in the development and progression of squamous cell carcinoma of the lung. *Human Pathology* 31: 1068-1073.
128. Myers RB, Oelschlagel DK, Weiss HL, Frost AR, Grizzle WE (2001) Fatty acid synthase: an early molecular marker of progression of prostatic adenocarcinoma to androgen independence. *Journal of Urology* 165: 1027-1032.
129. Swinnen JV, Roskams T, Joniau S, Van Poppel H, Oyen R, et al. (2002) Overexpression of fatty acid synthase is an early and common event in the development of prostate cancer. *International Journal of Cancer* 98: 19-22.
130. Jones AC, Trujillo KA, Phillips GK, Fleet TM, Murton JK, et al. (2012) Early growth response 1 and fatty acid synthase expression is altered in tumor adjacent prostate tissue and indicates field cancerization. *Prostate* 72: 1159-1170.
131. Kusakabe T, Nashimoto A, Honma K, Suzuki T (2002) Fatty acid synthase is highly expressed in carcinoma, adenoma and in regenerative epithelium and intestinal metaplasia of the stomach. *Histopathology* 40: 71-79.
132. Consolazio A, Alo PL, Rivera M, Iacopini F, Paoluzi OA, et al. (2006) Overexpression of fatty acid synthase in ulcerative colitis. *American Journal of Clinical Pathology* 126: 113-118.
133. Kapur P, Rakheja D, Balani JP, Roy LC, Amirkhan RH, et al. (2007) Phosphorylated histone H3, Ki-67, p21, fatty acid synthase, and cleaved caspase-3 expression in benign and atypical granular cell tumors. *Archives of Pathology & Laboratory Medicine* 131: 57-64.
134. Silva SD, Cunha IW, Rangel AL, Jorge J, Zecchin KG, et al. (2008) Differential expression of fatty acid synthase (FAS) and ErbB2 in nonmalignant and malignant oral keratinocytes. *Virchows Archiv* 453: 57-67.

135. Crispino P, Alo PL, Rivera M, Barilla D, Nardi F, et al. (2009) Evaluation of fatty acid synthase expression in oesophageal mucosa of patients with oesophagitis, Barrett's oesophagus and adenocarcinoma. *Journal of Cancer Research and Clinical Oncology* 135: 1533-1541.
136. Ishimura N, Amano Y, Sanchez-Siles AA, Fukuhara H, Takahashi Y, et al. (2011) Fatty acid synthase expression in Barrett's esophagus: implications for carcinogenesis. *Journal of Clinical Gastroenterology* 45: 665-672.
137. do Prado RF, da Silva Machado AL, Colombo CE, Carvalho YR (2011) Immunohistochemical study of the expression of fatty acid synthase and Ki-67 in salivary gland tumors. *Journal of Oral Pathology & Medicine* 40: 467-475.
138. Baron A, Migita T, Tang D, Loda M (2004) Fatty acid synthase: a metabolic oncogene in prostate cancer? *Journal of Cellular Biochemistry* 91: 47-53.
139. Vazquez-Martin A, Colomer R, Brunet J, Lupu R, Menendez JA (2008) Overexpression of fatty acid synthase gene activates HER1/HER2 tyrosine kinase receptors in human breast epithelial cells. *Cell Proliferation* 41: 59-85.
140. Migita T, Ruiz S, Fornari A, Fiorentino M, Priolo C, et al. (2009) Fatty acid synthase: a metabolic enzyme and candidate oncogene in prostate cancer. *Journal of the National Cancer Institute* 101: 519-532.
141. Fiorentino M, Zadra G, Palescandolo E, Fedele G, Bailey D, et al. (2008) Overexpression of fatty acid synthase is associated with palmitoylation of Wnt1 and cytoplasmic stabilization of beta-catenin in prostate cancer. *Laboratory Investigation* 88: 1340-1348.
142. Wang D, Dubois RN (2010) Eicosanoids and cancer. *Nature Reviews Cancer* 10: 181-193.
143. Locke JA, Guns ES, Lehman ML, Ettinger S, Zoubeidi A, et al. (2010) Arachidonic acid activation of intratumoral steroid synthesis during prostate cancer progression to castration resistance. *Prostate* 70: 239-251.
144. Balsinde J, Balboa MA, Insel PA, Dennis EA (1999) Regulation and inhibition of phospholipase A2. *Annual Review of Pharmacology and Toxicology* 39: 175-189.
145. Swinnen JV, Van Veldhoven PP, Timmermans L, De Schrijver E, Brusselmans K, et al. (2003) Fatty acid synthase drives the synthesis of phospholipids partitioning into detergent-resistant membrane microdomains. *Biochemical and Biophysical Research Communications* 302: 898-903.
146. Yoshii Y, Furukawa T, Oyama N, Hasegawa Y, Kiyono Y, et al. (2013) Fatty acid synthase is a key target in multiple essential tumor functions of prostate cancer: uptake of radiolabeled acetate as a predictor of the targeted therapy outcome. *PLoS One* 8: e64570.
147. Nagasaki S, Suzuki T, Miki Y, Akahira J, Kitada K, et al. (2009) 17Beta-hydroxysteroid dehydrogenase type 12 in human breast carcinoma: a prognostic factor via potential regulation of fatty acid synthesis. *Cancer Research* 69: 1392-1399.
148. Liu H, Liu Y, Zhang JT (2008) A new mechanism of drug resistance in breast cancer cells: fatty acid synthase overexpression-mediated palmitate overproduction. *Molecular Cancer Therapeutics* 7: 263-270.

149. Yang Y, Liu H, Li Z, Zhao Z, Yip-Schneider M, et al. (2011) Role of fatty acid synthase in gemcitabine and radiation resistance of pancreatic cancers. *International Journal of Biochemistry and Molecular Biology* 2: 89-98.
150. Kao YC, Lee SW, Lin LC, Chen LT, Hsing CH, et al. (2013) Fatty acid synthase overexpression confers an independent prognosticator and associates with radiation resistance in nasopharyngeal carcinoma. *Tumour Biology* 34: 759-768.
151. Liu HL, Wu X, Dong ZZ, Luo ZY, Zhao ZW, et al. (2013) Fatty acid synthase causes drug resistance by inhibiting TNF-alpha and ceramide production. *Journal of Lipid Research* 54: 776-785.
152. Wu X, Qin L, Fako V, Zhang JT (2014) Molecular mechanisms of fatty acid synthase (FASN)-mediated resistance to anti-cancer treatments. *Advances in Biological Regulation* 54C: 214-221.
153. Peetla C, Bhawe R, Vijayaraghavalu S, Stine A, Kooijman E, et al. (2010) Drug resistance in breast cancer cells: biophysical characterization of and doxorubicin interactions with membrane lipids. *Mol Pharm* 7: 2334-2348.
154. Pancreatic Cancer. American Cancer Society. <http://www.cancer.org/acs/groups/cid/documents/webcontent/003131-pdf.pdf>. (Accessed 5/12/14).
155. Greenlee RT, Murray T, Bolden S, Wingo PA (2000) Cancer statistics, 2000. *CA: A Cancer Journal for Clinicians* 50: 7-33.
156. Janes RH, Jr., Niederhuber JE, Chmiel JS, Winchester DP, Ocwieja KC, et al. (1996) National patterns of care for pancreatic cancer. Results of a survey by the Commission on Cancer. *Annals of Surgery* 223: 261-272.
157. Jemal A, Siegel R, Xu J, Ward E (2010) Cancer statistics, 2010. *CA: A Cancer Journal for Clinicians* 60: 277-300.
158. Poston GJ, Williamson RC (1990) Causes, diagnosis, and management of exocrine pancreatic cancer. *Comprehensive Therapy* 16: 36-42.
159. Maitra A, Fukushima N, Takaori K, Hruban RH (2005) Precursors to invasive pancreatic cancer. *Advances in Anatomic Pathology* 12: 81-91.
160. Maitra A, Hruban RH (2008) Pancreatic cancer. *Annual Review of Pathology Mechanisms of Disease* 3: 157-188.
161. Caldas C, Kern SE (1995) K-ras mutation and pancreatic adenocarcinoma. *International Journal of Pancreatology* 18: 1-6.
162. Hingorani SR, Tuveson DA (2003) Ras redux: rethinking how and where Ras acts. *Current Opinion in Genetics & Development* 13: 6-13.
163. Schutte M, Hruban RH, Geradts J, Maynard R, Hilgers W, et al. (1997) Abrogation of the Rb/p16 tumor-suppressive pathway in virtually all pancreatic carcinomas. *Cancer Research* 57: 3126-3130.
164. Redston MS, Caldas C, Seymour AB, Hruban RH, da Costa L, et al. (1994) p53 mutations in pancreatic carcinoma and evidence of common involvement of homocopolymer tracts in DNA microdeletions. *Cancer Research* 54: 3025-3033.
165. Vogelstein B, Kinzler KW (2004) Cancer genes and the pathways they control. *Nature Medicine* 10: 789-799.
166. Hahn SA, Schutte M, Hoque AT, Moskaluk CA, da Costa LT, et al. (1996) DPC4, a candidate tumor suppressor gene at human chromosome 18q21.1. *Science* 271: 350-353.

167. Siegel PM, Massague J (2003) Cytostatic and apoptotic actions of TGF-beta in homeostasis and cancer. *Nature Reviews Cancer* 3: 807-821.
168. Jones S, Zhang X, Parsons DW, Lin JC, Leary RJ, et al. (2008) Core signaling pathways in human pancreatic cancers revealed by global genomic analyses. *Science* 321: 1801-1806.
169. Li D, Xie K, Wolff R, Abbruzzese JL (2004) Pancreatic cancer. *Lancet* 363: 1049-1057.
170. Burris HA, 3rd, Moore MJ, Andersen J, Green MR, Rothenberg ML, et al. (1997) Improvements in survival and clinical benefit with gemcitabine as first-line therapy for patients with advanced pancreas cancer: a randomized trial. *Journal of Clinical Oncology* 15: 2403-2413.
171. Heinemann V, Hertel LW, Grindey GB, Plunkett W (1988) Comparison of the cellular pharmacokinetics and toxicity of 2',2'-difluorodeoxycytidine and 1-beta-D-arabinofuranosylcytosine. *Cancer Research* 48: 4024-4031.
172. Huang P, Chubb S, Hertel LW, Grindey GB, Plunkett W (1991) Action of 2',2'-difluorodeoxycytidine on DNA synthesis. *Cancer Research* 51: 6110-6117.
173. Gandhi V, Plunkett W (1990) Modulatory activity of 2',2'-difluorodeoxycytidine on the phosphorylation and cytotoxicity of arabinosyl nucleosides. *Cancer Research* 50: 3675-3680.
174. Conroy T, Desseigne F, Ychou M, Bouche O, Guimbaud R, et al. (2011) FOLFIRINOX versus gemcitabine for metastatic pancreatic cancer. *New England Journal of Medicine* 364: 1817-1825.
175. Warsame R, Grothey A (2012) Treatment options for advanced pancreatic cancer: a review. *Expert Review of Anticancer Therapy* 12: 1327-1336.
176. Moore MJ, Goldstein D, Hamm J, Figer A, Hecht JR, et al. (2007) Erlotinib plus gemcitabine compared with gemcitabine alone in patients with advanced pancreatic cancer: a phase III trial of the National Cancer Institute of Canada Clinical Trials Group. *Journal of Clinical Oncology* 25: 1960-1966.
177. Cunningham D, Chau I, Stocken DD, Valle JW, Smith D, et al. (2009) Phase III randomized comparison of gemcitabine versus gemcitabine plus capecitabine in patients with advanced pancreatic cancer. *Journal of Clinical Oncology* 27: 5513-5518.
178. Alo PL, Amini M, Piro F, Pizzuti L, Sebastiani V, et al. (2007) Immunohistochemical expression and prognostic significance of fatty acid synthase in pancreatic carcinoma. *Anticancer Research* 27: 2523-2527.
179. De Schrijver E, Brusselmans K, Heyns W, Verhoeven G, Swinnen JV (2003) RNA interference-mediated silencing of the fatty acid synthase gene attenuates growth and induces morphological changes and apoptosis of LNCaP prostate cancer cells. *Cancer Research* 63: 3799-3804.
180. Bandyopadhyay S, Zhan R, Wang Y, Pai SK, Hirota S, et al. (2006) Mechanism of apoptosis induced by the inhibition of fatty acid synthase in breast cancer cells. *Cancer Research* 66: 5934-5940.
181. Knowles LM, Smith JW (2007) Genome-wide changes accompanying knockdown of fatty acid synthase in breast cancer. *BMC Genomics* 8: 168.

182. Zaytseva YY, Rychahou PG, Gulhati P, Elliott VA, Mustain WC, et al. (2012) Inhibition of fatty acid synthase attenuates CD44-associated signaling and reduces metastasis in colorectal cancer. *Cancer Research* 72: 1504-1517.
183. Loftus TM, Jaworsky DE, Frehywot GL, Townsend CA, Ronnett GV, et al. (2000) Reduced food intake and body weight in mice treated with fatty acid synthase inhibitors. *Science* 288: 2379-2381.
184. Funabashi H, Kawaguchi A, Tomoda H, Omura S, Okuda S, et al. (1989) Binding site of cerulenin in fatty acid synthetase. *Journal of Biochemistry* 105: 751-755.
185. Pizer ES, Wood FD, Pasternack GR, Kuhajda FP (1996) Fatty acid synthase (FAS): a target for cytotoxic antimetabolites in HL60 promyelocytic leukemia cells. *Cancer Research* 56: 745-751.
186. Pizer ES, Jackisch C, Wood FD, Pasternack GR, Davidson NE, et al. (1996) Inhibition of fatty acid synthesis induces programmed cell death in human breast cancer cells. *Cancer Research* 56: 2745-2747.
187. Furuya Y, Akimoto S, Yasuda K, Ito H (1997) Apoptosis of androgen-independent prostate cell line induced by inhibition of fatty acid synthesis. *Anticancer Research* 17: 4589-4593.
188. Pizer ES, Wood FD, Heine HS, Romantsev FE, Pasternack GR, et al. (1996) Inhibition of fatty acid synthesis delays disease progression in a xenograft model of ovarian cancer. *Cancer Research* 56: 1189-1193.
189. Murata S, Yanagisawa K, Fukunaga K, Oda T, Kobayashi A, et al. (2010) Fatty acid synthase inhibitor cerulenin suppresses liver metastasis of colon cancer in mice. *Cancer Science* 101: 1861-1865.
190. Pizer ES, Chrest FJ, DiGiuseppe JA, Han WF (1998) Pharmacological inhibitors of mammalian fatty acid synthase suppress DNA replication and induce apoptosis in tumor cell lines. *Cancer Research* 58: 4611-4615.
191. Kuhajda FP, Pizer ES, Li JN, Mani NS, Frehywot GL, et al. (2000) Synthesis and antitumor activity of an inhibitor of fatty acid synthase. *Proceedings of the National Academy of Sciences of the United States of America* 97: 3450-3454.
192. Tomek K, Wagner R, Varga F, Singer CF, Karlic H, et al. (2011) Blockade of fatty acid synthase induces ubiquitination and degradation of phosphoinositide-3-kinase signaling proteins in ovarian cancer. *Molecular Cancer Research* 9: 1767-1779.
193. Li JN, Gorospe M, Chrest FJ, Kumaravel TS, Evans MK, et al. (2001) Pharmacological inhibition of fatty acid synthase activity produces both cytostatic and cytotoxic effects modulated by p53. *Cancer Research* 61: 1493-1499.
194. Menendez JA, Lupu R (2005) RNA interference-mediated silencing of the p53 tumor-suppressor protein drastically increases apoptosis after inhibition of endogenous fatty acid metabolism in breast cancer cells. *International Journal of Molecular Medicine* 15: 33-40.
195. Alli PM, Pinn ML, Jaffee EM, McFadden JM, Kuhajda FP (2005) Fatty acid synthase inhibitors are chemopreventive for mammary cancer in neu-N transgenic mice. *Oncogene* 24: 39-46.
196. Pizer ES, Thupari J, Han WF, Pinn ML, Chrest FJ, et al. (2000) Malonyl-coenzyme-A is a potential mediator of cytotoxicity induced by fatty-acid synthase inhibition in human breast cancer cells and xenografts. *Cancer Research* 60: 213-218.

197. Thupari JN, Landree LE, Ronnett GV, Kuhajda FP (2002) C75 increases peripheral energy utilization and fatty acid oxidation in diet-induced obesity. *Proceedings of the National Academy of Sciences of the United States of America* 99: 9498-9502.
198. McFadden JM, Medghalchi SM, Thupari JN, Pinn ML, Vadlamudi A, et al. (2005) Application of a flexible synthesis of (5R)-thiolactomycin to develop new inhibitors of type I fatty acid synthase. *Journal of Medicinal Chemistry* 48: 946-961.
199. Orita H, Coulter J, Lemmon C, Tully E, Vadlamudi A, et al. (2007) Selective inhibition of fatty acid synthase for lung cancer treatment. *Clinical Cancer Research* 13: 7139-7145.
200. Orita H, Coulter J, Tully E, Kuhajda FP, Gabrielson E (2008) Inhibiting fatty acid synthase for chemoprevention of chemically induced lung tumors. *Clinical Cancer Research* 14: 2458-2464.
201. Zhou W, Han WF, Landree LE, Thupari JN, Pinn ML, et al. (2007) Fatty acid synthase inhibition activates AMP-activated protein kinase in SKOV3 human ovarian cancer cells. *Cancer Research* 67: 2964-2971.
202. Wang X, Tian W (2001) Green tea epigallocatechin gallate: a natural inhibitor of fatty-acid synthase. *Biochemical and Biophysical Research Communications* 288: 1200-1206.
203. Brusselmans K, De Schrijver E, Heyns W, Verhoeven G, Swinnen JV (2003) Epigallocatechin-3-gallate is a potent natural inhibitor of fatty acid synthase in intact cells and selectively induces apoptosis in prostate cancer cells. *International Journal of Cancer* 106: 856-862.
204. Khan N, Afaq F, Saleem M, Ahmad N, Mukhtar H (2006) Targeting multiple signaling pathways by green tea polyphenol (-)-epigallocatechin-3-gallate. *Cancer Research* 66: 2500-2505.
205. Lee JS, Lee MS, Oh WK, Sul JY (2009) Fatty acid synthase inhibition by amentoflavone induces apoptosis and antiproliferation in human breast cancer cells. *Biological & Pharmaceutical Bulletin* 32: 1427-1432.
206. Brusselmans K, Vrolix R, Verhoeven G, Swinnen JV (2005) Induction of cancer cell apoptosis by flavonoids is associated with their ability to inhibit fatty acid synthase activity. *Journal of Biological Chemistry* 280: 5636-5645.
207. Li BH, Tian WX (2004) Inhibitory effects of flavonoids on animal fatty acid synthase. *Journal of Biochemistry* 135: 85-91.
208. Tian WX (2006) Inhibition of fatty acid synthase by polyphenols. *Current Medicinal Chemistry* 13: 967-977.
209. Puig T, Relat J, Marrero PF, Haro D, Brunet J, et al. (2008) Green tea catechin inhibits fatty acid synthase without stimulating carnitine palmitoyltransferase-1 or inducing weight loss in experimental animals. *Anticancer Research* 28: 3671-3676.
210. Puig T, Vazquez-Martin A, Relat J, Petriz J, Menendez JA, et al. (2008) Fatty acid metabolism in breast cancer cells: differential inhibitory effects of epigallocatechin gallate (EGCG) and C75. *Breast Cancer Research and Treatment* 109: 471-479.

211. Puig T, Turrado C, Benhamu B, Aguilar H, Relat J, et al. (2009) Novel inhibitors of fatty acid synthase with anticancer activity. *Clinical Cancer Research* 15: 7608-7615.
212. Kridel SJ, Axelrod F, Rozenkrantz N, Smith JW (2004) Orlistat is a novel inhibitor of fatty acid synthase with antitumor activity. *Cancer Research* 64: 2070-2075.
213. Pemble CW, Johnson LC, Kridel SJ, Lowther WT (2007) Crystal structure of the thioesterase domain of human fatty acid synthase inhibited by Orlistat. *Nature Structural & Molecular Biology* 14: 704-709.
214. Carvalho MA, Zecchin KG, Seguin F, Bastos DC, Agostini M, et al. (2008) Fatty acid synthase inhibition with Orlistat promotes apoptosis and reduces cell growth and lymph node metastasis in a mouse melanoma model. *International Journal of Cancer* 123: 2557-2565.
215. Zecchin KG, Rossato FA, Raposo HF, Melo DR, Alberici LC, et al. (2011) Inhibition of fatty acid synthase in melanoma cells activates the intrinsic pathway of apoptosis. *Laboratory Investigation* 91: 232-240.
216. Dowling S, Cox J, Cenedella RJ (2009) Inhibition of fatty acid synthase by Orlistat accelerates gastric tumor cell apoptosis in culture and increases survival rates in gastric tumor bearing mice in vivo. *Lipids* 44: 489-498.
217. Browne CD, Hindmarsh EJ, Smith JW (2006) Inhibition of endothelial cell proliferation and angiogenesis by orlistat, a fatty acid synthase inhibitor. *FASEB Journal* 20: 2027-2035.
218. Knowles LM, Axelrod F, Browne CD, Smith JW (2004) A fatty acid synthase blockade induces tumor cell-cycle arrest by down-regulating Skp2. *Journal of Biological Chemistry* 279: 30540-30545.
219. Little JL, Wheeler FB, Fels DR, Koumenis C, Kridel SJ (2007) Inhibition of fatty acid synthase induces endoplasmic reticulum stress in tumor cells. *Cancer Research* 67: 1262-1269.
220. Knowles LM, Yang C, Osterman A, Smith JW (2008) Inhibition of fatty-acid synthase induces caspase-8-mediated tumor cell apoptosis by up-regulating DDIT4. *Journal of Biological Chemistry* 283: 31378-31384.
221. Zhi J, Melia AT, Eggers H, Joly R, Patel IH (1995) Review of limited systemic absorption of orlistat, a lipase inhibitor, in healthy human volunteers. *Journal of Clinical Pharmacology* 35: 1103-1108.
222. Zhi J, Melia AT, Funk C, Viger-Chougnnet A, Hopfgartner G, et al. (1996) Metabolic profiles of minimally absorbed orlistat in obese/overweight volunteers. *Journal of Clinical Pharmacology* 36: 1006-1011.
223. Ma G, Zancanella M, Oyola Y, Richardson RD, Smith JW, et al. (2006) Total synthesis and comparative analysis of orlistat, valilactone, and a transposed orlistat derivative: Inhibitors of fatty acid synthase. *Organic Letters* 8: 4497-4500.
224. Purohit VC, Richardson RD, Smith JW, Romo D (2006) Practical, catalytic, asymmetric synthesis of beta-lactones via a sequential ketene dimerization/hydrogenation process: inhibitors of the thioesterase domain of fatty acid synthase. *Journal of Organic Chemistry* 71: 4549-4558.
225. Richardson RD, Ma G, Oyola Y, Zancanella M, Knowles LM, et al. (2008) Synthesis of novel beta-lactone inhibitors of fatty acid synthase. *Journal of Medicinal Chemistry* 51: 5285-5296.

226. Zhang W, Richardson RD, Chamni S, Smith JW, Romo D (2008) Beta-lactam congeners of orlistat as inhibitors of fatty acid synthase. *Bioorganic & Medicinal Chemistry Letters* 18: 2491-2494.
227. Liu B, Wang Y, Fillgrove KL, Anderson VE (2002) Triclosan inhibits enoyl-reductase of type I fatty acid synthase in vitro and is cytotoxic to MCF-7 and SKBr-3 breast cancer cells. *Cancer Chemotherapy and Pharmacology* 49: 187-193.
228. Oku H, Wongtangintharn S, Iwasaki H, Toda T (2003) Conjugated linoleic acid (CLA) inhibits fatty acid synthetase activity in vitro. *Bioscience, Biotechnology, and Biochemistry* 67: 1584-1586.
229. Zhao WH, Zhang JF, Zhe W, Zhang YX, Tian WX (2006) The extract of leaves of *Acer truncatum* Bunge: A natural inhibitor of fatty acid synthase with antitumor activity. *Journal of Enzyme Inhibition and Medicinal Chemistry* 21: 589-596.
230. Zhao WH, Gao C, Zhang YX, Tian WX (2007) Evaluation of the inhibitory activities of aceraceous plants on fatty acid synthase. *Journal of Enzyme Inhibition and Medicinal Chemistry* 22: 501-510.
231. Zhao WH, Zhao CY, Gao LF, Feng FF, Gao W, et al. (2008) The novel inhibitory effect of Pangdahai on fatty acid synthase. *IUBMB Life* 60: 185-194.
232. Zhang SY, Zheng CG, Yan XY, Tian WX (2008) Low concentration of condensed tannins from catechu significantly inhibits fatty acid synthase and growth of MCF-7 cells. *Biochemical and Biophysical Research Communications* 371: 654-658.
233. Na M, Hung TM, Oh WK, Min BS, Lee SH, et al. (2010) Fatty acid synthase inhibitory activity of dibenzocyclooctadiene lignans isolated from *Schisandra chinensis*. *Phytotherapy Research* 24 Suppl 2: S225-228.
234. Oh J, Hwang IH, Hong CE, Lyu SY, Na M (2013) Inhibition of fatty acid synthase by ginkgolic acids from the leaves of *Ginkgo biloba* and their cytotoxic activity. *Journal of Enzyme Inhibition and Medicinal Chemistry* 28: 565-568.
235. Wang Y, Tian WX, Ma XF (2012) Inhibitory effects of onion (*Allium cepa* L.) extract on proliferation of cancer cells and adipocytes via inhibiting fatty acid synthase. *Asian Pacific Journal of Cancer Prevention* 13: 5573-5579.
236. Richardson RD, Smith JW (2007) Novel antagonists of the thioesterase domain of human fatty acid synthase. *Molecular Cancer Therapy* 6: 2120-2126.
237. Rivkin A, Kim YR, Goulet MT, Bays N, Hill AD, et al. (2006) 3-Aryl-4-hydroxyquinolin-2(1H)-one derivatives as type I fatty acid synthase inhibitors. *Bioorganic and Medicinal Chemistry Letters* 16: 4620-4623.
238. Vazquez MJ, Leavens W, Liu R, Rodriguez B, Read M, et al. (2008) Discovery of GSK837149A, an inhibitor of human fatty acid synthase targeting the beta-ketoacyl reductase reaction. *FEBS Journal* 275: 1556-1567.
239. Zeng XF, Li WW, Fan HJ, Wang XY, Ji P, et al. (2011) Discovery of novel fatty acid synthase (FAS) inhibitors based on the structure of ketoacyl synthase (KS) domain. *Bioorganic and Medicinal Chemistry Letters* 21: 4742-4744.
240. Menendez JA, Vellon L, Lupu R (2005) Targeting fatty acid synthase-driven lipid rafts: a novel strategy to overcome trastuzumab resistance in breast cancer cells. *Medical Hypotheses* 64: 997-1001.

241. Menendez JA, Lupu R, Colomer R (2004) Inhibition of tumor-associated fatty acid synthase hyperactivity induces synergistic chemosensitization of HER -2/ neu - overexpressing human breast cancer cells to docetaxel (taxotere). *Breast Cancer Research and Treatment* 84: 183-195.
242. Menendez JA, Colomer R, Lupu R (2004) Inhibition of tumor-associated fatty acid synthase activity enhances vinorelbine (Navelbine)-induced cytotoxicity and apoptotic cell death in human breast cancer cells. *Oncology Reports* 12: 411-422.
243. Menendez JA, Vellon L, Colomer R, Lupu R (2005) Pharmacological and small interference RNA-mediated inhibition of breast cancer-associated fatty acid synthase (oncogenic antigen-519) synergistically enhances Taxol (paclitaxel)-induced cytotoxicity. *International Journal of Cancer* 115: 19-35.
244. Vazquez-Martin A, Ropero S, Brunet J, Colomer R, Menendez JA (2007) Inhibition of Fatty Acid Synthase (FASN) synergistically enhances the efficacy of 5-fluorouracil in breast carcinoma cells. *Oncology Reports* 18: 973-980.
245. Luciani F, Spada M, De Milito A, Molinari A, Rivoltini L, et al. (2004) Effect of proton pump inhibitor pretreatment on resistance of solid tumors to cytotoxic drugs. *Journal of the National Cancer Institute* 96: 1702-1713.
246. Holt S (1991) Proton-pump inhibition for acid-related disease. *Southern Medical Journal* 84: 1078-1087.
247. Stedman CA, Barclay ML (2000) Review article: comparison of the pharmacokinetics, acid suppression and efficacy of proton pump inhibitors. *Alimentary Pharmacology and Therapeutics* 14: 963-978.
248. Der G (2003) An overview of proton pump inhibitors. *Gastroenterology Nursing* 26: 182-190.
249. Fellenius E, Berglindh T, Sachs G, Olbe L, Elander B, et al. (1981) Substituted benzimidazoles inhibit gastric acid secretion by blocking (H⁺ + K⁺)ATPase. *Nature* 290: 159-161.
250. Sachs G, Shin JM, Besancon M, Prinz C (1993) The continuing development of gastric acid pump inhibitors. *Alimentary Pharmacology and Therapeutics* 7 Suppl 1: 4-12, discussion 29-31.
251. Sachs G, Shin JM, Briving C, Wallmark B, Hersey S (1995) The pharmacology of the gastric acid pump: the H⁺,K⁺ ATPase. *Annual Review of Pharmacology and Toxicology* 35: 277-305.
252. Sachs G, Shin JM, Howden CW (2006) Review article: the clinical pharmacology of proton pump inhibitors. *Alimentary Pharmacology and Therapeutics* 23 Suppl 2: 2-8.
253. Lindberg P, Brandstrom A, Wallmark B, Mattsson H, Rikner L, et al. (1990) Omeprazole - the 1st Proton Pump Inhibitor. *Medicinal Research Reviews* 10: 1-54.
254. Fitton A, Wiseman L (1996) Pantoprazole. A review of its pharmacological properties and therapeutic use in acid-related disorders. *Drugs* 51: 460-482.
255. Barradell LB, Faulds D, McTavish D (1992) Lansoprazole. A review of its pharmacodynamic and pharmacokinetic properties and its therapeutic efficacy in acid-related disorders. *Drugs* 44: 225-250.
256. Williams MP, Pounder RE (1999) Review article: the pharmacology of rabeprazole. *Alimentary Pharmacology and Therapeutics* 13 Suppl 3: 3-10.

257. McKeage K, Blick SK, Croxtall JD, Lyseng-Williamson KA, Keating GM (2008) Esomeprazole: a review of its use in the management of gastric acid-related diseases in adults. *Drugs* 68: 1571-1607.
258. Thomson AB, Sauve MD, Kassam N, Kamitakahara H (2010) Safety of the long-term use of proton pump inhibitors. *World Journal of Gastroenterology* 16: 2323-2330.
259. De Milito A, Marino ML, Fais S (2012) A Rationale for the Use of Proton Pump Inhibitors as Antineoplastic Agents. *Current Pharmaceutical Design* 18: 1395-1406.
260. Hernandez A, Serrano-Bueno G, Perez-Castineira JR, Serrano A (2012) Intracellular proton pumps as targets in chemotherapy: V-ATPases and cancer. *Current Pharmaceutical Design* 18: 1383-1394.
261. De Milito A, Fais S (2005) Proton pump inhibitors may reduce tumour resistance. *Expert Opinion on Pharmacotherapy* 6: 1049-1054.
262. De Milito A, Fais S (2005) Tumor acidity, chemoresistance and proton pump inhibitors. *Future Oncology* 1: 779-786.
263. Scaringi L, Cornacchione P, Ayroldi E, Corazzi L, Capodicasa E, et al. (2004) Omeprazole induces apoptosis in jurkat cells. *International Journal of Immunopathology and Pharmacology* 17: 331-342.
264. De Milito A, Iessi E, Logozzi M, Lozupone F, Spada M, et al. (2007) Proton pump inhibitors induce apoptosis of human B-cell tumors through a caspase-independent mechanism involving reactive oxygen species. *Cancer Research* 67: 5408-5417.
265. Yeo M, Kim DK, Kim YB, Oh TY, Lee JE, et al. (2004) Selective induction of apoptosis with proton pump inhibitor in gastric cancer cells. *Clinical Cancer Research* 10: 8687-8696.
266. Vishvakarma NK, Singh SM (2011) Mechanisms of tumor growth retardation by modulation of pH regulation in the tumor-microenvironment of a murine T cell lymphoma. *Biomedicine & Pharmacotherapy* 65: 27-39.
267. Marino ML, Fais S, Djavaheri-Mergny M, Villa A, Meschini S, et al. (2010) Proton pump inhibition induces autophagy as a survival mechanism following oxidative stress in human melanoma cells. *Cell Death & Disease* 1: e87.
268. Pauli-Magnus C, Rekersbrink S, Klotz U, Fromm MF (2001) Interaction of omeprazole, lansoprazole and pantoprazole with P-glycoprotein. *Naunyn-Schmiedeberg's Archives of Pharmacology* 364: 551-557.
269. Darby RA, Callaghan R, McMahon RM (2011) P-glycoprotein inhibition: the past, the present and the future. *Current Drug Metabolism* 12: 722-731.
270. Udelnow A, Kreyes A, Ellinger S, Landfester K, Walther P, et al. (2011) Omeprazole inhibits proliferation and modulates autophagy in pancreatic cancer cells. *PLoS One* 6: e20143.
271. Shen Y, Wu Y, Chen M, Shen W, Huang S, et al. (2012) Effects of pantoprazole as a HIF-1alpha inhibitor on human gastric adenocarcinoma sgc-7901 cells. *Neoplasma* 59: 142-149.
272. Shen W, Zou X, Chen M, Shen Y, Huang S, et al. (2013) Effect of pantoprazole on human gastric adenocarcinoma SGC7901 cells through regulation of

- phosphoLRP6 expression in Wnt/beta-catenin signaling. *Oncology Reports* 30: 851-855.
273. Chen M, Huang SL, Zhang XQ, Zhang B, Zhu H, et al. (2012) Reversal effects of pantoprazole on multidrug resistance in human gastric adenocarcinoma cells by down-regulating the V-ATPases/mTOR/HIF-1alpha/P-gp and MRP1 signaling pathway in vitro and in vivo. *Journal of Cellular Biochemistry* 113: 2474-2487.
274. Huang S, Chen M, Ding X, Zhang X, Zou X (2013) Proton pump inhibitor selectively suppresses proliferation and restores the chemosensitivity of gastric cancer cells by inhibiting STAT3 signaling pathway. *International Immunopharmacology* 17: 585-592.
275. Spugnini EP, Baldi A, Buglioni S, Carocci F, de Bazzichini GM, et al. (2011) Lansoprazole as a rescue agent in chemoresistant tumors: a phase I/II study in companion animals with spontaneously occurring tumors. *Journal of Translational Medicine* 9: 221.
276. University Health Network, Toronto; Princess Margaret Hospital, Canada. Study evaluating pantoprazole with doxorubicin for advanced cancer patients with extension cohort of patients with solid tumors. In: *ClinicalTrials.gov* [Internet]. Bethesda (MD): National Library of Medicine (US). 2000- [cited 2014 Jan 29]. Available from: <http://clinicaltrials.gov/ct2/show/NCT01163903> NLM Identifier: NCT01163903.
277. Cornell WD, Cieplak P, Bayly CI, Kollman PA (1993) Application of resp charges to calculate conformational energies, hydrogen-bond energies, and free-energies of solvation. *Journal of the American Chemical Society* 115: 9620-9631.
278. Pettersen EF, Goddard TD, Huang CC, Couch GS, Greenblatt DM, et al. (2004) UCSF Chimera--a visualization system for exploratory research and analysis. *Journal of Computational Chemistry* 25: 1605-1612.
279. Fiser A, Sali A (2003) ModLoop: automated modeling of loops in protein structures. *Bioinformatics* 19: 2500-2501.
280. Zhang W, Chakravarty B, Zheng F, Gu Z, Wu H, et al. (2011) Crystal structure of FAS thioesterase domain with polyunsaturated fatty acyl adduct and inhibition by dihomogamma-linolenic acid. *Proceedings of the National Academy of Sciences of the United States of America* 108: 15757-15762.
281. Meng EC, Shoichet BK, Kuntz ID (1992) Automated docking with grid-based energy evaluation. *Journal of Computational Chemistry* 13: 505-524.
282. Shoichet BK, Bodian DL, Kuntz ID (1992) Molecular docking using shape descriptors. *Journal of Computational Chemistry* 13: 380-397.
283. Irwin JJ, Shoichet BK (2005) ZINC - A free database of commercially available compounds for virtual screening. *Journal of Chemical Information and Modeling* 45: 177-182.
284. Irwin J, Shoichet B (2005) The ZINC database as a new research tool for ligand discovery. *Abstracts of Papers of the American Chemical Society* 230: U1009-U1009.
285. Irwin JJ, Sterling T, Mysinger MM, Bolstad ES, Coleman RG (2012) ZINC: a free tool to discover chemistry for biology. *Journal of Chemical Information and Modeling* 52: 1757-1768.

286. Jacks TJ, Kircher HW (1967) Fluorometric assay for the hydrolytic activity of lipase using fatty acyl esters of 4-methylumbelliferone. *Analytical Biochemistry* 21: 279-285.
287. Cer RZ, Mudunuri U, Stephens R, Lebeda FJ (2009) IC50-to-Ki: a web-based tool for converting IC50 to Ki values for inhibitors of enzyme activity and ligand binding. *Nucleic Acids Research* 37: W441-445.
288. Cheng Y, Prusoff WH (1973) Relationship between the inhibition constant (K1) and the concentration of inhibitor which causes 50 per cent inhibition (I50) of an enzymatic reaction. *Biochemical Pharmacology* 22: 3099-3108.
289. Mosmann T (1983) Rapid colorimetric assay for cellular growth and survival: application to proliferation and cytotoxicity assays. *Journal of Immunological Methods* 65: 55-63.
290. Folch J, Lees M, Sloane Stanley GH (1957) A simple method for the isolation and purification of total lipids from animal tissues. *Journal of Biological Chemistry* 226: 497-509.
291. Lineweaver H, Burk D (1934) The determination of enzyme dissociation constants. *Journal of the American Chemical Society* 56: 658-666.
292. Cheng F, Wang Q, Chen M, Quioco FA, Ma J (2008) Molecular docking study of the interactions between the thioesterase domain of human fatty acid synthase and its ligands. *Proteins* 70: 1228-1234.
293. Polgar L (2005) The catalytic triad of serine peptidases. *Cellular and Molecular Life Sciences* 62: 2161-2172.
294. Karplus M, Petsko GA (1990) Molecular dynamics simulations in biology. *Nature* 347: 631-639.
295. Karplus M, McCammon JA (2002) Molecular dynamics simulations of biomolecules. *Nature Structural & Molecular Biology* 9: 646-652.
296. Pearlman DA, Case DA, Caldwell JW, Ross WS, Cheatham TE, et al. (1995) Amber, a package of computer-programs for applying molecular mechanics, normal-mode analysis, molecular-dynamics and free-energy calculations to simulate the structural and energetic properties of molecules. *Computer Physics Communications* 91: 1-41.
297. Duan Y, Wu C, Chowdhury S, Lee MC, Xiong G, et al. (2003) A point-charge force field for molecular mechanics simulations of proteins based on condensed-phase quantum mechanical calculations. *Journal of Computational Chemistry* 24: 1999-2012.
298. Kawatkar SP, Kuntz DA, Woods RJ, Rose DR, Boons GJ (2006) Structural basis of the inhibition of Golgi alpha-mannosidase II by mannosatin A and the role of the thiomethyl moiety in ligand-protein interactions. *Journal of the American Chemical Society* 128: 8310-8319.
299. Rosenbaum DM, Zhang C, Lyons JA, Holl R, Aragao D, et al. (2011) Structure and function of an irreversible agonist-beta(2) adrenoceptor complex. *Nature* 469: 236-240.
300. At IU, what was Big Red? <https://kb.iu.edu/data/avjx.html>. (accessed 05/12/14).
301. What are Parallel Computing, Grid Computing, and Supercomputing? <https://kb.iu.edu/data/angf.html>. (accessed 05/12/14).

302. Cornell WD, Cieplak P, Bayly CI, Gould IR, Merz KM, et al. (1995) A second generation force field for the simulation of proteins, nucleic acids, and organic molecules. *Journal of the American Chemical Society* 117: 5179-5197.
303. Singer PT, Smalas A, Carty RP, Mangel WF, Sweet RM (1993) The hydrolytic water molecule in trypsin, revealed by time-resolved Laue crystallography. *Science* 259: 669-673.
304. Wilmouth RC, Clifton IJ, Robinson CV, Roach PL, Aplin RT, et al. (1997) Structure of a specific acyl-enzyme complex formed between beta-casomorphin-7 and porcine pancreatic elastase. *Nature Structural Biology* 4: 456-462.
305. Wilmouth RC, Edman K, Neutze R, Wright PA, Clifton IJ, et al. (2001) X-ray snapshots of serine protease catalysis reveal a tetrahedral intermediate. *Nature Structural Biology* 8: 689-694.
306. Burgi HB, Dunitz JD, Lehn JM, Wipff G (1974) Stereochemistry of reaction paths at carbonyl centres. *Tetrahedron* 30: 1563-1572.
307. Kridel SJ, Lowther WT, Pemble CWt (2007) Fatty acid synthase inhibitors: new directions for oncology. *Expert Opinion on Investigational Drugs* 16: 1817-1829.
308. Sebastiani V, Visca P, Botti C, Santeusanio G, Galati GM, et al. (2004) Fatty acid synthase is a marker of increased risk of recurrence in endometrial carcinoma. *Gynecologic Oncology* 92: 101-105.
309. Takahiro T, Shinichi K, Toshimitsu S (2003) Expression of fatty acid synthase as a prognostic indicator in soft tissue sarcomas. *Clinical Cancer Research* 9: 2204-2212.
310. Innocenzi D, Alo PL, Balzani A, Sebastiani V, Silipo V, et al. (2003) Fatty acid synthase expression in melanoma. *Journal of Cutaneous Pathology* 30: 23-28.
311. Liu H, Liu JY, Wu X, Zhang JT (2010) Biochemistry, molecular biology, and pharmacology of fatty acid synthase, an emerging therapeutic target and diagnosis/prognosis marker. *International Journal of Biochemistry and Molecular Biology* 1: 69-89.
312. Visca P, Sebastiani V, Botti C, Diodoro MG, Lasagni RP, et al. (2004) Fatty acid synthase (FAS) is a marker of increased risk of recurrence in lung carcinoma. *Anticancer Research* 24: 4169-4173.
313. Zhi J, Mulligan TE, Hauptman JB (1999) Long-term systemic exposure of orlistat, a lipase inhibitor, and its metabolites in obese patients. *Journal of Clinical Pharmacology* 39: 41-46.
314. Drawz SM, Bonomo RA (2010) Three decades of beta-lactamase inhibitors. *Clinical Microbiology Reviews* 23: 160-201.
315. Maveyraud L, Massova I, Birck C, Miyashita K, Samama JP, et al. (1996) Crystal structure of 6 alpha-(hydroxymethyl)penicillanate complexed to the TEM-1 beta-lactamase from *Escherichia coli*: Evidence on the mechanism of action of a novel inhibitor designed by a computer-aided process. *Journal of the American Chemical Society* 118: 7435-7440.
316. Shoichet BK (2004) Virtual screening of chemical libraries. *Nature* 432: 862-865.
317. Beddell CR, Goodford PJ, Norrington FE, Wilkinson S, Wootton R (1976) Compounds designed to fit a site of known structure in human hemoglobin. *British Journal of Pharmacology* 57: 201-209.

318. Cohen SS (1977) Strategy for Chemotherapy of Infectious-Disease. *Science* 197: 431-432.
319. Kuntz ID, Blaney JM, Oatley SJ, Langridge R, Ferrin TE (1982) A geometric approach to macromolecule-ligand interactions. *Journal of Molecular Biology* 161: 269-288.
320. Rizzo RC, Wang DP, Tirado-Rives J, Jorgensen WL (2000) Validation of a model for the complex of HIV-1 reverse transcriptase with sustiva through computation of resistance profiles. *Journal of the American Chemical Society* 122: 12898-12900.
321. Rosenfeld RJ, Goodsell DS, Musah RA, Morris GM, Goodin DB, et al. (2003) Automated docking of ligands to an artificial active site: augmenting crystallographic analysis with computer modeling. *Journal of Computer-Aided Molecular Design* 17: 525-536.
322. Doman TN, McGovern SL, Witherbee BJ, Kasten TP, Kurumbail R, et al. (2002) Molecular docking and high-throughput screening for novel inhibitors of protein tyrosine phosphatase-1B. *Journal of Medicinal Chemistry* 45: 2213-2221.
323. Lipinski CA, Lombardo F, Dominy BW, Feeney PJ (1997) Experimental and computational approaches to estimate solubility and permeability in drug discovery and development settings. *Advanced Drug Delivery Reviews* 23: 3-25.
324. Varney MD, Marzoni GP, Palmer CL, Deal JG, Webber S, et al. (1992) Crystal-structure-based design and synthesis of benz[cd]indole-containing inhibitors of thymidylate synthase. *Journal of Medicinal Chemistry* 35: 663-676.
325. von Itzstein M, Wu WY, Kok GB, Pegg MS, Dyason JC, et al. (1993) Rational design of potent sialidase-based inhibitors of influenza virus replication. *Nature* 363: 418-423.
326. Peng H, Huang N, Qi J, Xie P, Xu C, et al. (2003) Identification of novel inhibitors of BCR-ABL tyrosine kinase via virtual screening. *Bioorganic & Medicinal Chemistry Letters* 13: 3693-3699.
327. Vangrevelinghe E, Zimmermann K, Schoepfer J, Portmann R, Fabbro D, et al. (2003) Discovery of a potent and selective protein kinase CK2 inhibitor by high-throughput docking. *Journal of Medicinal Chemistry* 46: 2656-2662.
328. Enyedy IJ, Ling Y, Nacro K, Tomita Y, Wu XH, et al. (2001) Discovery of small-molecule inhibitors of bcl-2 through structure-based computer screening. *Journal of Medicinal Chemistry* 44: 4313-4324.
329. Zou XQ, Sun YX, Kuntz ID (1999) Inclusion of solvation in ligand binding free energy calculations using the generalized-born model. *Journal of the American Chemical Society* 121: 8033-8043.
330. Kitchen DB, Decornez H, Furr JR, Bajorath J (2004) Docking and scoring in virtual screening for drug discovery: methods and applications. *Nature Reviews Drug Discovery* 3: 935-949.
331. Tan MH, Nowak NJ, Loor R, Ochi H, Sandberg AA, et al. (1986) Characterization of a new primary human pancreatic tumor line. *Cancer Investigation* 4: 15-23.
332. Lieber M, Mazzetta J, Nelson-Rees W, Kaplan M, Todaro G (1975) Establishment of a continuous tumor-cell line (panc-1) from a human carcinoma of the exocrine pancreas. *International Journal of Cancer* 15: 741-747.

333. Menke A, Philippi C, Vogelmann R, Seidel B, Lutz MP, et al. (2001) Down-regulation of E-cadherin gene expression by collagen type I and type III in pancreatic cancer cell lines. *Cancer Research* 61: 3508-3517.
334. Stahle M, Veit C, Bachfischer U, Schierling K, Skripczynski B, et al. (2003) Mechanisms in LPA-induced tumor cell migration: critical role of phosphorylated ERK. *Journal of Cell Science* 116: 3835-3846.
335. Takada M, Nakamura Y, Koizumi T, Toyama H, Kamigaki T, et al. (2002) Suppression of human pancreatic carcinoma cell growth and invasion by epigallocatechin-3-gallate. *Pancreas* 25: 45-48.
336. Greco E, Basso D, Fogar P, Mazza S, Navaglia F, et al. (2005) Pancreatic cancer cells invasiveness is mainly affected by interleukin-1beta not by transforming growth factor-beta1. *International Journal of Biological Markers* 20: 235-241.
337. Deer EL, Gonzalez-Hernandez J, Coursen JD, Shea JE, Ngatia J, et al. (2010) Phenotype and genotype of pancreatic cancer cell lines. *Pancreas* 39: 425-435.
338. Yip-Schneider MT, Barnard DS, Billings SD, Cheng L, Heilman DK, et al. (2000) Cyclooxygenase-2 expression in human pancreatic adenocarcinomas. *Carcinogenesis* 21: 139-146.
339. Luo J, Guo P, Matsuda K, Truong N, Lee A, et al. (2001) Pancreatic cancer cell-derived vascular endothelial growth factor is biologically active in vitro and enhances tumorigenicity in vivo. *International Journal of Cancer* 92: 361-369.
340. Mosmann T (1983) Rapid colorimetric assay for cellular growth and survival: application to proliferation and cytotoxicity assays. *Journal of Immunological Methods* 65: 55-63.
341. Puck TT, Marcus PI (1956) Action of x-rays on mammalian cells. *Journal of Experimental Medicine* 103: 653-666.
342. Franken NA, Rodermond HM, Stap J, Haveman J, van Bree C (2006) Clonogenic assay of cells in vitro. *Nature Protocols* 1: 2315-2319.
343. Salgame P, Varadhachary AS, Primiano LL, Fincke JE, Muller S, et al. (1997) An ELISA for detection of apoptosis. *Nucleic Acids Research* 25: 680-681.
344. Elmore S (2007) Apoptosis: a review of programmed cell death. *Toxicologic Pathology* 35: 495-516.
345. Menendez JA, Lupu R (2007) Fatty acid synthase and the lipogenic phenotype in cancer pathogenesis. *Nature Reviews Cancer* 7: 763-777.
346. Yang YX, Metz DC (2010) Safety of proton pump inhibitor exposure. *Gastroenterology* 139: 1115-1127.
347. Freston JW, Pilmer BL, Chiu YL, Wang Q, Stolle JC, et al. (2004) Evaluation of the pharmacokinetics and pharmacodynamics of intravenous lansoprazole. *Alimentary Pharmacology & Therapeutics* 19: 1111-1122.
348. Loftus TM, Jaworsky DE, Frehywot GL, Townsend CA, Ronnett GV, et al. (2000) Reduced food intake and body weight in mice treated with fatty acid synthase inhibitors. *Science* 288: 2379-2381.
349. Flavin R, Peluso S, Nguyen PL, Loda M (2010) Fatty acid synthase as a potential therapeutic target in cancer. *Future Oncology* 6: 551-562.
350. Yang X, Ren Z, Kuk J, Moffat K (2011) Temperature-scan cryocrystallography reveals reaction intermediates in bacteriophytochrome. *Nature* 479: 428-432.

Curriculum Vitae

Valerie Fako Miller

Education

Indiana University Doctor of Philosophy in Pharmacology	August 2009-August 2014 Cumulative GPA: 3.98/4.0
University of Wisconsin-Madison Master of Science in Analytical Chemistry	August 2007-May 2009 Cumulative GPA: 3.71/4.0
University of Illinois at Urbana-Champaign Bachelor of Science in Chemistry, ACS Certified Minor in Anthropology	August 2003-December 2006 Cumulative GPA: 3.83/4.0

Research Experience

Indiana University School of Medicine

Graduate Research Assistant: May 2010-August 2014

Department of Pharmacology: Dr. J. T. Zhang

- Used molecular dynamics simulations to study the interaction between fatty acid synthase and its antagonist orlistat
- Used *in-silico* drug screening to identify novel candidate inhibitors against fatty acid synthase, which is overexpressed in a wide variety of cancers, for lead compound determination for use in pancreatic cancer

University of Wisconsin

Graduate Research Assistant: July 2008-May 2009

Division of Pharmaceutical Sciences: Dr. Darin Furgeson

- Used a zebrafish model to conservatively estimate the toxicity of possible drug delivery polymers

Graduate Research Assistant: November 2007-July 2008

Department of Chemistry: Dr. James Weisshaar

- Used optical microscopy and fluorescence recovery after photobleaching (FRAP) to study diffusion in *Escherichia coli*

University of Illinois

Undergraduate Research Assistant: January 2007-May 2007

Department of Chemistry: Dr. Neil Kelleher

- Used mass spectrometry for natural product discovery

Undergraduate Research Assistant: June 2005-December 2006

Department of Chemistry: Dr. Paul Hergenrother Lab

- Focused on drug design and discovery via organic syntheses of various derivatives of the small molecule cancer drug our lab discovered and is currently investigating
- Synthesized and characterized building blocks and building block precursors for the 165 compound library we completed

University of Minnesota

Undergraduate Research Assistant: June 2006-August 2006

Department of Chemistry: Dr. Gianluigi Veglia

- Focused on the expression and purification of various membrane proteins found in the heart for study via solution and solid-state NMR

Research Support

- 5F31 CA165603-03 (Fako) Molecular mechanism of orlistat hydrolysis by FASN for targeted drug discovery. NIH/NCI NRSA, April 2012-August 2014.

Publications

- Wu, X.; Qin, L.; **Fako, V.**; Zhang, J. T. Molecular mechanisms of fatty acid synthase (FASN)-mediated resistance to anti-cancer treatments, *Advances in Biological Regulation* 54 (1), 214-221 (2014).
- **Fako, V. E.**; Furgeson, D. Y. Zebrafish as a correlative and predictive model for assessing biomaterial toxicity, *Advanced Drug Delivery Reviews* 61 (6), 478-486 (2009).
- Bar-Ilan, O.; Albrecht, R. M.; **Fako, V. E.**; Furgeson, D. Y. Toxicity assessments of multi-sized gold and silver nanoparticles in zebrafish embryos, *Small* 5 (16), 1897-1910 (2009).
- **Fako, V. E.**; Liu, J. Y.; Zhang, J. T. Mechanism of orlistat hydrolysis by the thioesterase of human fatty acid synthase (in revision).
- **Fako, V. E.**; Liu, J. Y.; Zhang, J. T. Proton pump inhibitors act as novel inhibitors of the thioesterase of human fatty acid synthase (in preparation).

Patents

- Hergenrother, P. J.; Putt, K. S.; Peterson, Q. P.; **Fako, V. E.** Compositions and methods including cell death inducers and procaspase activation. U. S. Patent 8,592,584, November 26, 2013.

Presentations and Abstracts

- **Fako, V. E.**; Liu, J. Y.; Zhang, J. T. Mechanism of orlistat hydrolysis by FASN for targeted drug discovery. Poster Presentation. Great Lakes Drug Metabolism and Disposition Group Meeting 2014, Indianapolis, IN

- **Fako, V. E.;** Liu, J. Y.; Zhang, J. T. Molecular mechanism of orlistat hydrolysis by FASN for targeted drug discovery. Accepted Abstract. National Institutes of Health National Graduate Student Research Conference 2013, Bethesda, MD
- **Fako, V. E.;** Liu, J. Y.; Zhang, J. T. Novel inhibitors of human fatty acid synthase thioesterase. Poster Presentation. Molecular Therapeutics of Cancer Research Conference 2013, Boulder, CO.
- **Fako, V. E.;** Liu, J. Y.; Zhang, J. T. Mechanism of orlistat hydrolysis by the thioesterase in fatty acid synthase. Poster Presentation. IU Simon Cancer Center Cancer Research Day 2012, Indianapolis, IN
- **Fako, V. E.;** Liu, J. Y.; Zhang, J. T. Mechanism of orlistat hydrolysis by the thioesterase in fatty acid synthase. Poster Presentation. IUPUI Research Day 2012, Indianapolis, IN
- **Fako, V. E.;** Liu, J. Y.; Zhang, J. T. Mechanism of orlistat hydrolysis by the thioesterase in fatty acid synthase. Poster Presentation. American Association for Cancer Research Annual Meeting 2012, Chicago, IL
- **Fako, V. E.;** Liu, J. Y.; Zhang, J. T. Mechanism of orlistat hydrolysis by fatty acid synthase thioesterase. Platform Presentation. Sigma Xi Graduate Student Research Competition 2011, Indianapolis, IN

Honors and Awards

Graduated from the University of Illinois *Cum Laude* with James Scholar Distinction and Highest Distinction in the Chemistry Curriculum
 National Society of Collegiate Scholars
 Chemical Industry Council of Illinois Scholarship Winner, 2003
 National Starch Company Scholarship Winner, 2005
 Hughes Undergraduate Research Fellow; University of Illinois, 2005-2006
 Lando Summer Undergraduate Research Fellow; University of Minnesota, 2006
 First Place in Sigma Xi Research Presentation Competition at IUSM, 2011
 AACR Travel Award; Indiana University Simon Cancer Center, 2012
 IUSM Department of Pharmacology and Toxicology Student President, 2013-2014
 Paradise Travel Award; IUSM Department of Pharmacology and Toxicology, 2013
 Accepted to attend NIH National Graduate Student Research Conference, 2013
 K.K. Chen Fellowship Recipient; IUSM Department of Pharmacology and Toxicology, 2014

Memberships

American Association for the Advancement of Science, Student Member, 2010-present
 American Association for Cancer Research, Associate Member, 2011-present
 Sigma Xi, The Scientific Research Society, Associate Member, 2012-2013